

# Fast and Robust Sparsity-Aware Block Diagonal Representation

Aylin Taştan\*, Michael Muma†, and Abdelhak M. Zoubir‡

**Abstract**—The block diagonal structure of an affinity matrix is a commonly desired property in cluster analysis because it represents clusters of feature vectors by non-zero coefficients that are concentrated in blocks. However, recovering a block diagonal affinity matrix is challenging in real-world applications, in which the data may be subject to outliers and heavy-tailed noise that obscure the hidden cluster structure. To address this issue, we first analyze the effect of different fundamental outlier types in graph-based cluster analysis. A key idea that simplifies the analysis is to introduce a vector that represents a block diagonal matrix as a piece-wise linear function of the similarity coefficients that form the affinity matrix. We reformulate the problem as a robust piece-wise linear fitting problem and propose a Fast and Robust Sparsity-Aware Block Diagonal Representation (FRS-BDR) method, which jointly estimates cluster memberships and the number of blocks. Comprehensive experiments on a variety of real-world applications demonstrate the effectiveness of FRS-BDR in terms of clustering accuracy, robustness against corrupted features, computation time and cluster enumeration performance.

**Index Terms**—Block diagonal representation, affinity matrix, similarity matrix, eigenvalues, subspace clustering.

## I. INTRODUCTION

A BLOCK diagonally structured affinity matrix represents clusters of feature vectors by non-zero coefficients that are concentrated in blocks. Such a structure is an informative model to describe hidden relationships. It has numerous applications, e.g., denoising [1]-[2], recognition [3], semi-supervised learning [4]-[6], subspace learning and clustering/classification [6]-[16].

Commonly used existing block diagonal representation (BDR) methods impose a structure on the affinity matrix using regularization with block diagonal (BD) priors, e.g. based on a low-rank property [17]-[20], sparsity [21]-[23] or a known number of blocks  $K$  [6]-[9]. For example the method in [6], which is one of the current benchmarks BDR methods, controls the number of connected components in the affinity matrix by imposing a rank constraint on the Laplacian matrix. An alternative popular approach [7], proposes a  $K$ -block regularizer that is defined by the sum of the  $K$  smallest eigenvalues of the Laplacian matrix to compute a BD affinity matrix. A major challenge of these methods is the need to

\*The author was with the Signal Processing Group, Technische Universität Darmstadt, Darmstadt, Germany and is now with the Pattern Recognition Group, University of Bern, Bern, Switzerland (e-mail: a.tastan@spg.tu-darmstadt.de; aylin.tastan@unibe.ch).

†The author is with the Robust Data Science Group, Technische Universität Darmstadt, Darmstadt, Germany (e-mail: michael.muma@tu-darmstadt.de).

‡The author is with the Signal Processing Group, Technische Universität Darmstadt, Darmstadt, Germany (e-mail: zoubir@spg.tu-darmstadt.de).

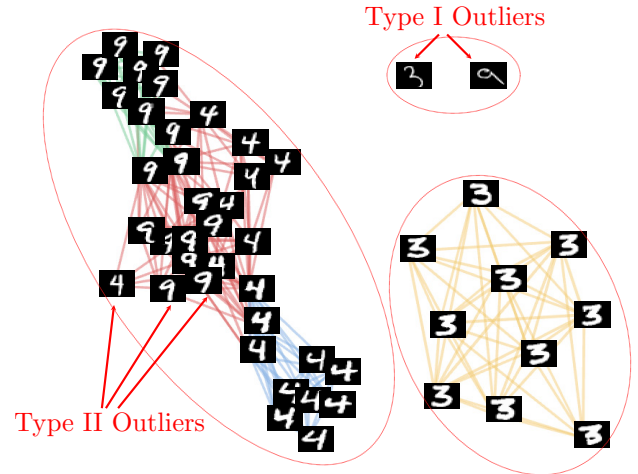


Fig. 1: Exemplary graph partitioning digit samples from MNIST data base [32].

determine appropriate BD priors which play a crucial role in achieving accurate BDR results. Due to its key role in BDR methods, the determination of sparsity/low-rank level has been intensively investigated from different viewpoints, e.g. similarity coefficients’ distribution [24], connectedness [25], geometric analysis [26] and supervised learning [27]-[28]. Recently, in [9], an alternative unsupervised approach based on eigenvalues has been proposed to deduce the sparsity level in a BD matrix. The eigenvalue analysis is, however, restricted to the setting of independent blocks.

A further significant challenge when working with real-world data is the presence of heavy-tailed noise and outliers [29]-[31], that might obscure the eigenvalue structure in corrupted data sets. This results in a performance degradation for BDR approaches that rely on estimating eigenvalues to determine connectedness. To illustrate the necessity for robustness, a graph partitioning application is shown in Fig. 1 for a defined level of sparsity using the well-known handwritten digit samples from the MNIST data base [32]. In the exemplary graph model, the red edges represent connections to outliers while the remaining edges are the informative edges, where green, blue and yellow lines represent the within-cluster edges of digits 9, 4 and 3, respectively. The red ellipses indicate cluster assignments that are computed based on the general graph partitioning principle, in which the number of edges that cross the cut is minimized [33]. As can be seen, unconnected outlying digit samples (‘Type I outliers’) are assigned into a small cluster while a different type of outliers (‘Type II outliers’) that create

false positive connections between multiple clusters cause a merging of characters four and nine into one large cluster.

In this work, we propose a method for robustly estimating an underlying BD structure, given an outlier-corrupted affinity matrix. We call this method: *Fast and Robust Sparsity-Aware Block Diagonal Representation*. We build upon the definition of a vector  $\mathbf{v}$  that we recently introduced in [9] to represent the BD affinity matrix as a piece-wise linear function. Compared to existing popular BDR approaches, such as, [6]-[8], the optimization is efficiently performed in a vector space instead of matrix space. Additionally and in contrast to [9], the method is robust against outliers. Our main contributions are summarized as follows:

- 1) We perform comprehensive robustness analysis that quantifies the effects of outliers. In particular, our theoretical analysis shows how the vector  $\mathbf{v}$  and the eigenvalues, which carry substantial information about the BD structure, are influenced by outliers.
- 2) Our analysis enables the development of a BDR algorithm that is (i) robust against outliers that obscure the target BD structure and (ii) computationally efficient by re-formulating the problem as a piece-wise linear function optimization instead of a matrix-optimization. We show that our proposed method provides mathematically interpretable results in challenging settings where deriving eigenvalue information is no longer possible (i.e., in the extreme case when all blocks are connected because of corruption by outliers).

The paper is organized as follows. Section II contains a summary of notations and a brief discussion on eigen-decomposition. The detailed eigenvalue analysis and outlier effects are presented in Section III. The simplification of the graph Laplacian matrix analysis by means of vector  $\mathbf{v}$  and the associated outlier effect analysis are the subject of Section IV. The proposed FRS-BDR method is detailed in Section V and experimental evaluations demonstrating the performance of FRS-BDR in comparison to popular BDR approaches are shown in Section VI. Finally, conclusions are drawn in Section VII. The codes that implement the FRS-BDR method are available at: <https://github.com/A-Tastan/FRS-BDR>

## II. PRELIMINARIES

### A. Summary of Notation

Lower and upper-case bold letters denote vectors and matrices, respectively;  $|x|$  denotes the absolute value of  $x$ ;  $\|\mathbf{x}\|$  denotes the norm of vector  $\mathbf{x}$  while  $\text{med}(\mathbf{x})$  denotes its median;  $\text{sign}(x) = x/|x|$ ;  $\text{diag}(x_1, \dots, x_N)$  denotes a diagonal matrix of size  $N \times N$  with  $x_1, \dots, x_N$  on its diagonal;  $\mathbf{I}$  denotes the identity matrix;  $\mathbf{1}$  denotes the column vector of ones;  $\hat{\mathbf{x}}$  denotes the estimate of vector  $\mathbf{x}$ ;  $\tilde{\mathbf{W}}$  refers to a corrupted affinity matrix;  $i, j$  and  $k$  are index operators for the blocks, e.g.  $\tilde{\mathbf{W}}_i$  denotes  $i$ th block in  $\tilde{\mathbf{W}}$ ;  $m, n$  and  $r$  are index operators for the samples; finally I and II denote, respectively, index operators for the Type I and Type II outliers.

### B. Eigen-decomposition of Laplacian Matrix

Let data set  $\mathbf{X} = [\mathbf{x}_1 \dots \mathbf{x}_N] \in \mathbb{R}^{M \times N}$  with  $M$  denoting the feature dimension and  $N$  being the number of feature vectors,

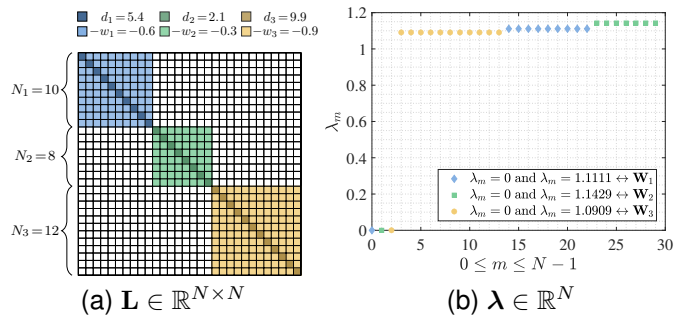


Fig. 2: Exemplary target Laplacian matrix and its eigenvalues ( $\mathbf{n} = [10, 8, 12]^T \in \mathbb{R}^K$ ,  $N = 30$ ,  $K = 3$ ).

be represented as a graph  $G = \{V, E, \mathbf{W}\}$ , where  $V$  denotes the vertices,  $E$  represents the edges, and  $\mathbf{W} \in \mathbb{R}^{N \times N}$  is the symmetric affinity matrix. The affinity matrix is computed from  $\mathbf{X}$  by choosing an appropriate similarity measure, such as, the cosine similarity for which  $w_{m,n} = \mathbf{x}_m^T \mathbf{x}_n$ ,  $m \neq n$  s.t.  $\|\mathbf{x}_m\|_2 = 1$ ,  $\|\mathbf{x}_n\|_2 = 1$ . Let  $\mathbf{L} \in \mathbb{R}^{N \times N}$  denote the nonnegative definite Laplacian matrix that is defined by the eigen-problem

$$\mathbf{L}\mathbf{y}_m = \lambda_m \mathbf{y}_m, \quad (1)$$

or in a generalized eigenvalue problem form

$$\mathbf{L}\mathbf{y}_m = \lambda_m \mathbf{D}\mathbf{y}_m, \quad (2)$$

with associated eigenvalues  $0 \leq \lambda_0 \leq \lambda_1 \leq \dots \leq \lambda_{N-1}$  sorted in ascending order. Here,  $\mathbf{L} = \mathbf{D} - \mathbf{W}$ , where  $\mathbf{D} \in \mathbb{R}^{N \times N}$  is a diagonal weight matrix with edge weights  $d_{m,m} = \sum_n w_{m,n}$  on the diagonal,  $\lambda_m$  denotes the  $m$ th eigenvalue and  $\mathbf{y}_m \in \mathbb{R}^N$  is the eigenvector associated with  $\lambda_m$ .

## III. EIGENVALUE ANALYSIS AND OUTLIER EFFECTS

The eigen-decomposition of a Laplacian matrix has numerous applications [33]-[37] and, in particular, it plays a crucial role in graph-based cluster analysis [14], [38]-[44]. However, isolated outliers and outliers that induce undesired correlations between different clusters may negatively impact the eigen-decomposition, leading to a breakdown of clustering algorithms [38]-[39]. Section III-A summarizes briefly our previous findings in [9]. A new series of solutions based on the standard eigen-decomposition in Eq. (1) is provided in Appendix B of the accompanying material. Then, the effect of outliers and group similarity on eigenvalues is analyzed in Section III-B for both eigen-decompositions, i.e. for Eqs. (1) and (2).

### A. Target Eigenvalues for Graph-based Clustering

As graph partitioning approaches seek to partition the set of vertices in  $G$  into disjoint sets and minimizing the number of the edges that cross the cut [26], [45]-[46], an ideal, i.e., target BD affinity matrix is defined in [9] as follows.

**Definition III.1. (Target BD Affinity Matrix, [9])** Let  $\mathbf{W} \in \mathbb{R}^{N \times N}$  be a  $K$  block zero-diagonal symmetric affinity matrix with blocks  $\mathbf{W}_1, \mathbf{W}_2, \dots, \mathbf{W}_K$  on its diagonal. Each block  $\mathbf{W}_i$ ,  $i=1, \dots, K$  is associated with a number  $N_i \in \mathbb{Z}_+ > 1$  of feature vectors and concentrated around a similarity constant  $w_i \in \mathbb{R}^+$ ,  $i=1, \dots, K$  with negligibly small variations.  $\mathbf{W}$  is called

the target affinity matrix if and only if the similarity coefficients between different blocks are all zero-valued.

Based on this definition, the corresponding ideal graph  $G$  includes only edges between vertices associated with the same block. In [9], using spectral analysis, we showed that if there exists a  $\mathbf{W}$  as in Definition III.1, the eigenvalues of the associated Laplacian matrix  $\mathbf{L} \in \mathbb{R}^{N \times N}$  will be of the following form

$$\boldsymbol{\lambda} = \text{sort} \left( \underbrace{0, \dots, 0}_K, \underbrace{\frac{N_1}{N_1-1}, \dots, \frac{N_1}{N_1-1}}_{N_1-1}, \dots, \underbrace{\frac{N_K}{N_K-1}, \dots, \frac{N_K}{N_K-1}}_{N_K-1} \right), \quad (3)$$

where  $\boldsymbol{\lambda} \in \mathbb{R}^N$  denotes the vector of target eigenvalues and  $\text{sort}(\cdot)$  is the sorting operation in ascending order.

Fig. 2 illustrates the vector of target eigenvalues  $\boldsymbol{\lambda}$  associated with a Laplacian matrix of  $K=3$  blocks where each block is assumed to be concentrated around a constant  $w_i \in \mathbb{R}^+$ , e.g.  $\mathbf{w} = [0.6, 0.3, 0.9]^\top \in \mathbb{R}^K$ . Fig. 2b confirms the findings of [9], i.e., that the smallest eigenvalue is zero-valued and the remaining  $N_i - 1$  number of eigenvalues are  $\frac{N_i}{N_i-1}$  for each block  $i = 1, \dots, K$ .

For clustered data, the target block diagonal model in Definition III.1 represents the optimal level of sparsity with internally dense and externally disjoint groups of vertices. If the observed data would ideally follow this model, it would not contain outliers and the sparsity level could directly be deduced from the percentage of zero-valued entries in the affinity matrix. It is evident that setting additional entries in the affinity matrix in Definition III.1 to zero (resulting in an overly sparse graph) will reduce the internally dense structure of a cluster and lead to the occurrence of Type I outliers (see Definition III.2). In contrast, an overly dense graph, is obtained by adding undesired edges between blocks, which is consistent with the occurrence of Type II outliers (see Definition III.3) and its extreme case of group similarity (see Definition III.4). The introduced theoretical analysis in the following section describes the effect of these fundamental outlier types on the optimal level of sparsity and shows how optimizing the level of sparsity based on the determined target block diagonal model prevents these fundamental outlier effects and addresses robustness and sparsity jointly.

### B. Outlier Effects on Target Eigenvalues

From Eq. (3), it follows that the non-zero components of the target eigenvalues contain the block size information. However, in practice, such a target vector is not available. Especially for outlier-corrupted affinity matrices, the blocks might be obscured (see also Fig. 8 for an example), which results, e.g., in a performance degradation of an eigenvalue-based block size estimate. To quantify this more precisely, and subsequently derive robust BDR methods, we next define some fundamental outlier types and analyze their effects on the target eigenvalues.

**Definition III.2. (Type I Outliers, [31])** *The feature vectors corresponding to the vertices that do not share edges with any of the samples are called Type I outliers.*

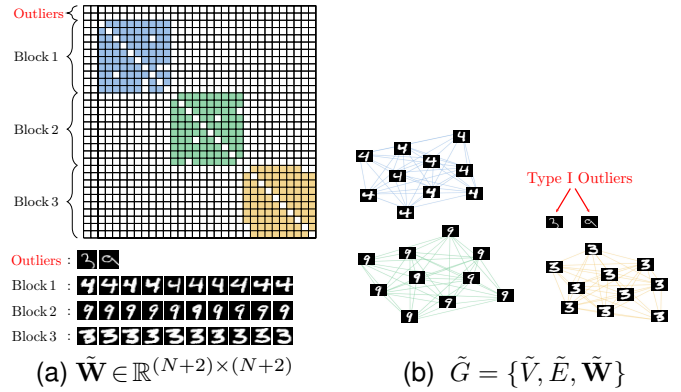


Fig. 3: Illustration of Type I outliers. The colored cells in the corrupted BD affinity matrix  $\tilde{\mathbf{W}}$  represent non-zero edge weights in graph  $\tilde{G}$ .

Definition III.2 is illustrated in Fig. 3 in which the unconnected vertices in  $\tilde{G}$  are Type I outliers. Since the multiplicity of the zero-valued eigenvalues of  $\mathbf{L}$  equals the number of connected components [47], this means that  $N_I$  Type I outliers lead to  $N_I$  additional zero-valued eigenvalues [31].

In real-world scenarios the number of Type I outliers varies and their occurrence, generally speaking, is affected by multiple factors: One significant delimiter for the number of Type I outliers is the data structure. For example, a simple similarity measure, i.e.  $\mathbf{W} = \mathbf{X}^\top \mathbf{X}$  will produce a sparse affinity matrix only when the feature vectors are sparse. In practice, using images or medical observations as feature vectors usually generates non-sparse affinity matrices for a simple similarity measure (e.g.  $\mathbf{W} = \mathbf{X}^\top \mathbf{X}$ ) while using, e.g. a term-document matrix as data matrix may result in a sparse matrix and consequently to the occurrence of Type I outliers. The second important delimiter is the affinity matrix construction. In more details, for a sparse affinity matrix construction method increasing sparsity produces Type I outliers. An example illustrating the link between Type I outliers and sparse affinity matrix construction is shown in Fig. 10 and in Appendix E.1 of the accompanying material for the MNIST data base.

Next, we study the effect of Type II outliers, defined as follows:

**Definition III.3. (Type II Outliers, [31])** *The feature vectors corresponding to the vertices that share edges with more than one group of feature vectors are called Type II outliers.*

Definition III.3 is illustrated in Fig. 4, which shows that the connectedness of Type II outliers to multiple groups of feature vectors obscures the target group structure and poses a challenge to BDR methods.

In contrast to Type I outliers studied in [31], the effect of Type II outliers on eigenvalues is still an open problem. Therefore, an analysis of the Type II outliers' effect on the eigenvalues of the Laplacian matrix is provided for the generalized eigen-decomposition in Eq. (2) as follows.<sup>1</sup>

<sup>1</sup>For an analysis based on the standard eigen-decomposition in Eq. (1), see Appendix B of the accompanying material.

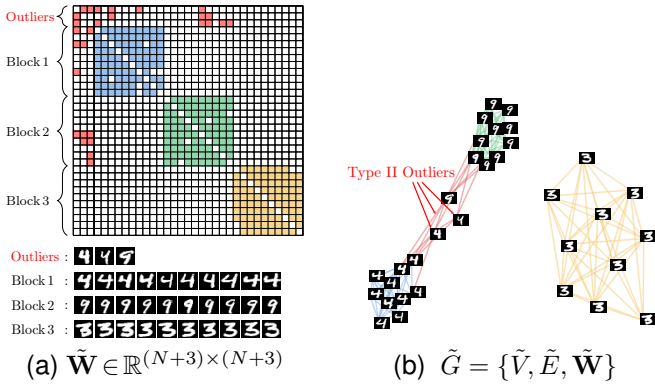


Fig. 4: Illustration of Type II outliers. The red colored cells in  $\tilde{W}$  correspond to edges of Type II outliers.

**Theorem 1.** Let  $\tilde{W} \in \mathbb{R}^{(N+1) \times (N+1)}$  define a symmetric affinity matrix, that is equal to  $W$ , except for an additional Type II outlier that shares similarity coefficients with  $K$  blocks where  $\tilde{w}_{\Pi,K} > 0$  denotes the similarity coefficient between the Type II outlier and the  $K$ th block. Then, for the associated corrupted Laplacian matrix  $\tilde{L} \in \mathbb{R}^{(N+1) \times (N+1)}$  with eigenvalues  $\tilde{\lambda} \in \mathbb{R}^{N+1}$ , it holds that

$$\left\{ \begin{array}{l} N_1 - 1 \text{ elements of } \tilde{\lambda} \text{ are equal to } \frac{N_1 w_1 + \tilde{w}_{\Pi,1}}{\tilde{d}_1}, \\ N_2 - 1 \text{ elements of } \tilde{\lambda} \text{ are equal to } \frac{N_2 w_2 + \tilde{w}_{\Pi,2}}{\tilde{d}_2}, \\ \vdots \\ N_K - 1 \text{ elements of } \tilde{\lambda} \text{ are equal to } \frac{N_K w_K + \tilde{w}_{\Pi,K}}{\tilde{d}_K}, \\ \text{the smallest element of } \tilde{\lambda} \text{ is equal to zero,} \end{array} \right.$$

and the remaining  $K$  eigenvalues are the roots of

$$\prod_{j=1}^K (\tilde{w}_{\Pi,j} - \tilde{\lambda} \tilde{d}_j) \left( - \sum_{j=1}^K \frac{N_j \tilde{w}_{\Pi,j} \tilde{d}_j}{\tilde{w}_{\Pi,j} - \tilde{\lambda} \tilde{d}_j} - \tilde{d}_{\Pi} \right) = 0,$$

where  $\tilde{d}_{\Pi} = \sum_{j=1}^K N_j \tilde{w}_{\Pi,j}$  and  $\tilde{d}_j = (N_j - 1)w_j + \tilde{w}_{\Pi,j}$ .

*Proof.* See Appendix A.1 of the accompanying material.  $\square$

We next introduce an extreme case of Type II outliers based on the following definition.

**Definition III.4. (Group Similarity)** If an entire group of vertices shares edges with another group of vertices we call this, group similarity.

The Laplacian matrix of Definition III.4 can be considered as a single connected component which means that the number of zero-valued eigenvalues equals to one [47]. In contrast to this simple interpretation, the remaining eigenvalues can be formulated as a function of intra-blocks and inter-blocks similarity coefficients where inter-blocks similarity coefficients are generally smaller-valued than those of intra-blocks in real-world scenarios. To provide a mathematical understanding of this, the following theorem quantifies the effect of group similarity on the target eigenvalues.

**Theorem 2.** Let  $\tilde{W} \in \mathbb{R}^{N \times N}$  define an affinity matrix that is equal to  $W$ , except that block  $i$  has similarity with the remaining  $K - 1$  blocks with  $\tilde{w}_{i,j} = \tilde{w}_{j,i} > 0$  denoting the

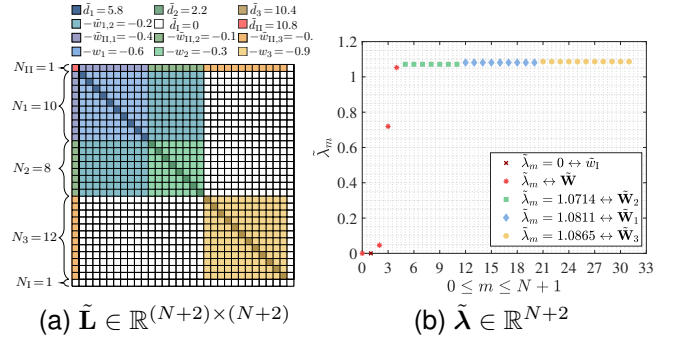


Fig. 5: Exemplary corrupted Laplacian matrix and its eigenvalues ( $\mathbf{n} = [10, 8, 12]^T \in \mathbb{R}^K$ ,  $N = 30$ ,  $K = 3$ ).

value around which the similarity coefficients between blocks  $i$  and  $j$  are concentrated for  $j = 1, \dots, K$  and  $i \neq j$ . Then, the eigenvalues  $\tilde{\lambda} \in \mathbb{R}^N$  of  $\tilde{L} \in \mathbb{R}^{N \times N}$  are as follows:

$$\left\{ \begin{array}{l} N_i - 1 \text{ elements of } \tilde{\lambda} \text{ are equal to } \frac{N_i w_i + \sum_{\substack{j=1, \\ j \neq i}}^K N_j \tilde{w}_{i,j}}{\tilde{d}_i}, \\ N_j - 1 \text{ elements of } \tilde{\lambda} \text{ are equal to } \frac{N_j w_j + N_i \tilde{w}_{i,j}}{\tilde{d}_j}, \\ \vdots \\ N_K - 1 \text{ elements of } \tilde{\lambda} \text{ are equal to } \frac{N_K w_K + N_i \tilde{w}_{i,K}}{\tilde{d}_K}, \\ \text{the smallest element of } \tilde{\lambda} \text{ is equal to zero,} \end{array} \right.$$

and the remaining  $K - 1$  eigenvalues in  $\tilde{\lambda}$  are the roots of

$$\prod_{\substack{j=1 \\ j \neq i}}^K (N_i \tilde{w}_{i,j} - \tilde{\lambda} \tilde{d}_j) \left( - \sum_{\substack{j=1 \\ j \neq i}}^K \frac{\tilde{d}_j N_j \tilde{w}_{i,j}}{N_i \tilde{w}_{i,j} - \tilde{\lambda} \tilde{d}_j} - \tilde{d}_i \right) = 0,$$

where  $\tilde{d}_j = (N_j - 1)w_j + N_i \tilde{w}_{i,j}$ ,  $\tilde{d}_i = (N_i - 1)w_i + \sum_{\substack{j=1 \\ j \neq i}}^K N_j \tilde{w}_{i,j}$ .

*Proof.* See Appendix A.2 of the accompanying material.  $\square$

A Laplacian matrix  $\tilde{L}$  that is corrupted with all discussed outlier types is displayed in Fig. 5a, while the above derived outlier effects on the eigenvalues are visually summarized in Fig. 5b.

**Remark 1.** To derive the theoretical results, simplifying assumptions<sup>2</sup>, such as, concentration of the similarity coefficients within a block around a mean value are required. In practice, these assumptions may only be approximately fulfilled. However, will see later in Section VI that the numerical performance gain obtained by suppressing outliers' effects outweigh the model mismatch in the considered benchmark data sets. Further, existing theoretical works on the spectrum of BDR methods, e.g. [49]-[52], make even stricter assumptions, because the spectrum of an adjacency matrix can be found in closed form for simple models [50]. According to the most recent generic analyses [49] and [50], the spectrum of a BDR has been computed for planted partition model (PPM) with equal community sizes which is a special case of stochastic block model (SBM) assuming that the probability of having an edge within the cluster is constant and equal for all clusters while probability of having an edge

<sup>2</sup>For our further analysis about loosening assumptions based on eigenvectors, see Theorem 1 in [48].

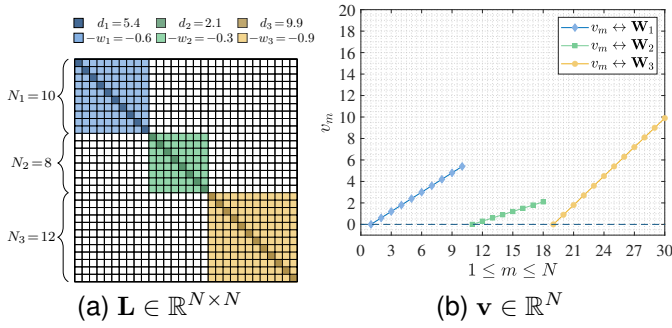


Fig. 6: Exemplary target Laplacian matrix and corresponding vector  $\mathbf{v}$  ( $\mathbf{n} = [10, 8, 12]^T \in \mathbb{R}^K$ ,  $N = 30$ ,  $K = 3$ ).

to a different cluster is also constant and the same for all clusters. There are also some other researches on eigenvalues to determine the limiting distribution of the edge eigenvalues [51] and that of the outlier eigenvalues [52]. Even though these previously introduced spectral properties of random matrices are interesting to understand the complex graph structures, the available information about the spectrum of a BD matrix is limited to the considered simple models, i.e. PPM, and the available information about the eigenvalues is limited to eigenvalues of non-weighted graphs.

#### IV. SIMPLIFIED LAPLACIAN MATRIX ANALYSIS AND OUTLIER EFFECTS

In the preceding sections, outlier effects have been analyzed for  $N \times N$  Laplacian matrices, which may lead to computationally heavy methods for large graphs. In this section, we therefore re-formulate the problem in  $N \times 1$  vector space. In particular, assuming that  $\mathbf{W}$  is symmetric and BD<sup>3</sup>, the analysis is simplified by defining the vector  $\mathbf{v} \in \mathbb{R}^N$  as follows [9]

$$v_m = \sum_{n=m}^N l_{m,n}, \quad (4)$$

where  $v_m$  and  $l_{m,n}$ , respectively, denote the  $m$ th and  $(m, n)$ th components of  $\mathbf{v}$  and  $\mathbf{L}$ .

##### A. Target Vector $\mathbf{v}$ for Graph-based Clustering

In [9], we have shown that the target vector  $\mathbf{v}$  is a piece-wise linear function of the following form.

**Definition IV.1. (Target Vector  $\mathbf{v}$ , [9])** The target vector  $\mathbf{v}$  is a piece-wise linear function of the following form

$$v_m = f(m) = \begin{cases} (m - \ell_1)w_1 & \text{if } \ell_1 \leq m \leq u_1 \\ \vdots & \\ (m - \ell_K)w_K & \text{if } \ell_K \leq m \leq u_K, \end{cases}$$

where  $\ell_1 = 1$ ,  $u_1 = N_1$ ,  $\ell_i = \sum_{k=1}^{i-1} N_k + 1$  and  $u_i = \sum_{k=1}^i N_k$  for  $i=2, \dots, K$ .

An illustration is provided in Fig 6 for a  $K = 3$  block Laplacian matrix. As can be seen, the changepoints of the piece-wise linear function provide information about the block size. To arrive at robust methods, we next determine the outlier effects on  $\mathbf{v}$ .

<sup>3</sup>A sparse matrix can be transformed into a BD form using the Reverse Cuthill-McKee (RCM) algorithm [53].

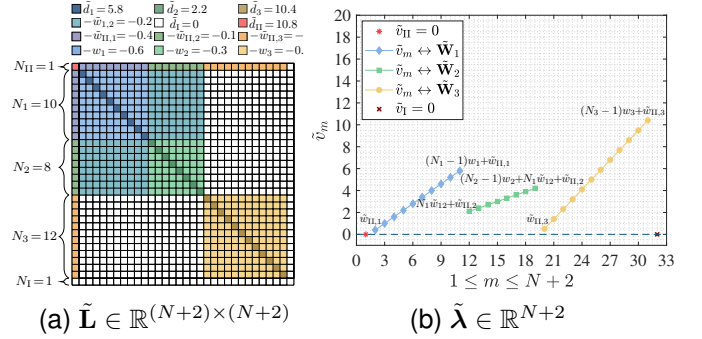


Fig. 7: Exemplary corrupted Laplacian matrix and corresponding  $\tilde{\mathbf{v}}$  ( $\mathbf{n} = [10, 8, 12]^T \in \mathbb{R}^K$ ,  $N = 30$ ,  $K = 3$ ).

##### B. Outlier Effects on Target Vector $\mathbf{v}$

For a Type I outlier-corrupted affinity matrix  $\tilde{\mathbf{W}} \in \mathbb{R}^{(N+1) \times (N+1)}$  that is identical to  $\mathbf{W}$ , except for a single Type I outlier  $o_I$ , the overall edge weight associated with  $o_I$  is zero-valued, i.e.  $\tilde{d}_I = 0$ . Based on Def. IV.1, it is straightforward to show that the component in the associated corrupted vector  $\tilde{\mathbf{v}} \in \mathbb{R}^{N+1}$  that is associated with Type I outliers is zero valued, i.e.,  $\tilde{v}_I = 0$ . The Type II outliers' effect on  $\mathbf{v}$  is as follows.

**Theorem 3.** Let  $\tilde{\mathbf{W}} \in \mathbb{R}^{(N+1) \times (N+1)}$  define a Type II outlier-corrupted BD affinity matrix that is identical to  $\mathbf{W} \in \mathbb{R}^{N \times N}$  except for a single Type II outlier that has non-zero similarity coefficients with all blocks. Assuming that the similarity coefficients associated with the outlier  $o_{II}$  and the blocks  $j \in \{1, \dots, K\}$  are concentrated around  $\tilde{w}_{II,j}$ , the components, whose indexes are valued between the outlier index and the largest index of the  $j$ th block, such that  $m_{II} < m \leq u_j$ , increase by  $\tilde{w}_{II,j}$  in the corrupted vector  $\tilde{\mathbf{v}} \in \mathbb{R}^{N+1}$ . Further, the component associated with the Type II outlier is given by

$$\tilde{v}_{II} = \begin{cases} 0 & \text{if } 0 < m_{II} < \ell_1 \\ (m_{II} - \ell_1)\tilde{w}_{II,1} & \text{if } \ell_1 < m_{II} < \ell_2 \\ \vdots & \\ \sum_{j=1}^{K-1} N_j \tilde{w}_{II,j} + (m_{II} - \ell_K)\tilde{w}_{II,K} & \text{if } \ell_K < m_{II} \leq N+1 \end{cases},$$

where  $\ell_j$  denotes the lowest index of the  $j$ th block.

*Proof.* See Appendix C.1 of the accompanying material.  $\square$

The effect of group similarity on  $\mathbf{v}$  is as follows.

**Theorem 4.** Let  $\tilde{\mathbf{W}} \in \mathbb{R}^{N \times N}$  define a corrupted affinity matrix that is identical to  $\mathbf{W} \in \mathbb{R}^{N \times N}$ , except that block  $i$  has non-zero similarity coefficients with the remaining  $K - 1$  blocks with  $\tilde{w}_{i,j} = \tilde{w}_{j,i} > 0$  denoting the similarity coefficients around which, blocks  $i$  and  $j$  are concentrated. These similarities result in an increase by  $N_i \tilde{w}_{i,j}$  in the components associated with the blocks  $j = i + 1, \dots, K$  of  $\tilde{\mathbf{v}} \in \mathbb{R}^N$  while the components of  $j < i$  remain the same. Further, the components associated with block  $i$  remain the same for  $i = 1$  and increase by  $\sum_{j=1}^{i-1} N_j \tilde{w}_{i,j}$  for  $2 \leq i \leq K$ .

*Proof.* See Appendix C.2 of the accompanying material.  $\square$

In the sequel, we analyze the worst case of group similarity, i.e., similarity of all blocks. Note that, in this case, eigenvalues can not be formulated as a function of similarity coefficients

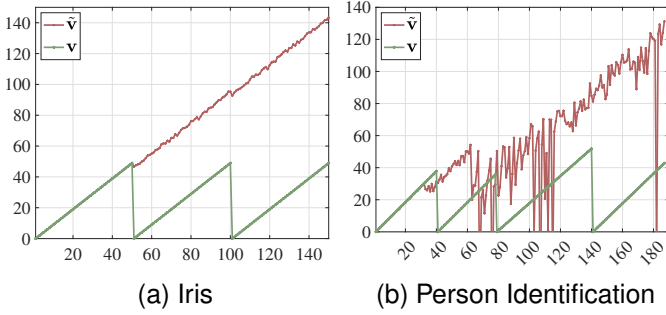


Fig. 8: Exemplary deviations from the target vector  $\mathbf{v}$ . The affinity matrix is defined by  $\mathbf{W} = \mathbf{X}^\top \mathbf{X}$ .

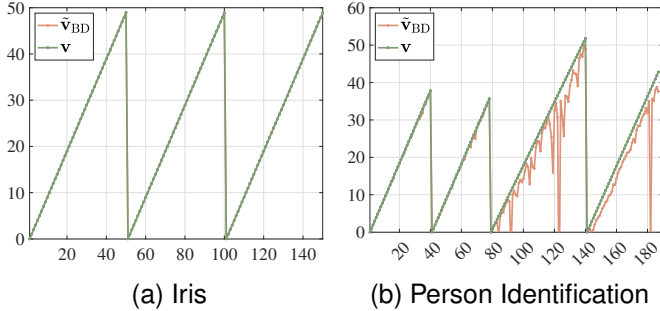


Fig. 9: Exemplary deviations from the target vector  $\mathbf{v}$ . The BD affinity matrix is defined by removing the undesired similarity coefficients between different blocks of  $\mathbf{W} = \mathbf{X}^\top \mathbf{X}$ .

due to the impossibility of simplifying determinants of full matrices via Gaussian elimination. However, recovering the structure of  $\mathbf{W}$  based on  $\mathbf{v}$  is possible based on the following result.

**Corollary 4.1.** *Let  $\tilde{\mathbf{W}} \in \mathbb{R}^{N \times N}$  define a corrupted affinity matrix that is identical to  $\mathbf{W} \in \mathbb{R}^{N \times N}$ , except that each block  $i = 1, \dots, K$  has non-zero similarity coefficients with the remaining  $K - 1$  blocks with  $\tilde{w}_{i,j} = \tilde{w}_{j,i} > 0$  denoting the similarity coefficients around which, blocks  $i$  and  $j$  are concentrated for  $j = 1, \dots, K$  and  $i \neq j$ . This leads to a piece-wise linear function given by*

$$\tilde{v}_m = \begin{cases} (m - \ell_1)w_1 & \text{if } \ell_1 \leq m \leq u_1 \\ (u_1 - \ell_1 + 1)\tilde{w}_{1,2} + (m - \ell_2)w_2 & \text{if } \ell_2 \leq m \leq u_2 \\ \vdots & \vdots \\ \sum_{i=1}^{K-1} (u_i - \ell_i + 1)\tilde{w}_{i,K} + (m - \ell_K)w_K & \text{if } \ell_K \leq m \leq u_K \end{cases}$$

where  $\ell_1 = 1$ ,  $u_1 = N_1$ ,  $\ell_i = \sum_{k=1}^{i-1} N_k + 1$  and  $u_i = \sum_{k=1}^i N_k$  for  $i = 2, \dots, K$ .

*Proof.* See Appendix C.2 of the accompanying material.  $\square$

An exemplary corrupted Laplacian matrix  $\tilde{\mathbf{L}}$  and corresponding  $\tilde{\mathbf{v}}$  illustrating our theoretical findings are shown in Fig. 7a and Fig. 7b, respectively. Consistent with Section III-B, outliers of Type I result in zeros in  $\tilde{\mathbf{v}}$ . Additionally, Type II outliers and group similarity lead to an increase in the target vector  $\mathbf{v}$  as quantified in Theorems 3 and 4, respectively.

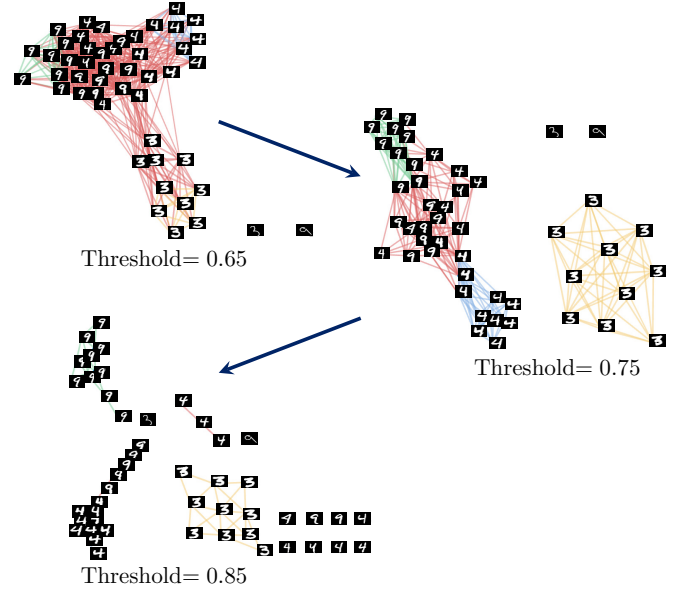


Fig. 10: Example graphs for increasing sparsity. An initial affinity matrix is defined by  $\mathbf{W} = \mathbf{X}^\top \mathbf{X}$  and the example graphs are obtained by removing the edges whose corresponding edge weight is smaller than the defined threshold value.

To demonstrate the degree of model mismatch in the considered real-world data sets due to the simplifying assumptions that were necessary to derive our theory, exemplary vectors associated with the corrupted affinity matrices that are subject to group similarity as in Corollary 4.1 and the corresponding target vector  $\mathbf{v}$ 's are illustrated in Figs. 8a and 8b, respectively, for the Iris [54] and Person Identification [55] data sets. As can be seen, undesired similarity coefficients between different blocks result in shifts from the target piece-wise linear functions starting from the second linear pieces, consistent with our theory in Corollary 4.1. In particular, assumptions and findings of Corollary 4.1 hold well in real-world data sets, especially, when the data sets include densely connected clusters of points, e.g. Ceramic [56] and Iris [54].<sup>4</sup> Additionally, corrupted data sets, e.g. Person Identification [55] whose corresponding affinity matrix is subject to Type I outliers and group similarity results in large deviations from the target piece-wise linear function with group similarity shifts and small-valued  $\tilde{\mathbf{v}}$  components corresponding to Type I outliers as it has been theoretically shown in previous. A further analysis illustrating the degree of model mismatch between the target BD model and a BD model with varying similarity coefficients within the blocks is shown in Figs. 9a and 9b, respectively, for the Iris and Person Identification data sets. Even though highly corrupted data sets generate large deviations from the assumed models in real-world scenarios, an appropriate BDR suppresses these outlier effects by providing an optimal level of sparsity which is a major motivation of our proposed algorithm that will be detailed in the sequel.

<sup>4</sup>For further real-world data examples, see Appendix E.2 of the accompanying material.

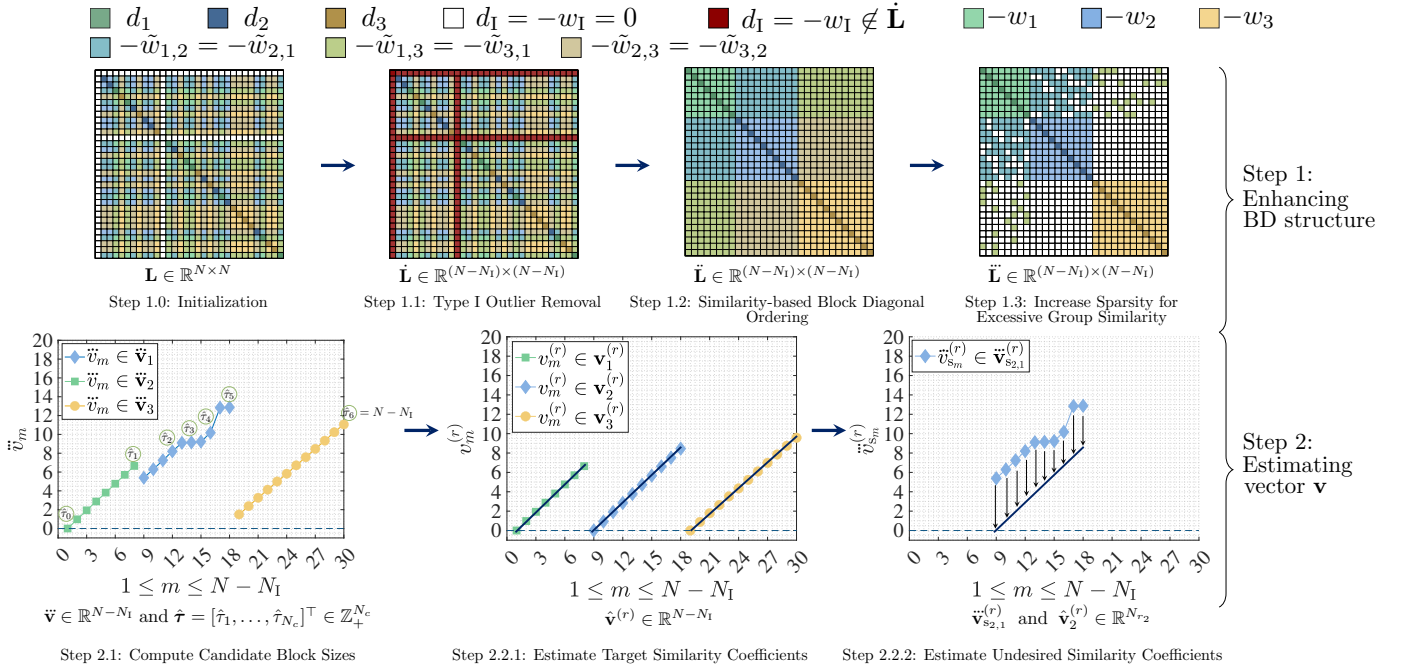


Fig. 11: High-level flow diagram illustrating the key steps of FRS-BDR using a generic example with  $K = 3$  clusters.

## V. THE PROPOSED METHOD

In Section V-B, we briefly discuss the key ideas of the proposed method. Following this, a step-by-step detailed mathematical explanation is provided in Section V-C. We then analyze the computational complexity in Section V-D. Additionally, a comprehensive visual summary is provided in Appendix F.1 of the accompanying material and a pseudo-code algorithm of FRS-BDR is given in Algorithm 2.

### A. Problem Statement: Jointly Addressing Robustness and Sparsity

With the results of Sections III and IV in place, we are ready to understand the relationship between the level of sparsity and the previously defined outlier types to highlight the importance of jointly addressing robustness and sparsity. In a generic example, Fig. 10 shows that a dense graph (top) contains high amounts of group similarity while increasing sparsity reduces the number of Type II outliers (middle). Finally, further increasing sparsity generates Type I outliers until at some point the underlying true cluster structure is completely lost. This means that an inaccurate determination of the sparsity level leads to the above discussed outlier effects for existing approaches, such as, e.g. [21]-[23]. In this section, we therefore propose a new method that addresses robustness and sparsity *jointly*.

More precisely, let a given data set of feature vectors  $\mathbf{X} \in \mathbb{R}^{M \times N}$  be represented as a weighted graph  $G = \{V, E, \mathbf{W}\}$ , i.e.,  $\mathbf{W} = \mathbf{X}^T \mathbf{X}$  and  $\|\mathbf{x}_m\| = 1$ ,  $m = 1, \dots, N$ . Further, let  $\mathbf{D}$  and  $\mathbf{L} \in \mathbb{R}^{N \times N}$  denote, respectively, the overall edge weight and the Laplacian matrices associated with  $\mathbf{W}$ . Then, the goal of this work is to robustly estimate a  $K$  block zero-diagonal symmetric affinity matrix  $\mathbf{W} \in \mathbb{R}^{N \times N}$  using the available information about the vector  $\mathbf{v}$  and an eigen-decomposition.

The number of blocks  $K$  is assumed to be unknown and  $\mathbf{X}$  may be subject to heavy-tailed noise and outliers which results in undesired effects, such as group similarity. The number of outliers is assumed to be unknown. Computational efficiency is also of fundamental interest. *Thus, in brief, the overall aim is to develop a fast and sparsity aware BDR method that is robust against outliers and group similarity.*

### B. Main Ideas and Outline of Proposed Method

This section summarizes the main ideas of our proposed *Fast and Robust Sparsity-Aware Block Diagonal Representation (FRS-BDR)* method. The full details of each step are given in Section V-C.

To provide a general understanding, a high-level flow diagram illustrating the key steps of FRS-BDR is provided in Fig. 11. As shown in the figure, the method consists of two general steps, i.e., enhancing BD structure (Step 1) and estimating vector  $\mathbf{v}$  (Step 2). The computation step starts with a given Type I outlier-corrupted and non-sparse Laplacian matrix  $\mathbf{L}$  (Step 1.0: Initialization in Fig. 11). According to the explicit Definition III.2 of Type I outliers, the method first removes the similarity coefficients associated with Type I outliers, which are represented in red color, from  $\mathbf{L}$  (Step 1.1: Type I Outlier Removal in Fig. 11). Then, the next step is to structure the resulting matrix  $\tilde{\mathbf{L}}$  in a BD form  $\tilde{\tilde{\mathbf{L}}}$  with a similarity-based BD ordering that we present in the sequel (Step 1.2: Similarity-based Block Diagonal Ordering in Fig. 11). The last part of Step 1 is, to obtain vector  $\mathbf{v}$  in form of  $K$  discrete linear segments by computing an ordered sparse Laplacian matrix  $\tilde{\tilde{\tilde{\mathbf{L}}}}$  (Step 1.3: Sparsity for Excessive Group Similarity in Fig. 11). Then, the estimation step starts with a changepoint detection that we propose, to compute the possible block sizes (Step 2.1: Compute Candidate Block

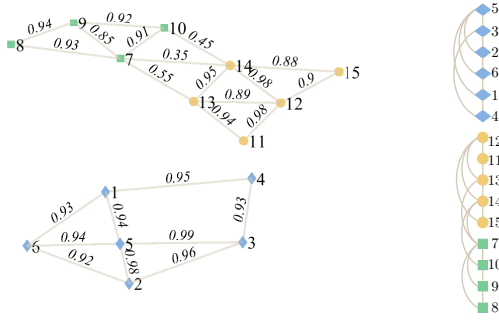


Fig. 12: Exemplary plot of the sBDO algorithm.

Sizes in Fig. 11). For each possible block size vector, i.e.,  $\mathbf{n}_r = [8, 10, 12]^T \in \mathbb{Z}_+^K$  in this illustrating example, the method computes a target vector  $\mathbf{v}^{(r)}$  and a corresponding estimate  $\hat{\mathbf{v}}^{(r)}$  as a function of the estimated target similarity coefficients (Step 2.2.1: Estimate Target Similarity Coefficients in Fig. 11). Further, for every undesired similarity coefficient around which the blocks are concentrated, the shifted vectors (see Corollary 4.1) are computed separately and the undesired similarity coefficients are estimated (Step 2.2.2: Estimate Undesired Similarity Coefficients in Fig. 11). Finally, the estimate  $\hat{\mathbf{v}} \in \mathbb{R}^{N-N_I}$  is computed for the block size vector which provides the best fit to the computed vector  $\hat{\mathbf{v}}$ .

### C. FRS-BDR Algorithm

1) *Step 1 : Enhancing BD Structure*: The key requirement for computing vector  $\mathbf{v}$  based on Eq. (4) is recovering an approximately BD structured Laplacian matrix. Assuming that  $\mathbf{W}$  (and the associated  $\mathbf{L}$ ) are symmetric and sparse matrices, they can be ordered in a BD form [53] based on which vector  $\mathbf{v}$  can be directly computed. However, in general, similarity measures may not produce sparse affinity matrices. We therefore discuss the most challenging scenario, i.e., that  $\mathbf{W}$  is subject to Type I outliers and all blocks exhibit similarity. Considering the Type I outliers' effect on the target vector  $\mathbf{v}$  (see, Section IV-B), the proposed vector  $\mathbf{v}$  computation starts with Type I outlier detection (Step 1.1). Then, a new BD ordering based on the similarity coefficients is proposed to generate a BD ordered Laplacian matrix (Step 1.2). Lastly, a sparse Laplacian matrix design is detailed for the case of excessive group similarity (Step 1.3).

a) *Step 1.1 : Type I Outlier Removal*: Type I outliers are detected according to

$$\mathbf{x}_m \in \mathbf{O}_I \text{ if } w_{m,n} = 0 \text{ for } \forall n = 1, \dots, N \text{ and } m \neq n, \quad (5)$$

where  $\mathbf{O}_I \in \mathbb{R}^{M \times N_I}$  denotes the matrix of Type I outliers,  $\mathbf{x}_m \in \mathbb{R}^M$  is the  $m$ th feature vector for  $m = 1, \dots, N$ ,  $w_{m,n}$  is the  $m, n$ th similarity coefficient corresponding to  $\mathbf{x}_m$  (due to the symmetry of  $\mathbf{W}$ ,  $w_{m,n} = w_{n,m}$ ).

Type I outlier removal based on Eq. (5) directly follows Definition III.2 which means that the operation does not require a determination of the number of outliers. It is an important preliminary step since the presence of Type I outliers may lead to an inaccurate sparsity increase in Step 1.3 due to their effects on the eigenvalues or an incorrect candidate block size estimation in Step 2.1 based on their effects on the vector  $\mathbf{v}$ .

### Algorithm 1: sBDO

---

**Input:**  $\hat{\mathbf{W}}, \hat{\mathbf{D}} \in \mathbb{R}^{(N-N_I) \times (N-N_I)}$   
*Initialization:*  
 Find the node of maximum overall edge weight  $\hat{d}_{\max}$   
**for**  $s = 2, \dots, (N - N_I)$  **do**  
   Adding the most similar neighbor to  $\hat{\mathbf{b}}^{(s)}$ :  
   **if** at least one neighbor exists **then**  
     Estimate  $\hat{b}_s$  using Eq. (6) and stack into  $\hat{\mathbf{b}}^{(s)}$   
   **else**  
     Find the node with maximum overall edge weight  
     among unselected nodes and stack  $\hat{b}_s$  into  $\hat{\mathbf{b}}^{(s)}$   
   **end**  
**end**  
**Output:** Estimated order vector  $\hat{\mathbf{b}}^{(s)} \in \mathbb{Z}_+^{(N-N_I)}$

---

b) *Step 1.2 : Similarity-based BD Ordering (sBDO)*: Let  $\hat{\mathbf{X}} \in \mathbb{R}^{M \times (N-N_I)}$ ,  $\hat{\mathbf{W}}, \hat{\mathbf{D}}$  and  $\hat{\mathbf{L}} \in \mathbb{R}^{(N-N_I) \times (N-N_I)}$  be the resulting matrices after Step 1.1. The vector of the BD order, i.e.,  $\hat{\mathbf{b}} \in \mathbb{Z}_+^{N-N_I}$  is determined based on the following steps.

*Step 1.2.1: Initialization*: The BD order vector  $\hat{\mathbf{b}}^{(1)}$  is comprised of the node index of maximum overall edge weight (i.e.,  $\hat{d}_{\max}$ ).

*Step 1.2.2: Adding the most similar neighbor to  $\hat{\mathbf{b}}^{(s)}$* : Let  $\hat{\mathbf{b}}^{(s)} = [\hat{b}_1, \dots, \hat{b}_{s-1}]^T \in \mathbb{Z}_+^{s-1}$ , with  $s = 2, \dots, N - N_I$ , denote the BD order vector at the  $s$ th stage. Assuming that the neighbors set is non-empty<sup>5</sup>, the most similar neighbor to  $\hat{\mathbf{b}}^{(s)}$  at the  $s$ th stage is determined by

$$\hat{b}_s = \arg \max_{m \in \{1, 2, \dots, N - N_I\}} \left\{ \sum_{n=1}^{s-1} \hat{w}_{m, \hat{b}_n} \right\}, \quad (6)$$

where  $m \in \mathbb{Z}_+$  such that  $1 \leq m \leq N - N_I$  denotes a neighbor node.

An example of the sBDO algorithm is illustrated in Fig. 12 and technically summarized in Algorithm 1. As can be seen from Fig.12, starting from node five, whose overall edge weight is largest valued, the method selects the neighbors based on their edge weights that represent the similarity to previously selected nodes. After selecting all neighbors, the method jumps to the node that has the maximum overall edge weight among the remaining nodes and determines the ordering of the associated neighbors.

Different from the Reverse Cuthill-McKee (RCM) [53], which is a well-known block diagonal ordering method, the proposed sBDO algorithm incorporates useful information from the similarity coefficients. By doing this, the sBDO ordering method does not require making specific assumptions<sup>6</sup>. on the similarity coefficients or a sparse matrix structure that is necessary in RCM algorithm. In challenging scenarios, for example, starting the ordering with a Type II outlier the sBDO algorithm continues selecting vertices from the most similar cluster therewith quickly suppressing the effect of Type II outlier's similarity coefficients.<sup>7</sup>

<sup>5</sup>If it is empty the method simply stacks the node index of maximum overall edge weight into  $\hat{\mathbf{b}}^{(s)}$ .

<sup>6</sup>For examples of similarity coefficients' empirical distributions, see Appendix E.3 of the accompanying material.

<sup>7</sup>For the analysis of sBDO performance, see Appendix F.4.5 of the accompanying material.



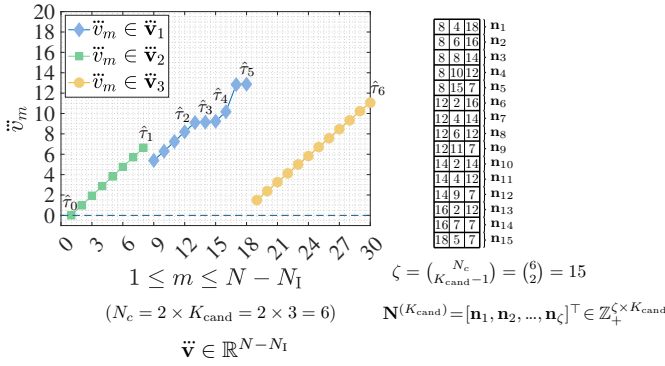


Fig. 13: Exemplary plot of computing candidate block sizes.

*c) Step 1.3: Increase Sparsity for Excessive Group Similarity:* Let  $\tilde{\mathbf{W}}$ ,  $\tilde{\mathbf{D}}$  and  $\tilde{\mathbf{L}} \in \mathbb{R}^{(N-N_1) \times (N-N_1)}$  be the matrices resulting from Step 1.2. A sparsity improved Laplacian matrix  $\tilde{\mathbf{L}} \in \mathbb{R}^{(N-N_1) \times (N-N_1)}$  is designed<sup>8</sup> by increasing sparsity as long as, at least, the two smallest eigenvalues are close to zero<sup>9</sup>. After computing  $\tilde{\mathbf{L}}$ , the vector  $\tilde{\mathbf{v}} \in \mathbb{R}^{N-N_1}$  is obtained using Eq. (4)<sup>10</sup>.

Increasing sparsity for excessive group similarity is an optional step for the FRS-BDR algorithm. In particular, it is designed to obtain a sparsity improved Laplacian matrix  $\tilde{\mathbf{L}}$  whose associated vector  $\tilde{\mathbf{v}}$  provides distinct changepoints that can be easily computed in Step 2.1. In this way, the negative impact of excessive group similarity, which obscures the piece-wise linear functions (for details, see Corollary 4.1), is suppressed and changepoints become more visible. However, this operation does not enforce a block diagonal affinity matrix since it eliminates only a small portion of the undesired similarity coefficients. Therefore, the following steps estimate the vector  $\mathbf{v}$  as a function of desired similarity coefficients and that of undesired that will be removed to obtain a BDR.

2) *Step 2: Estimating Vector v:* This step models  $\tilde{\mathbf{v}}$  as a  $K$ -piece linear function of similarity coefficients around which the blocks are assumed to be concentrated (for details, see Corollary 4.1.), i.e.,

$$\tilde{v}_i = v_i + \mathbf{1} \sum_{\substack{j=1 \\ j \neq i}}^{i-1} N_j \tilde{w}_{i,j}, \quad i = 1, \dots, K, \quad (7)$$

where

$$\mathbf{v}_i = [0, w_i, \dots, (N_i - 1)w_i]^\top \in \mathbb{R}^{N_i} \quad (8)$$

denotes the  $i$ th linear segment of the target vector  $\mathbf{v}_i$ ,  $w_i$  is the similarity coefficient around which the block  $i$  is concentrated and  $\tilde{w}_{i,j}$  is the undesired similarity coefficient between blocks  $i$  and  $j$  around which they are concentrated,  $\mathbf{1} \in \mathbb{R}^{N_i}$  is the column vector of ones,  $N_i$  and  $N_j$  are, respectively, the size of block  $i$  and  $j$ .

*a) Step 2.1: Computing Candidate Block Sizes:* Let  $N_c \in \mathbb{Z}_+$  denote the number of changepoints, let  $\boldsymbol{\tau} = [\tau_1, \tau_2, \dots, \tau_{N_c}]^\top \in \mathbb{Z}_+^{N_c}$  be the vector containing the

<sup>8</sup>For the exemplary sparse Laplacian matrix design algorithms, see Appendix F.3 of the accompanying material.

<sup>9</sup>For the definition of *close to zero*, see Appendix F.2 in of the accompanying material.

<sup>10</sup>The vector  $\mathbf{v}$  can alternatively be computed using  $\tilde{\mathbf{L}} \in \mathbb{R}^{(N-N_1) \times (N-N_1)}$  after executing Steps 1.1 and 1.2 if, at least, the two smallest eigenvalues of  $\tilde{\mathbf{L}}$  are close to zero.

corresponding locations in  $\tilde{\mathbf{v}}$ , and let  $\tau_0 = 0$  and  $\tau_{N_c+1} = N$ . Then, to estimate the model for vector  $\tilde{\mathbf{v}}$  based on Eq. (7), our first step is to detect the changepoints in  $\tilde{\mathbf{v}}$  by minimizing the following penalized least-squares function as in [57]

$$\sum_{i=1}^{N_c+1} \sum_{m=\tau_{i-1}+1}^{\tau_i} (\tilde{v}_m - \hat{v}_m)^2 + \gamma N_c, \quad (9)$$

where  $\tilde{v}_m$  and  $\hat{v}_m$  denote, respectively, the  $m$ th point in the  $i$ th linear segment of  $\tilde{\mathbf{v}}$  and the corresponding least-squares linear fit.  $\gamma$  is the penalty parameter that controls the number of changepoints  $N_c$ . In particular, Eq. (9) considers all possible changepoints for  $\gamma = 0$  and it rejects including additional changepoints if the residual error is smaller than the determined penalty parameter  $\gamma$ . Different from determining  $\gamma$  directly, this step increases the value of  $\gamma$  gradually as long as the function finds a lower number of changepoints than a predefined maximum number of changepoints  $N_{c_{\max}} \in \mathbb{Z}_+$  which is a reasonably small number satisfying  $K - 1 \leq N_{c_{\max}}$ . Then, for a candidate number of blocks from a given vector, i.e.,  $K_{\text{cand}} \in [K_{\min}, \dots, K_{\max}]^\top \in \mathbb{Z}_+^{N_c}$ , the resulting number of changepoints  $N_c$  and corresponding locations  $\boldsymbol{\tau}$  in Eq. (9) are used to compute the candidate size vectors  $\mathbf{n}_r = [N_{r_1}, N_{r_2}, \dots, N_{r_{K_{\text{cand}}}}]^\top \in \mathbb{Z}_+^{K_{\text{cand}}}$ ,  $r = 1, \dots, \zeta$  that are designed by combination of all possible size vectors with  $\zeta = \binom{N_c}{K_{\text{cand}} - 1}$ . Lastly, the block-size matrix associated with a candidate number of blocks, i.e.,

$$\mathbf{N}^{(K_{\text{cand}})} = [\mathbf{n}_1, \mathbf{n}_2, \dots, \mathbf{n}_\zeta]^\top \in \mathbb{Z}_+^{\zeta \times K_{\text{cand}}}, \quad (10)$$

is formed.<sup>11</sup>

The computation of candidate block sizes illustrated in Fig. 13 for a candidate block number  $K_{\text{cand}} = 3$ . After estimating the changepoints using Eq. (9), a possible block size matrix, i.e.  $\mathbf{N}^{(K_{\text{cand}})} \in \mathbb{Z}_+^{\zeta \times K_{\text{cand}}}$ , with  $\zeta = 15$  is computed for all possible block size combinations.

In this step, the changepoint locations are determined based on a piece-wise linear fit of the vector  $\tilde{\mathbf{v}}$  using Eq. (9). This is a fundamental step to compute the candidate block sizes. However, the obtained information from Eq. (9) does not provide the target and undesired similarity coefficients which are needed to structure the affinity matrix in a block diagonal form. In other words, the estimated piece-wise linear fit is a combination of these similarity coefficients as it has been illustrated in Fig. 7b. Therefore, Step 2.2, i.e. estimating the target and undesired similarity coefficients individually is a necessary step to obtain information about all similarity coefficients. A more detailed explanation of similarity coefficients' estimation is provided in the following.

*b) Step 2.2: Estimating Matrix of Similarity Coefficients:*

*b.1) Step 2.2.1: Estimate Target Similarity Coefficients*

Suppose that  $N_{r_i}$  denotes the size of the  $i$ th linear segment from a candidate size vector  $\mathbf{n}_r$ , as defined in Eq. (10). Further, let  $\mathbf{v}^{(r)} \in \mathbb{R}^{(N-N_1)}$  denote the target vector  $\mathbf{v}$  associated with  $\mathbf{n}_r$  defined by

<sup>11</sup>In practice, the candidate size vectors including the block sizes that are smaller than a predefined minimum number of nodes in the blocks  $N_{\min}$  can be removed from  $\mathbf{N}^{(K_{\text{cand}})}$ .

$$v_m^{(r)} = \sum_{n=m}^{u_{r_i}} \ddot{l}_{m,n} \quad \text{s.t.} \quad \begin{aligned} \ell_{r_i} \leq m \leq u_{r_i} \\ i = 1, \dots, K_{\text{cand}} \end{aligned} \quad (11)$$

where the  $m$ th and  $(m, n)$ th components of  $\mathbf{v}^{(r)}$  and  $\ddot{\mathbf{L}}$  are denoted, respectively, by  $v_m^{(r)}$  and  $\ddot{l}_{m,n}$ ,  $\ell_{r_1} = 1$ ,  $u_{r_1} = N_{r_1}$ ,  $\ell_{r_i} = \sum_{k=1}^{i-1} N_{r_k} + 1$  and  $u_{r_i} = \sum_{k=1}^i N_{r_k}$  for  $i = 2, \dots, K_{\text{cand}}$ . After computing  $\mathbf{v}^{(r)}$  using Eq. (11), with Definition IV.1, we model it as a  $K$ -piece linear function of the target similarity coefficients. The model parameters are estimated in the FRS-BDR algorithm by applying the algorithm from [58] that determines a plane-based piece-wise linear fit. In more details, for every linear segment  $i = 1, \dots, K_{\text{cand}}$  associated with  $K_{\text{cand}}$ , the method first estimates the parameters of the linear fit. Then, it estimates the target similarity coefficients  $w_i, \dots, w_{K_{\text{cand}}}$  based on the slope of piece-wise linear fit estimates. A step-by-step detailed description of the plane-based piece-wise linear fit algorithm to determine  $\mathbf{v}^{(r)}$  is given in Section IX.A of the supplementary material.

### b.2) Step 2.2.2: Estimate Undesired Similarity Coefficients

In this step, the shifted vectors of  $\mathbf{v}^{(r)}$  are computed as follows

$$\ddot{\mathbf{v}}_{s_{i,j}}^{(r)} = \mathbf{v}_i^{(r)} + \ddot{\mathbf{v}}_{i,j}^{(r)}, \quad \begin{aligned} i = 2, \dots, K_{\text{cand}}, \\ j = 1, \dots, i-1 \end{aligned} \quad (12)$$

where  $\ddot{\mathbf{v}}_{i,j}^{(r)} \in \mathbb{R}^{N_{r_i}}$  denotes the vector of increase, associated with the undesired group similarity between block  $i$  and  $j$ , and  $\ddot{\mathbf{v}}_{s_{i,j}}^{(r)}$  is the associated shifted target vector.<sup>12</sup> Then, combining the results from Eq. (7), Eq. (11) and Eq. (12), the undesired similarity coefficients between different blocks can be estimated as

$$\hat{w}_{i,j}^{(r)} = \frac{\text{med}(\ddot{\mathbf{v}}_{s_{i,j}}^{(r)} - \hat{\mathbf{v}}_i^{(r)})}{N_{r_j}} \quad \begin{aligned} i = 2, \dots, K_{\text{cand}} \\ j = 1, \dots, i-1 \end{aligned} \quad (13)$$

where  $\text{med}(\cdot)$  denotes the median operator,  $N_{r_j}$  is defined in Eq. (10), and  $\hat{w}_{i,j}^{(r)}$  is the undesired similarity coefficient estimate between  $i$  and  $j$ .

**Remark 2.** Alternative to using the median operator as an estimator in Eq. (13), one could consider using the sample mean estimator based on the theory in Section III and IV. However, for the sample mean, a single outlying component has an unbounded effect on estimating undesired similarity coefficient, while the median operator provide robustness with the highest possible breakdown value of 50% (for a detailed discussion about robustness comparisons, see Section 1.3 in [29]). This property of the median provides robustness even in real-world cases where our theoretical assumptions are not fully fulfilled.

To clarify Steps 2.2.1 and 2.2.2, an example with  $K_{\text{cand}} = K$  illustrating the computation of vector  $\ddot{\mathbf{v}}$  and a matrix  $\mathbf{W}_{\text{sim}} \in \mathbb{R}^{K \times K}$  is shown in Fig 14. As can be seen, the target similarity coefficients, which are the diagonal elements of  $\mathbf{W}_{\text{sim}}$ , i.e.,  $\text{diag}(\mathbf{W}_{\text{sim}}) = [w_1, w_2, \dots, w_K]^T \in \mathbb{R}^K$ , represent an estimate of the slopes of the  $K_{\text{cand}} = K$  linear segments in  $\ddot{\mathbf{v}}$ . Further, off-diagonal elements of  $\mathbf{W}_{\text{sim}}$  represent undesired similarity coefficients between different blocks and are calculated by computing the undesired shifts that have been highlighted as shaded areas in Fig 14.

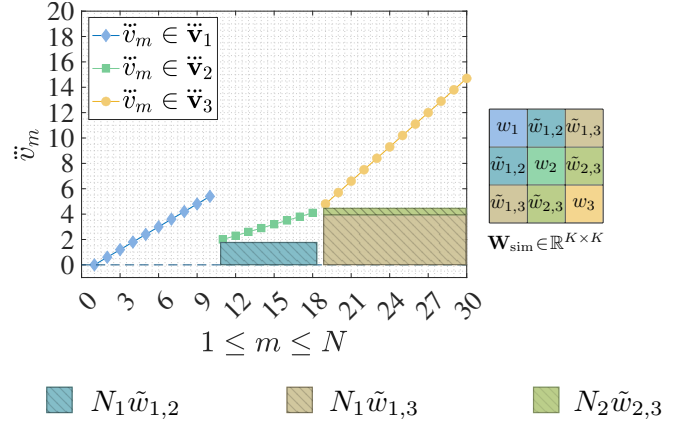


Fig. 14: Exemplary plot of  $\ddot{\mathbf{v}}$  and  $\mathbf{W}_{\text{sim}}$  with  $K_{\text{cand}} = K$ ,  $\mathbf{n} = [10, 8, 12]^T \in \mathbb{R}^K$ ,  $\text{diag}(\mathbf{W}_{\text{sim}}) = [0.6, 0.3, 0.9]^T \in \mathbb{R}^K$ ,  $\tilde{w}_{1,2} = 0.2$ ,  $\tilde{w}_{1,3} = 0.4$ , and  $\tilde{w}_{2,3} = 0.1$ .

### b.3) Step 2.3: Estimating vector $\ddot{\mathbf{v}}$ and $\mathbf{W}_{\text{sim}}$

From the computed estimates  $\hat{\mathbf{W}}_{\text{sim}}^{(r)} \in \mathbb{R}^{K_{\text{cand}} \times K_{\text{cand}}}$  and  $\hat{\mathbf{v}}^{(r)} \in \mathbb{R}^{(N-N_i)}$ , the vector  $\hat{\mathbf{v}}_i^{(r)}$  is computed by plugging in the associated intermediate estimates for all  $r=1, \dots, \zeta$  and  $K_{\text{cand}} = K_{\text{min}}, \dots, K_{\text{max}}$  into Eq. (7) and determining the final estimate as

$$\hat{\mathbf{v}} = \underset{\mathbf{n}_r \in \mathbf{N}^{(K_{\text{cand}})}}{\text{argmin}} \|\ddot{\mathbf{v}} - \hat{\mathbf{v}}^{(r)}\|_2 \quad (14)$$

where  $\forall \hat{w}_i^{(r)} \in \text{diag}(\hat{\mathbf{W}}_{\text{sim}}^{(r)})$ ,  $\hat{w}_i^{(r)} > \hat{w}_{i,j}^{(r)}$  holds for  $i = 1, \dots, K_{\text{cand}}$ ,  $j = 1, \dots, K_{\text{cand}}$  and  $i \neq j$ .

Since the target block diagonal model with internally dense externally disjoint clusters represents the optimum level of sparsity, the closeness of the estimate of  $\ddot{\mathbf{v}}$  to the target piece-wise linear function directly provides information of how well the algorithm was able to remove the undesired edges and therewith determine the sparsity level. In particular, the estimate of vector  $\ddot{\mathbf{v}}$  provides fundamental information about the number of blocks, the number of elements for every block, desired and undesired similarity coefficients associated with each block that have been collected in the matrix  $\mathbf{W}_{\text{sim}}$ . To design a BDR that provides a good balance with internally dense externally sparse clusters, the desired similarity coefficients, the proposed strategy preserves the similarity coefficients corresponding to the diagonal entries of  $\mathbf{W}_{\text{sim}}$  while removing that of undesired similarity coefficients corresponding to the off-diagonal entries of  $\mathbf{W}_{\text{sim}}$ .<sup>13</sup>

The proposed FRS-BDR is summarized in Algorithm 2. The codes are provided at: <https://github.com/A-Tastan/FRS-BDR>

### D. Computational Analysis of FRS-BDR

A comprehensive computational analysis is computed in Section X of the supplementary material by determining the number of fladd, flmlt, fldiv and flam. The Landau's big  $O$  symbol is used for the cases when the complexity is not specified as above operations. For a detailed information, see [59]-[60]. Our analysis showed that the complexity of FRS-BDR strongly depends on the initial structure of the affinity

<sup>12</sup>For details, see Section IX.B of the supplementary material.

<sup>13</sup>For examples that analyze the mismatch between the target and estimated BD structure, see Appendix E.2 of the accompanying material.

**Algorithm 2: FRS-BDR**


---

**Input:**  $\mathbf{X} \in \mathbb{R}^{M \times N}$ ,  $K_{\min}$ ,  $K_{\max}$ ,  $N_{c_{\max}}$ ,  $N_{\min}(\text{opt.})$   
 Compute  $\mathbf{W} \in \mathbb{R}^{N \times N}$  i.e.  $\mathbf{W} = \mathbf{X}^T \mathbf{X}$  for  $\forall \mathbf{x}_m \in \mathbf{X}$ ,  $\|\mathbf{x}_m\|=1$

**Step 1: Enhancing BD Structure**  
*Step 1.1: Type I Outlier Removal*  
 Compute  $\hat{\mathbf{W}}$ ,  $\hat{\mathbf{D}}$  and  $\hat{\mathbf{L}} \in \mathbb{R}^{(N-N_1) \times (N-N_1)}$  via Eq. (5)  
*Step 1.2: Similarity-based Block Diagonal Ordering*  
 Perform Algorithm 1 to achieve  $\hat{\mathbf{b}}^{(s)} \in \mathbb{Z}_+^{(N-N_1)}$   
 Obtain  $\hat{\mathbf{W}}$ ,  $\hat{\mathbf{D}}$  and  $\hat{\mathbf{L}} \in \mathbb{R}^{(N-N_1) \times (N-N_1)}$  using  $\hat{\mathbf{b}}^{(s)}$   
*Step 1.3 (opt.): Sparsity for Excessive Group Similarity*  
 Design  $\tilde{\mathbf{L}} \in \mathbb{R}^{(N-N_1) \times (N-N_1)}$  for the desired method, i.e. Algorithm 3 or 4 of the accompanying material.  
 Compute  $\tilde{\mathbf{v}} \in \mathbb{R}^{(N-N_1) \times 1}$  corresponding to  $\tilde{\mathbf{L}}$  using Eq. (4) (or alternatively  $\tilde{\mathbf{v}} \in \mathbb{R}^{(N-N_1) \times 1}$  corresponding to  $\hat{\mathbf{L}}$ )

**Step 2: Estimating Vector  $\mathbf{v}$**   
**for**  $K_{\text{cand}} = K_{\min}, \dots, K_{\max}$  **do**  
*Step 2.1: Computing Candidate Block Sizes*  
 Compute  $\mathbf{N}^{(K_{\text{cand}})} \in \mathbb{Z}_+^{K_{\text{cand}} \times K_{\text{cand}}}$  using Eqs. (9)-(10)  
*Step 2.2: Estimating  $\mathbf{W}_{\text{sim}}$*   
**for**  $\mathbf{n}_r = \mathbf{n}_1, \dots, \mathbf{n}_\zeta$  **do**  
*Step 2.2.1: Estimating Target Similarity Coefficients*  
 Compute  $\mathbf{v}^{(r)} \in \mathbb{R}^{(N-N_1)}$  using Eq. (11)  
**for**  $i = 1, \dots, K_{\text{cand}}$  **do**  
   Calculate  $\Sigma_i^{(r)} \in \mathbb{R}^{2 \times 2}$  and  $\mu_i^{(r)} \in \mathbb{R}^2$  for  $\Upsilon_i^{(r)}$   
   Find  $\hat{\mathbf{v}}_i^{(r)} \in \mathbb{R}^2$  and  $\hat{\mathbf{b}}_i^{(r)} \in \mathbb{R}$   
   Find  $\hat{\mathbf{v}}_i^{(r)} \in \mathbb{R}^{N_r}$  and compute  $\hat{w}_i$   
**end**  
 Form  $\text{diag}(\hat{\mathbf{W}}_{\text{sim}}^{(r)}) = [\hat{w}_1^{(r)}, \hat{w}_2^{(r)}, \dots, \hat{w}_{K_{\text{cand}}}^{(r)}]^T \in \mathbb{R}^{K_{\text{cand}}}$   
 and  $\hat{\mathbf{v}}^{(r)} = [(\hat{\mathbf{v}}_1^{(r)})^T, (\hat{\mathbf{v}}_2^{(r)})^T, \dots, (\hat{\mathbf{v}}_{K_{\text{cand}}}^{(r)})^T]^T \in \mathbb{R}^{(N-N_1)}$   
*Step 2.2.2: Estimating Undesired Similarity Coefficients*  
**for**  $i = 2, \dots, K_{\text{cand}}$  **do**  
   **for**  $j = 1, \dots, i - 1$  **do**  
     Compute  $\tilde{\mathbf{v}}_{s_{i,j}}^{(r)} \in \mathbb{R}^{(N-N_1)}$  using Eqs. (12)  
     Compute  $\hat{w}_{i,j}^{(r)}$  using Eq. (13) and stack  $\hat{\mathbf{W}}_{\text{sim}}^{(r)}$   
   **end**  
**end**  
 Estimate  $\tilde{\mathbf{v}}^{(r)}$  using Eq. (7)  
 Update  $\hat{\mathbf{v}}$  based on Eq. (14)  
**end**  
**end**  
**Output:**  $\hat{\mathbf{v}}$ ,  $\hat{\mathbf{W}}_{\text{sim}}$ ,  $\hat{\mathbf{n}}$

---

matrix and the number of blocks  $K$ . In addition to the numeric analysis, the complexity is analyzed experimentally in the following sections.

## VI. EXPERIMENTAL RESULTS

This section benchmarks the proposed FRS-BDR method in a broad range of real data experiments, including cluster enumeration and handwritten digit, object and face clustering. *Data Sets:* The performance is analyzed using the well-known data sets for handwritten digit clustering [32], [61], for object clustering [62], for face clustering [63]-[65] and for cluster enumeration [66]-[70]. The detailed information about the data sets is given in the following sections.

*Baselines:* For the task of subspace clustering, FRS-BDR is benchmarked against seven state-of-the-art BDR approaches [6]-[10], two low-rank representation methods [17]-[18], a sparse representation method (SSC) [21], a robust principal component analysis method (FRPCAG) [71], a robust spectral clustering method (RSC) [72] and the initial affinity matrix

that is defined by  $\mathbf{W} = \mathbf{X}^T \mathbf{X}$ . For cluster enumeration<sup>14</sup>, the method is benchmarked against seven popular community detection methods, i.e. [73]-[78] and our previously proposed method that is called SPARCODE in [24].

*Parameter Setting:* In all experiments, the parameters are optimally tuned for the competitor approaches, while FRS-BDR is computed with the default parameters that are detailed in Section XI of the supplementary material.

*Evaluation Metrics:* The computation time ( $t$ ) and average clustering accuracy ( $\bar{c}_{\text{acc}}$ ) are used for the subspace clustering performance analysis. In cluster enumeration, the empirical probability of detection ( $p_{\text{det}}$ ), modularity ( $\text{mod}$ ) and conductance ( $\text{cond}$ ) are used in addition to  $t$ . The evaluation metrics are comprehensively explained in Section XI of the supplementary material.

### A. Handwritten Digit Clustering

The effectiveness of FRS-BDR in handwritten digit clustering is shown based on the following popular real-world data sets: *MNIST Data Set:* The data base includes 60,000 training and 10,000 test images corresponding to 10 digits. For a varying number of subjects  $K = \{2, 3, 5, 8, 10\}$ , the data matrix  $\mathbf{X}$  is generated using 100 randomly selected images from the test set for every subject where the images are used as feature vectors and normalized. As in [7],  $\mathbf{X}$  of size  $784 \times 100K$  is produced for the images of size  $28 \times 28$ .

*USPS Data Set:* 7291 training and 2007 test images of size  $16 \times 16$  are contained in the data set. The data matrix  $\mathbf{X}$  is computed by following the same procedure, except for using 50 randomly selected images from the test set for every subject. As a result, for the images of size  $16 \times 16$ , the data matrix  $\mathbf{X}$  of size  $256 \times 50K$  corresponding to a number of subjects  $K = \{2, 3, 5, 8, 10\}$ , is obtained.

In contrast to object and face applications that we will detail in the following sections, the data matrix  $\mathbf{X}$  of high dimensional feature vectors is directly used in initial affinity matrix design. The initial affinity matrix, i.e.  $\mathbf{W} = \mathbf{X}^T \mathbf{X}$  is used as an input to BDR approaches [6]-[10], low-rank representation methods [17]-[18] and the sparse representation method in [21] to design affinity matrices in a desired form. Then, spectral clustering<sup>15</sup> is applied to the resulting affinity matrices of different methods. Different from affinity matrix construction methods, FRPCAG [71] and RSC [72] algorithms use the data matrix  $\mathbf{X}$  as an input. These methods determine the affinity matrices based on their default construction where the number of neighbors is defined by gradually decreasing the number of all neighbors until the methods do not fail.

An example of digit clustering results is shown in Fig. 15 for the MNIST data base. A broad set of analyses including MNIST and USPS data bases is provided in Appendix F.4.1 of the accompanying material. Even though the performance of SSC [21], BDSSC [6], BDLRR [6], BDR-B [7], BDR-Z [7], IBDLR [8], LSR [10], LRR [17], RKLRR [18], FRPCAG [71] and RSC [72] is reported for an optimal tuning of the

<sup>14</sup>For the numerical cluster enumeration results, see Appendix F.4.4.2 of the accompanying material.

<sup>15</sup>For the details about spectral clustering, see Section XI of the supplementary material.

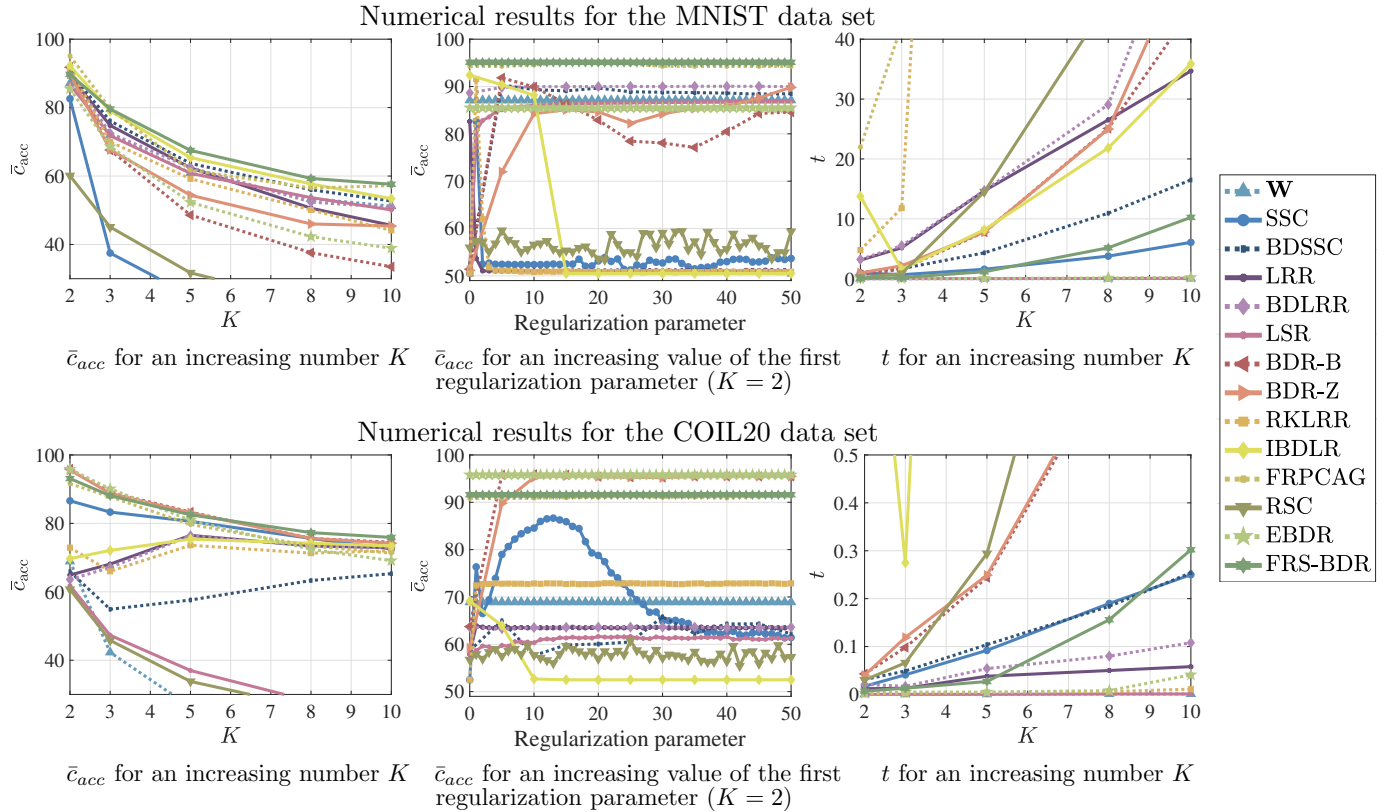


Fig. 15: Numerical results for the COIL20 and MNIST data sets. The regularization parameters of the competing methods are tuned for optimal performance in all settings while the proposed method determines the parameters using Algorithms 1 and 2. In the regularization parameter performance analysis, for all competing methods that use two parameters, the second one is tuned optimally while varying the first parameter.

parameters, which is not feasible in practice, the FRS-BDR achieves the highest clustering accuracy results in almost all cases. Further, the regularization parameter effect analysis in Fig. 15 shows that BDR-B and BDR-Z performances are sensitive to the choice of the first regularization parameter, even when tuning the second one optimally. Based on the computation time analysis, the main drawback of competitor approaches is that they are sensitive to the dimension of the feature space whereas FRS-BDR is an efficient algorithm for the data sets including high dimensional feature vectors.

To quantify the performance of different BDR approaches in terms of the sparsity, an additional set of experiments analyzing modularity (mod) and conductance (cond) scores, which are the commonly used quality metrics for this analysis, are introduced in Appendix F.4 of the accompanying material. The numerical analysis demonstrates that the proposed FRS-BDR algorithm provides a “good balance” in sparsity with large-valued modularity scores and small-valued conductance scores in most of the cases.<sup>16</sup> The analysis confirms the results of the clustering accuracy performance analysis that FRS-BDR algorithm shows a good performance compared to the optimally tuned BDR approaches while providing

<sup>16</sup>The modularity and conductance performance of the proposed FRS-BDR algorithm could be further improved by enforcing the estimated blocks to be distinct but such a step may result in a performance degradation in clustering accuracy which is more important in these clustering applications.

considerably better performance than optimally tuned low-rank representation methods. Different from structuring all clusters based on a single determined sparsity parameter (which may be difficult to tune in practice), our approach allows for treating every block differently, depending on the occurrence of the outliers’ effect within each block and this makes the proposed FRS-BDR method advantageous in terms of balancing the sparsity.

### B. Object Clustering

This section introduces a set of experiments that are performed on the COIL20 [62] data base of 20 objects. In COIL20, each object has 72 images where the images are taken by rotating the object on a turntable in five degree intervals. In our experiments, the processed COIL20 data set in [79] containing images of size  $32 \times 32$  pixels is used. Then, the data set  $\mathbf{X}$  of size  $1024 \times 400$  is generated by selecting 20 images randomly for every object. The feature space is reduced to 10 based on the PCA performance, which is provided in Appendix F.4.2.1 of the accompanying material.

As in [7], a performance analysis of every application is conducted for an increasing value of  $K$ , i.e.,  $K = \{2, 3, 5, 8, 10\}$  using 100 randomly selected subject combinations. To obtain the affinity matrices for the competing methods, the regularization parameters are manually tuned on a grid of 50 values. Finally, spectral clustering [47] is

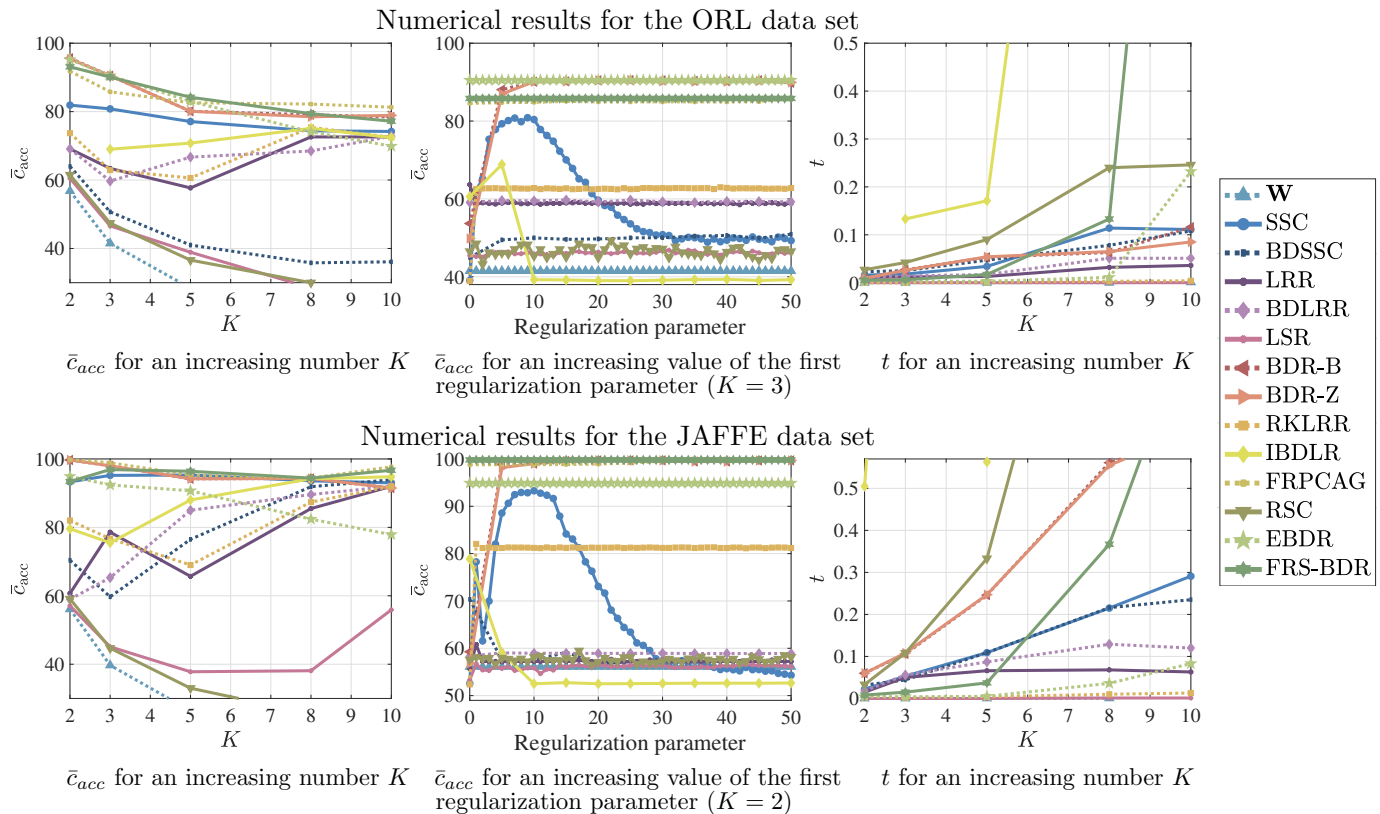


Fig. 16: Numerical results for the ORL and JAFFE data sets. The regularization parameters of the competing methods are tuned for optimal performance in all settings while the proposed method determines the parameters using Algorithms 1 and 2. In the regularization parameter performance analysis, for all competing methods that use two parameters, the second one is tuned optimally while varying the first parameter.

applied and the results in Fig. 15, for an increasing value of  $K$ , are obtained analogously to [7] (see Appendix F.4.2 of the accompanying material for further details). The average clustering accuracy  $\bar{c}_{acc}$  results show that FRS-BDR performs best while EBDR is an efficient method for small values of  $K$ . In terms of  $t$ , the main competitors BDR-B and BDR-Z show poor performance whereas FRS-BDR performs relatively good even for large values of  $K$ . This computational advantage of the proposed method can be explained with its simple nature, i.e. finding a piece-wise linear function robustly, which is easy to solve in comparison to analyzing the graph structure in a matrix space as in the existing BDR methods.

The BDR-B and BDR-Z methods show poor performance for small-valued regularization parameters even though the second regularization parameter is optimally tuned. An important point is that these approaches reach their best results lately in comparison to experiments on face clustering data sets that are explained in the following section.

### C. Face Clustering

In this section, the subspace clustering performances of different methods are benchmarked in terms of their  $\bar{c}_{acc}$  and  $t$  by using the following application details:

**ORL Data Set:** The data set includes 10 images of 40 different subjects that are taken at different times by varying the

lighting, facial expressions and details. As in [8], we resize all images to  $32 \times 32$  to obtain a data matrix  $\mathbf{X}$  of size  $1024 \times 400$  using normalized features. The feature space dimension is reduced to nine using Principal Component Analysis (PCA) in order to reduce the computation time<sup>17</sup>.

**JAFFE Data Set:** The JAFFE data set comprises 213 images of seven facial expressions from 10 Japanese female models. As in [8], the images are resized to  $64 \times 64$  pixels and the data set  $\mathbf{X}$  of size  $4096 \times 213$  is computed using resized images as normalized feature vectors before applying PCA to reduce the dimensionality to 14 features<sup>18</sup>.

**Yale Data Set:** 165 grayscale images of 15 different individuals. For every subject, the data set contains 11 images that capture different facial expressions. The data matrix  $\mathbf{X}$  of size  $1024 \times 165$  is constructed as in the ORL Data Set<sup>19</sup>.

After determining the number of PCA features, the same procedure as in object clustering is performed and the performance is reported for a different number of subjects  $K = \{2, 3, 5, 8, 10\}$  in Fig. 16. For a detailed performance analysis, see Appendix F.4.3 of the accompanying material.

<sup>17</sup>For the PCA analysis of the ORL data set, see Appendix F.4.3.1 of the accompanying material.

<sup>18</sup>For the PCA analysis of the JAFFE data set, see Appendix F.4.3.2 of the accompanying material.

<sup>19</sup>For the PCA analysis of the Yale data set, see Appendix F.4.3.3 of the accompanying material

Data Set	Subspace Clustering Performances for Different Block Diagonal Representation Methods													
	Minimum-Maximum Clustering Accuracy ( $c_{\text{accmin}} - c_{\text{accmax}}$ ) for Different Regularization Parameters													
	W	SSC	BD-SSC	LRR	BD-LRR	LSR	BDR-B	BDR-Z	RKLRR	IBDLR	FRPCAG	RSC	EBDR	FRS-BDR
Breast Cancer [66],	88.2	51.0-74.7	50.3-88.2	54.3-90.3	88.0-90.0	73.5-88.2	62.4-90.0	52.9-90.2	62.6-91.7	60.3-90.0	60.5-88.2	50.1-58.5	85.2	90.1
Ceramic [56],	98.9	51.1-98.9	51.1-100	95.5-98.9	95.5-98.9	54.5-98.9	51.1-100	51.1-98.9	51.1-95.5	51.1-98.9	50.0-100	50.0-69.3	98.9	98.9
Vertebral Column [67],	73.2	50.0-77.7	50.3-74.8	53.9-72.6	72.6-72.6	62.6-75.8	67.4-76.8	71.9-76.8	67.4-71.3	67.4-76.1	51.0-75.8	50.0-69.7	74.8	75.8
Iris [54],	78.0	34.7-82.7	34.0-83.3	38.7-80.7	80.0-98.0	78.0-82.7	34.0-96.7	65.3-96.7	34.0-80.0	34.7-84.0	34.0-89.3	35.3-50.0	98.0	96.7
Human Gait [68],	77.3	20.3-77.4	20.1-77.5	26.1-83.9	78.9-83.5	55.4-75.9	20.3-84.8	26.4-84.5	20.5-85.5	20.4-81.6	50.8-77.8	22.1-26.0	81.1	77.1
Ovarian Cancer [69],	61.7	51.4-73.6	50.9-71.3	52.3-76.4	54.2-76.4	51.9-66.2	53.7-75.9	51.9-74.1	55.6-88.4	55.6-75.5	77.8-89.3	50.0-69.4	77.8	77.3
Person Identification [55],	x	33.7-96.8	31.6-95.7	49.7-94.7	71.1-94.7	33.2-64.2	31.6-96.3	59.4-95.7	34.2-94.1	33.7-95.7	29.4-92.5	28.9-41.2	97.3	96.8
Parkinson [70],	61.3	50.4-58.8	50.0-61.3	50.4-54.2	50.4-61.3	57.9-61.3	50.4-61.3	50.0-61.3	50.4-61.7	50.4-61.3	50.0-67.5	50.4-72.1	56.7	58.2
Average	76.9	42.8-80.1	42.3-81.5	52.6-81.4	73.8-84.4	58.4-76.6	46.4-85.2	53.6-84.8	47.0-83.5	46.7-82.9	50.4-85.1	42.1-57.0	83.7	83.9

TABLE I: Subspace clustering performance of different block diagonal representation approaches on well-known clustering data sets.  $\mathbf{W}$  represents the subspace clustering results that are obtained by using the initial affinity matrix  $\mathbf{W} = \mathbf{X}^T \mathbf{X}$  as an input to spectral clustering algorithm. The remaining columns show affinity matrix construction methods that are using  $\mathbf{W}$  as input and performing spectral clustering on the sparse affinity matrix estimates. The performances are summarized in terms of  $\bar{c}_{\text{acc}}$  for parameter-free approaches including  $\mathbf{W}$ , EBDR and FRS-BDR while the remaining methods are shown for  $c_{\text{accmin}} - c_{\text{accmax}}$ . ‘x’ denotes the failed results due to the complex-valued eigenvectors.

The average clustering accuracy  $\bar{c}_{\text{acc}}$  and computation time  $t$  for the ORL and the JAFFE data sets are provided in Fig. 16. Consistent with the previous experiments, FRS-BDR shows the best clustering accuracy performance among all approaches in almost all cases. In terms of  $t$ , FRS-BDR shows a reasonably good performance until the number of subjects reaches  $K = 8$ . A reduction for a large value of  $K$  can be obtained by adjusting  $N_{c_{\text{max}}}$ . Extensive further numerical experiments are reported in Appendices E.5.3.1, E.5.3.2, and E.5.3.3. of the accompanying material.

#### D. Subspace Clustering on Well-Known Clustering Data Sets

This section investigates the subspace clustering performance of different approaches in terms of their average clustering accuracy using the following popular clustering data sets: Breast Cancer Wisconsin (Breast Cancer) [66], Chemical Composition of Ceramic (Ceramic) [56], Vertebral Column [67], Fisher’s iris (Iris) [54], Radar-based Human Gait (Human Gait) [68], Ovarian Cancer [69], Person Identification [55] and Parkinson [70]. To analyze subspace clustering performances on popular clustering data sets, subspace clustering is first performed on the initial affinity matrix that is defined by  $\mathbf{W} = \mathbf{X}^T \mathbf{X}$ . Analogous to the handwritten digit clustering application in Section VI-A, the data matrix is used as an input to the FRPCAG [71] and RSC [72] methods while state-of-the-art BDR methods use the initial affinity matrix that is defined by  $\mathbf{W} = \mathbf{X}^T \mathbf{X}$  as an input to design BD structured affinity matrices. Then, spectral clustering as detailed in Section XI of the supplementary material is performed on the BD affinity matrix estimates. For the FRPCAG [71] and RSC [72] methods, spectral clustering is performed based their eigenvector estimates. As in previous experiments, the competitor approaches’ results are shown for optimally tuned parameters while the proposed FRS-BDR is performed with the default parameters.

The clustering accuracy performances of different block-diagonal representation approaches are detailed in terms of their average clustering accuracy in Table I. As can be seen from Table I, FRS-BDR provides a similar performance as the maximum clustering accuracy of its strongest competitors (BDR-B, BDR-Z, BD-LRR) while it outperforms all other block diagonal representation approaches. The method is

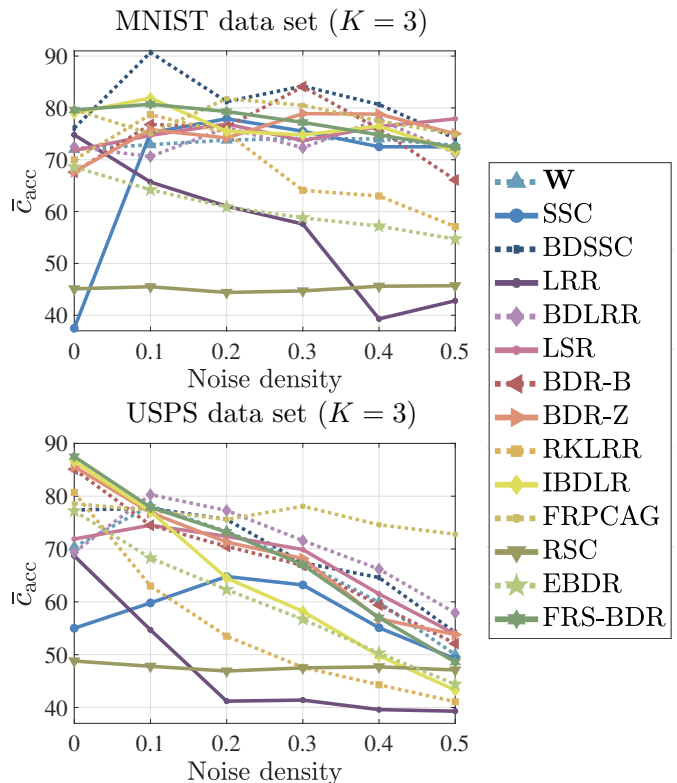


Fig. 17: Robustness analysis results for the MNIST and USPS data sets. The regularization parameters of the competing methods are tuned for optimal performance in all settings while the proposed method determines the parameters using Algorithms 1 and 2.  $\bar{c}_{\text{acc}}$  performances are shown for increasing density value of the salt and pepper noise.

also computationally efficient in comparison to most of the competitors based on the additional experiments that are given in Appendix F.4.4 of the accompanying material.

#### E. Robustness Analysis

A further analysis evaluating robustness of the proposed FRS-BDR method in noisy scenarios with corruptions in data/feature space, is reported in this section. To analyze robustness, against outliers, digit samples from MNIST [32]

and USPS [61] data sets are corrupted with salt and pepper noise and Poisson noise. Object and face recognition data sets are not included to robustness analysis due to the performance degradation of the (non-robust) PCA that is part of the feature generation.

The robustness analysis results of different methods are shown in Fig. 17 for the MNIST and USPS data sets that are corrupted with salt and pepper noise for an increasing percentage of outlier contamination. As in previously analyzed scenarios, the proposed FRS-BDR shows relatively good performance compared to the optimally tuned approaches for both data sets. This is because the proposed method leverages the derived theory on how an ideal block diagonal structure is disturbed by outliers and this allows to precisely remove the effects of Type I and Type II outliers as well as the group similarity. Many block diagonal affinity matrix construction methods that we compare against are not robust against outliers and it is well-known that performance of non-robust methods can severely be degraded in presence of outliers [29].

## VII. CONCLUSION

A robust method to recover a block diagonal affinity matrix in challenging scenarios has been presented. The proposed Fast and Robust Sparsity-Aware Block Diagonal Representation (FRS-BDR) method jointly estimates cluster memberships and the number of blocks. It builds upon our presented theoretical results that describe the effect of different fundamental outlier types in cluster analysis, allowing a reformulation of the problem as a robust piece-wise linear fitting problem. Comprehensive experiments, including a variety of real-world applications demonstrate the effectiveness of FRS-BDR compared to optimally tuned benchmark methods in terms of clustering accuracy, computation time and cluster enumeration performance. Since all codes are made available, the FRS-BDR method can also easily be benchmarked on other larger-scale data sets, e.g. [80]-[82].

## ACKNOWLEDGMENTS

The work of A. Taştan is supported by the Republic of Turkey Ministry of National Education. The work of M. Muma has been funded by the LOEWE initiative (Hesse, Germany) within the emergenCITY centre and is supported by the ERC Starting Grant ScReeningData (Project Number: 101042407).

## REFERENCES

- [1] Z. Kong and X. Yang, "Color image and multispectral image denoising using block diagonal representation," *IEEE Trans. Image Process.*, vol. 28, pp. 4247-4259, 2019.
- [2] Y. Dar, A. M. Bruckstein, M. Elad and R. Giryes, "Postprocessing of compressed images via sequential denoising," *IEEE Trans. Image Process.*, vol. 25, pp. 3044-3058, 2016.
- [3] Z. Zhang, Y. Xu, L. Shao and J. Yang, "Discriminative block diagonal representation learning for image recognition," *IEEE Trans. Neural Networks Learn. Syst.*, vol. 29, pp. 3111-3125, 2017.
- [4] C. -G. Li, Z. Lin, H. Zhang and J. Guo, "Learning semi-supervised representation towards a unified optimization framework for semi-supervised learning," in *Proc. IEEE Conf. Comp. Vision*, pp. 2767-2775, 2015.
- [5] Y. Qin, H. Wu, X. Zhang and G. Feng, "Semi-Supervised Structured Subspace Learning for Multi-View Clustering," *IEEE Trans. Image Process.*, vol. 31, pp. 1-14, 2021.
- [6] J. Feng, Z. Lin, H. Xu and S. Yan, "Robust subspace segmentation with block diagonal prior," in *Proc. IEEE Conf. Comp. Vision Pattern Recognit.*, pp. 3818-3825, 2014.
- [7] C. Lu, J. Feng, Z. Lin, T. Mei and S. Yan, "Subspace clustering by block diagonal representation," *IEEE Trans. Pattern Anal. Mach. Intell.*, vol. 41, pp. 487-501, 2018.
- [8] X. Xie, X. Guo, G. Liu and J. Wang, "Implicit block diagonal low-rank representation," *IEEE Trans. Image Process.*, vol. 27, pp. 477-489, 2017.
- [9] A. Taştan, M. Muma and A. M. Zoubir, "Eigenvalue-Based Block Diagonal Representation and Application to  $p$ -Nearest Neighbor Graphs," in *Proc. 30th European Signal Process. Conf.*, pp. 1761-1765, 2022.
- [10] C. -Y. Lu, H. Min, Z. -Q. Zhao, L. Zhu, D. -S. Huang and S. Yan, "Robust and efficient subspace segmentation via least squares regression," in *Proc. Eur. Conf. Comp. Vision*, pp. 347-360, 2012.
- [11] M. Liu, Y. Wang, J. Sun and Z. Ji, "Structured block diagonal representation for subspace clustering," *Appl. Intell.*, vol. 50, pp. 2523-2536, 2020.
- [12] F. Wu, Y. Hu, J. Gao, Y. Sun and Yin. B, "Ordered subspace clustering with block diagonal priors," *IEEE Trans. Cybern.*, vol. 46, pp. 3209-3219, 2015.
- [13] X. Zhang, F. Sun, G. Liu and Y. Ma, "Fast low-rank subspace segmentation," *IEEE Trans. Knowl. Data Eng.*, vol. 26, pp. 1293-1297, 2013.
- [14] X. Zhu, S. Zhang, Y. Li, J. Zhang, L. Yang and Y. Fang, "Low-rank sparse subspace for spectral clustering," *IEEE Trans. Knowl. Data Eng.*, vol. 31, pp. 1532-1543, 2018.
- [15] Y. Ding, S. Pan and Y. Chong, "Robust spatial-spectral block diagonal structure representation with fuzzy class probability for hyperspectral image classification," *IEEE Trans. Geosci. Remote Sens.*, vol. 58, pp. 1747-1762, 2019.
- [16] C. Xing, M. Wang, Z. Wang, C. Duan and Y. Liu, "Diagonalized Low-Rank Learning for Hyperspectral Image Classification," *IEEE Trans. Geosci. Remote Sens.*, vol. 60, pp. 1-12, 2021.
- [17] G. Liu, Z. Lin, S. Yan, J. Sun, Y. Yu and Y. Ma, "Robust recovery of subspace structures by low-rank representation," *IEEE Trans. Pattern Anal. Mach. Intell.*, vol. 35, pp. 171-184, 2012.
- [18] S. Xiao, M. Tan, D. Xu and Z.Y. Dong, "Robust kernel low-rank representation," *IEEE Trans. Neural Networks Learn. Syst.*, vol. 27, pp. 2268-2281, 2015.
- [19] G. Liu and S. Yan, "Latent low-rank representation for subspace segmentation and feature extraction," in *Proc. Int. Conf. Comp. Vision*, pp. 1615-1622, 2011.
- [20] G. Liu, Z. Lin and Y. Yu, "Robust subspace segmentation by low-rank representation," *Icml.*, vol. 1, pp. 8, 2010.
- [21] E. Elhamifar and R. Vidal, "Sparse subspace clustering: Algorithm, theory, and applications," *IEEE Trans. Pattern Anal. Mach. Intell.*, vol. 35, pp. 2765-2781, 2013.
- [22] L. Fan, G. Lu, Y. Wang and T. Liu, "Block Diagonal Sparse Subspace Clustering," in *Proc. 13th Int. Conf. Wireless Commun. Signal Process. (WCSP)*, pp. 1-6, 2021.
- [23] J. Wang, K. Zhang, P. Wang, K. Madani and C. Sabourin, "Unsupervised band selection using block diagonal sparsity for hyperspectral image classification," *IEEE Trans. Geosci. Remote Sens. Lett.*, vol. 14, pp. 2062-2066, 2017.
- [24] A. Taştan, M. Muma and A. M. Zoubir, "Sparsity-aware Robust Community Detection," *Signal Process.*, vol. 187, pp. 108147, 2021.
- [25] B. Nasihatkon and R. Hartley, "Graph connectivity in sparse subspace clustering," in *Proc. CVPR 2011*, pp. 2137-2144, 2011.
- [26] S. Arora, S. Rao and U. Vazirani, "Expander flows, geometric embeddings and graph partitioning" *J. ACM*, vol. 56, pp. 1-37, 2009.
- [27] N. García-Pedrajas, J. A. R. Del Castillo and G. Cerruela-García, "A proposal for local  $k$  values for  $k$ -nearest neighbor rule," *IEEE Trans. Neural Networks Learn. Syst.*, vol. 28, pp. 470-475, 2015.
- [28] S. S. Mullick, S. Datta and S. Das, "Adaptive learning-based  $k$ -nearest neighbor classifiers with resilience to class imbalance," *IEEE Trans. Neural Networks Learn. Syst.*, vol. 29, pp. 5713-5725, 2018.
- [29] A. M. Zoubir, V. Koivunen, E. Ollila and M. Muma, *Robust statistics for signal processing*, Cambridge, 2018.
- [30] P. J. Rousseeuw and A. M. Leroy, *Robust regression and outlier detection*, John Wiley & Sons, 2005.
- [31] A. Taştan, M. Muma and A. M. Zoubir, "Robust Regularized Locality Preserving Indexing for Fiedler Vector Estimation," *IEEE Trans. Knowl. Data Eng. (submitted)*, 2021.
- [32] T. Hastie and P. Y. Simard, "Metrics and models for handwritten character recognition," *Stat. Sci.*, pp. 54-65, 1998.
- [33] S. Arora, S. Rao and U. Vazirani, "Geometry, flows, and graph-partitioning algorithms," *Commun. ACM*, vol. 51, pp. 96-105, 2008.

- [34] D. Cai, X. He and J. Han, "Document clustering using locality preserving indexing" *IEEE Trans. Knowl. Data Eng.*, vol. 17, pp. 1624-1637, 2005.
- [35] D. Cai, X. He, W. V. Zhang and J. Han, "Regularized locality preserving indexing via spectral regression," in *Proc. 16th ACM Conf. Inf. Knowl. Manage.*, pp. 741-750, 2007.
- [36] J. Lu and Y. -P. Tan, "Regularized locality preserving projections and its extensions for face recognition," *IEEE Trans. Syst. Man Cybern. Part B Cybern.*, vol. 40, pp. 958-963, 2009.
- [37] M. Artac, M. Jogan and A. Leonardis, "Incremental PCA for on-line visual learning and recognition," in *Proc. Intl. Conf. Pattern Recognit.*, vol. 3, pp. 781-784, 2002.
- [38] A. Y. Ng, M. I. Jordan and Y. Weiss, "On spectral clustering: Analysis and an algorithm," *Adv. Process. Neural Inf. Syst.*, vol. 14, pp. 849-856, 2001.
- [39] D. Cai and X. Chen, "Large scale spectral clustering with landmark-based sparse representation," *IEEE Trans. Cybern.*, vol. 45, pp. 1669-1680, 2014.
- [40] A. Taştan, M. Muma and A. M. Zoubir, "Robust Spectral Clustering: A Locality Preserving Feature Mapping Based on M-estimation," in *Proc. 29th European Signal Process. Conf.*, 2021.
- [41] M. Belkin and P. Niyogi, "Laplacian eigenmaps and spectral techniques for embedding and clustering," in *Proc. Conf. Adv. Neural Inf. Process. Syst.*, vol. 14, 2001.
- [42] M. Belkin and P. Niyogi, "Laplacian eigenmaps for dimensionality reduction and data representation," *Neural Comput.*, vol. 15, pp. 1373-1396, 2003.
- [43] Z. Li, F. Nie, X. Chang, L. Nie, H. Zhang and Y. Yang, "Rank-constrained spectral clustering with flexible embedding," *IEEE Trans. Neural Networks Learn. Syst.*, vol. 29, pp. 6073-6082, 2018.
- [44] X. Li, W. Hu, C. Shen, A. Dick and Z. Zhang, "Context-aware hypergraph construction for robust spectral clustering," *IEEE Trans. Knowl. Data Eng.*, vol. 26, pp. 2588-2597, 2013.
- [45] D. Matula and F. Shahrokhi, "Sparsest cuts and bottlenecks in graphs," *Discrete Appl. Math.*, vol. 27, pp. 113-123, 1990.
- [46] R. Andersen and Y. Peres, "Finding sparse cuts locally using evolving sets," in *Proc. 41st Annu. Symp. Theory Comput.*, pp. 235-244, 2009.
- [47] U. Von Luxburg, "A tutorial on spectral clustering," *Stat. Comput.*, vol. 17, pp. 395-416, 2007.
- [48] A. Taştan, M. Muma, E. Ollila and A. M. Zoubir, "Sparsity-Aware Block Diagonal Representation for Subspace Clustering," in *Proc. 31th European Signal Process. Conf. (accepted)*, 2023.
- [49] K. Avrachenkov, L. Cottatellucci and A. Kadavankandy, "Spectral properties of random matrices for stochastic block model," in *Proc. 13th Int. Symp. Model. Optim. Mobile, Ad Hoc, Wireless Networks (WiOpt)*, pp. 537-544, 2015.
- [50] J. Miettinen, S. Vorobyov and E. Ollila, "Modelling and studying the effect of graph errors in graph signal processing," *Signal Process.*, vol. 189, p. 108256, 2021.
- [51] M. Tang, "The eigenvalues of stochastic blockmodel graphs," 2018. [Online]. Available: <https://arxiv.org/abs/1803.11551>
- [52] A. Athreya, J. Cape and M. Tang, "Eigenvalues of stochastic Blockmodel graphs and random graphs with low-rank edge probability matrices," *Sankhya A.*, vol. 46, pp. 1-28, 2021.
- [53] E. Cuthill, and J. McKee, "Reducing the bandwidth of sparse symmetric matrices," in *Proc. 24th Nat. Conf.*, 1969.
- [54] R. A. Fisher, "The use of multiple measurements in taxonomic problems," *Ann. Eugenics*, vol. 7, pp. 179-188, 1936.
- [55] F. K. Teklehaymanot, A. -K. Seifert, M. Muma, M. G. Amin and A. M. Zoubir, "Bayesian target enumeration and labeling using radar data of human gait," in *Proc. 26th European Signal Process. Conf. (EUSIPCO)*, pp. 1342-1346, 2018.
- [56] Z. He, M. Zhang and H. Zhang, "Data-driven research on chemical features of Jingdezhen and Longquan celadon by energy dispersive X-ray fluorescence," in *Ceramics Int.*, vol. 42, pp. 5123-5129, 2016.
- [57] R. Killick, P. Fearnhead and I. A. Eckley, "Optimal detection of changepoints with a linear computational cost," *J. Am. Stat. Assoc.*, vol. 107, pp. 1590-1598, 2012.
- [58] X. Yang, H. Yang, F. Zhang, L. Zhang, X. Fan, Q. Ye and L. Fu, "Piecewise linear regression based on plane clustering," *IEEE Access*, vol. 7, pp. 29845-29855, 2019.
- [59] G. W. Stewart, *Matrix Algorithms: Volume I Basic Decompositions*, Society for Industrial and Applied Mathematics, 1998.
- [60] G. W. Stewart, *Matrix Algorithms: Volume II Eigensystems*, Society for Industrial and Applied Mathematics, 2001.
- [61] J. J. Hull, "A database for handwritten text recognition research," *IEEE Trans. Pattern Anal. Mach. Intell.*, vol. 16, pp. 550-554, 1994.
- [62] S. A. Nene, S. K. Nayar and H. Murase, "Columbia object image library (coil-20)," 1995.
- [63] F. S. Samaria and A. C. Harter, "Parameterisation of a stochastic model for human face identification," in *Proc. IEEE Int. Workshop Appl. Comput. Vision*, pp. 138-142, 1994.
- [64] M. Lyons, S. Akamatsu, M. Kamachi and J. Gyoba, "Coding facial expressions with gabor wavelets," in *Proc. 3rd IEEE Int. Conf. Autom. Face Gesture Recognit.*, pp. 200-205, 1998.
- [65] P. N. Belhumeur, J. P. Hespanha and D. J. Kriegman, "Eigenfaces vs. fisherfaces: Recognition using class specific linear projection," *IEEE Trans. Pattern Anal. Mach. Intell.*, vol. 19, pp. 711-720, 1997.
- [66] W. H. Wolberg and O. L. Mangasarian, "Multisurface method of pattern separation applied to breast cytology diagnosis," in *Proc. Natl. Acad. Sci.*, vol. 87, pp. 9193-9196, 1989.
- [67] A. R. Rocha Neto, R. Sousa, G. A. Barreto and J. S. Cardoso, "Diagnostic of pathology on the vertebral column with embedded reject option," in *Proc. Iberian Conf. Pattern Recognit. Image Anal.*, pp. 588-595, 2011.
- [68] A. -K. Seifert, M. Amin and A. M. Zoubir, "Toward unobtrusive in-home gait analysis based on radar micro-Doppler signatures," *IEEE Trans. Biomed. Eng.*, vol. 66, pp. 1-11, 2019.
- [69] T. P. Conrads, V. A. Fusaro, S. Ross, D. Johann, V. Rajapakse, B. A. Hitt, S. M. Steinberg, E. C. Kohn, D. A. Fishman, G. Whitely, J. C. Barrett, L. A. Liotta, E. F. Petricoin and T. D. Veenstra, "High-resolution serum proteomic features for ovarian cancer detection," *Endocrine-related Cancer*, vol. 11, pp. 163-178, 2004.
- [70] L. Naranjo, C. J. Perez, Y. Campos-Roca and J. Martin, "Addressing voice recording replications for Parkinson's disease detection," *Expert Syst. Appl.*, vol. 46, pp. 286-292, 2016.
- [71] N. Shahid, N. Perraudin, V. Kalofolias, G. Puy and P. Vanderghyest, "Fast robust PCA on graphs," *IEEE J. Sel. Top. Signal Process.*, vol. 10, pp. 740-756, 2016.
- [72] A. Bojchevski, Y. Matkovic and S. Günnemann, "Robust spectral clustering for noisy data: Modeling sparse corruptions improves latent embeddings," in *Proc. 23rd ACM SIGKDD Int. Conf. Knowl. Discovery and Data Min.*, pp. 737-746, 2017.
- [73] V. D. Blondel, J. L. Guillaume, R. Lambiotte and E. Lefebvre, "Fast unfolding of communities in large networks," *J. Stat. Mech: Theory Exp.*, vol. 10, pp. P10008, 2008.
- [74] E. L. Martelot and C. Hankin, "Multi-scale community detection using stability as optimization criterion in a greedy algorithm," in *Proc. Int. Conf. Knowl. Discovery and Inf. Retrieval*, pp. 208-217, 2011.
- [75] I. Psorakis, S. Roberts, M. Ebden and B. Sheldon, "Overlapping community detection using Bayesian non-negative matrix factorization," *Phys. Rev. E*, vol. 83, p. 066114, 2011.
- [76] X. Bai, P. Yang and X. Shi, "An overlapping community detection algorithm based on density peaks," *Neurocomput.*, vol. 226, pp. 7-15, 2017.
- [77] S. Sobolevsky, R. Campari, A. Belyi and C. Ratti, "General optimization technique for high-quality community detection in complex networks," *Phys. Rev. E*, vol. 90, pp. 012811, 2014.
- [78] L. Bohlin, D. Edler, A. Lancichinetti, and M. Rosvall, "Community detection and visualization of networks with the map equation framework," *Measuring Scholarly Impact*, pp. 3-34, 2014.
- [79] D. Cai, X. He, J. Han and T. S. Huang, "Graph regularized nonnegative matrix factorization for data representation," *IEEE Trans. Pattern Anal. Mach. Intell.*, vol. 33, pp. 1548-1560, 2010.
- [80] L. Fei-Fei, R. Fergus and P. Perona, "One-shot learning of object categories," *IEEE Trans. Pattern Anal. Mach. Intell.*, vol. 28, pp. 594-611, 2006.
- [81] H. Xiao, K. Rasul and R. Vollgraf, "Fashion-mnist: a novel image dataset for benchmarking machine learning algorithms," 2017. [Online]. Available: <https://arxiv.org/abs/1708.07747>
- [82] Y. Netzer, T. Wang, A. Coates, A. Bissacco, B. Wu and A. Y. Ng, "Reading digits in natural images with unsupervised feature learning," in *NIPS Workshop Deep Learn. Unsupervised Feature Learn.*, 2011.



# Supplementary Information: Fast and Robust Sparsity-Aware Block Diagonal Representation

Aylin Taştan\*, Michael Muma†, and Abdelhak M. Zoubir‡

## STRUCTURE

The Supplementary Information for the paper Fast and Robust Sparsity-Aware Block Diagonal Representation (FRS-BDR) is organized as follows: In Section VIII exemplary solution paths are shown for eigenvalue and simplified Laplacian matrix analysis, respectively. Section IX comprises the additional information for FRS-BDR algorithm. A step-by-step analysis of computational complexity is presented in Section X. Finally, the details about experimental setting are introduced in Section XI.

A comprehensive supplementary file is given separately. The file is named by “Accompanying Material: Fast and Robust Sparsity-Aware Block Diagonal Representation” and it is organized as follows:

*Appendix A: The Generalized Eigen-decomposition based Eigenvalue Analysis*

The theorems (and corresponding corollaries) by reference to outlier effects on eigenvalues are proved based on the generalized eigen-decomposition and they are visually exemplified.

*Appendix B: The Standard Eigen-decomposition based Eigenvalue Analysis*

It includes analysis of outlier effects on eigenvalues theorems (and corresponding corollaries) based on the standard eigen-decomposition and their visual examples.

*Appendix C: Simplified Laplacian Matrix Analysis and Outlier Effects*

The proofs associated with simplified Laplacian matrix analysis and outlier effects are presented with visual illustrations in Appendix C.

*Appendix D: The Generalized Matrix Determinant Lemma*

The appendix explains the generalization of matrix determinant lemma.

*Appendix E: Real-world Data Examples*

The real-world data examples that are analyzing the model mismatch are introduced.

*Appendix F: Additional Information for FRS-BDR*

It contains a step by step detailed visual summary of FRS-BDR, an analysis for sparse Laplacian matrix design,

\*The author was with the Signal Processing Group, Technische Universität Darmstadt, Darmstadt, Germany and is now with the Pattern Recognition Group, University of Bern, Bern, Switzerland (e-mail: a.tastan@spg.tu-darmstadt.de; aylin.tastan@unibe.ch).

†The author is with the Robust Data Science Group, Technische Universität Darmstadt, Darmstadt, Germany (e-mail: michael.muma@tu-darmstadt.de).

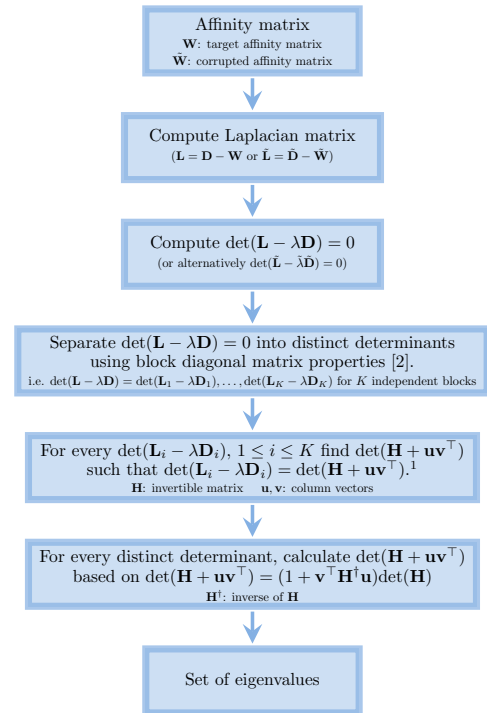
‡The author is with the Signal Processing Group, Technische Universität Darmstadt, Darmstadt, Germany (e-mail: zoubir@spg.tu-darmstadt.de).

additional algorithms for sparse Laplacian matrix design, and additional experimental results for all applications, respectively.

## VIII. EXAMPLARY SOLUTION PATHS

### A. Eigenvalue Analysis and Outlier Effects

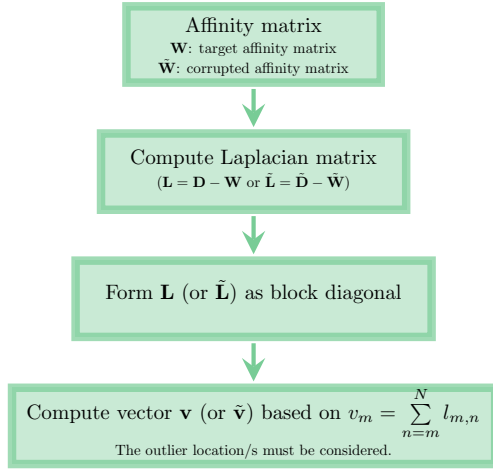
This section provides a high-level description of the solution path for the eigenvalue analysis and outlier effects detailed in Theorem 1 and 2 in Section III of the paper Fast and Robust Sparsity-Aware Block Diagonal Representation (FRS-BDR). The below diagram shows the steps involved from the input, which is an affinity matrix subject to outliers or group similarity, to the output, which is the set of eigenvalues. The detailed solutions are given in Appendix A of the accompanying material in accompanying material.



### B. Simplified Laplacian Matrix Analysis and Outlier Effects

This section provides a high-level description of the solution path to obtain vector  $\mathbf{v}$  for the Theorems 3-4 and Corollary 4.1 in Section IV of the paper Fast and Robust Sparsity-Aware Block Diagonal Representation. The detailed solutions are given in Appendix C of the accompanying material in accompanying material.

<sup>1</sup>If the matrix  $\det(\mathbf{L}_i - \lambda \mathbf{D}_i)$  can not be represented in terms of  $\mathbf{H}$ ,  $\mathbf{u}$  and  $\mathbf{v}$ , the generalized matrix determinant lemma can be used. For a detailed information, see Appendix D in accompanying material.



## IX. FRS-BDR ALGORITHM DETAILS

### A. Plane-based Piece-wise Linear Fit of $\mathbf{v}^{(r)}$

Assuming that  $\Upsilon_i^{(r)} = [\mathbf{v}_{i_1}^{(r)}, \mathbf{v}_{i_2}^{(r)}, \dots, \mathbf{v}_{i_{N_{r_i}}}^{(r)}]^\top \in \mathbb{R}^{N_{r_i} \times 2}$  denotes a sample matrix associated with the  $i$ th linear segment such that  $\mathbf{v}_{i_m}^{(r)} = [m, v_m^{(r)}]^\top \in \mathbb{R}^2$ ,  $m = 1, \dots, N_{r_i}$ , our goal is to approximate  $\mathbf{v}^{(r)} \in \mathbb{R}^{(N-N_i)}$ , using a piece-wise linear function that is determined by estimating  $K_{\text{cand}}$  planes, i.e.

$$\hat{\mathcal{P}}_i^{(r)} = \{\mathbf{v}_{i_m}^{(r)} | \mathbf{v}_{i_m}^{(r)} \in \mathbb{R}^2, (\hat{\boldsymbol{\theta}}_i^{(r)})^\top \mathbf{v}_{i_m}^{(r)} + \hat{b}_i^{(r)} = 0\}, \quad (1)$$

where  $\hat{\boldsymbol{\theta}}_i^{(r)} \in \mathbb{R}^2$  and  $\hat{b}_i^{(r)} \in \mathbb{R}$  denote, respectively, the normal vector and the bias associated with the estimated  $i$ th plane  $\hat{\mathcal{P}}_i^{(r)}$  for  $i = 1, \dots, K_{\text{cand}}$ . The estimation can be performed by solving the  $K_{\text{cand}}$  individual ordinary eigenvalue problems as in [2]

$$\boldsymbol{\Sigma}_i^{(r)} \hat{\boldsymbol{\theta}}_i^{(r)} = \Lambda_i^{(r)} \hat{\boldsymbol{\theta}}_i^{(r)} \quad i = 1, \dots, K_{\text{cand}} \quad (2)$$

and

$$\hat{b}_i^{(r)} = -(\hat{\boldsymbol{\theta}}_i^{(r)})^\top \boldsymbol{\mu}_i^{(r)} \quad i = 1, \dots, K_{\text{cand}}, \quad (3)$$

where  $\Lambda_i^{(r)} \in \mathbb{R}$  is the smallest eigenvalue associated with the  $i$ th plane, and  $\boldsymbol{\Sigma}_i^{(r)} \in \mathbb{R}^{2 \times 2}$  and  $\boldsymbol{\mu}_i^{(r)} \in \mathbb{R}^2$  are, respectively, the covariance and the mean matrices of  $\mathbf{v}_i^{(r)}$ . Then, using the estimated parameters of the  $K_{\text{cand}}$  planes, each segment in the vector  $\mathbf{v}^{(r)}$  is estimated as follows

$$(\hat{\boldsymbol{\theta}}_i^{(r)})^\top \begin{bmatrix} m \\ \hat{v}_{i_m}^{(r)} \end{bmatrix} + \hat{b}_i^{(r)} = 0, \quad i = 1, \dots, K_{\text{cand}}, \quad m = 1, \dots, N_{r_i}, \quad (4)$$

where  $\hat{v}_{i_m}^{(r)}$  denotes the  $m$ th estimated point correspond to the  $i$ th segment. Based on this linear function, the target similarity coefficients  $\text{diag}(\mathbf{W}_{\text{sim}}^{(r)})$  can be computed as

$$\hat{w}_i^{(r)} = -\frac{\hat{v}_{i_1}^{(r)}}{\hat{v}_{i_2}^{(r)}}, \quad i = 1, \dots, K_{\text{cand}} \quad (5)$$

where  $\hat{v}_{i_1}^{(r)}$  and  $\hat{v}_{i_2}^{(r)}$  are denote, respectively, the first and the second elements in  $\hat{\boldsymbol{\theta}}_i^{(r)}$ , and  $\hat{w}_i^{(r)}$  is the target similarity coefficient estimate associated with  $i$ th block.

### B. Computing vector of increases $\ddot{\mathbf{v}}_{u_{ij}}^{(r)}$

The vector of increase  $\ddot{\mathbf{v}}_{i,j}^{(r)} \in \mathbb{R}^{N_{r_i}}$  associated with group similarity between block  $i$  and  $j$ , is computed as follows

$$\ddot{\mathbf{v}}_{i,j}^{(r)} = \left[ \sum_{n=\ell_{r_j}}^{u_{r_j}} \ddot{l}_{\ell_{r_i},n}, \dots, - \sum_{n=\ell_{r_j}}^{u_{r_j}} \ddot{l}_{u_{r_i},n} \right]. \quad (6)$$

## X. COMPUTATIONAL COMPLEXITY ANALYSIS

Due to its essential role in graph analysis, the computational complexity of the proposed FRS-BDR method is analyzed in terms of its main operations. The computational analysis is detailed using the following terms [3], [4]:

fladd: an operation that consists of a floating-point addition

flmlt: an operation that consists of a floating-point multiplication

fldiv: an operation that consists of a floating-point division

flam: a compound operation that consists of one addition and one multiplication

Additionally, the Landau's big  $O$  symbol is used when the complexity is not specified as above terms. In the sequel, the computational complexity of the proposed approach is detailed for the fundamental steps.

### A. Initial Graph Construction

As in [5], the pairwise cosine similarity which takes  $\frac{1}{2}N^2M + 2NM$  flam can be used for constructing an initial graph  $G$ .

### B. Step 1: Enhancing BD Structure

1) *Step 1.1 (optional): Type I Outlier Removal:* Since removing unconnected vertices associated with Type I outliers results in negligibly smaller cost in comparison to remaining estimation steps, the complexity of preprocessing is ignored in the complexity analysis.

2) *Step 1.2: sBDO Algorithm:* In this step, the complexity of sBDO algorithm is detailed for two main operations as follows.

To determine the starting nodes, the overall edge weights must be sorted which is of complexity  $O(N \log N)$  and there are computationally efficient alternatives such as [6] for which the complexity is reduced to  $O(N \sqrt{\log N})$ .

The second main operation is adding the most similar node to the vector of previously estimated nodes. For a vector of previously estimated nodes  $\hat{\mathbf{b}}^{(s)} \in \mathbb{Z}_+^{s-1}$  at the  $s$ th stage, the method sums up the similarity coefficients that takes  $s-2$  additions for every neighbor. For  $N_{\text{neigh}}^{(s)}$  number of neighbors, it follows that

$$\sum_{s=2}^N (s-2) N_{\text{neigh}}^{(s)}$$

fladd. Even though the complexity is directly linked to number of neighbors, it can be explicitly calculated if every node is connected to remaining  $N-1$  number of nodes, i.e.

$$\sum_{s=2}^N (s-2)(N-s+1)$$

fladd. In addition to similarity computation, the method sorts vector of neighbor similarities to find the most similar node. This sorting operation results in minimum  $O(N_{\text{neigh}}^{(s)} \sqrt{\log N_{\text{neigh}}^{(s)}})$  complexity at every stage  $s = 2, \dots, N$ .

3) *Step 1.3 (optional): Increase Sparsity for Excessive Group Similarity:* This step evaluates computational complexity of sparse Laplacian matrix design for the two exemplary algorithms which have been provided in Appendix E.3 accompanying material.

**Sparse Laplacian Matrix Design based on Adaptive Thresholding:** As eigen-decomposition and sorting operations are computationally demanding in comparison to thresholding operation, the complexity is detailed in terms of these two main processes. The proposed sparse Laplacian matrix design computes eigenvalues for each iteration in which e.g. MATLAB uses a Krylov Schur decomposition [7]. The decomposition is built upon two main phases that are known as expansion and contraction. The computational cost of decomposition mainly depends on these phases when  $N$  is larger than  $N_{\text{Lan}}$ , where  $N_{\text{Lan}}$  denotes the number of Lanczos basis vectors (preferably chosen as  $N_{\text{Lan}} \geq 2N_{\text{eig}}$  for  $N_{\text{eig}}$  eigenvectors). In more details, the expansion phase requires between  $N(N_{\text{Lan}}^2 - N_{\text{eig}}^2)$  flam and  $2N(N_{\text{Lan}}^2 - N_{\text{eig}}^2)$  flam while the contraction phase requires  $NN_{\text{Lan}}N_{\text{eig}}$  flam [4]. To find the second smallest eigenvalues, the computed eigenvalues must be sorted which is of complexity  $O(N\sqrt{\log N})$  in [6]. When  $N_{\text{Lan}} \rightarrow N$ , the cost of eigen-decomposition dominates the sorting operation. Thus, sparse Laplacian matrix design using adaptive thresholding with respect to flam yields minimally

$$N_{\text{iter}}(N(N_{\text{Lan}}^2 - N_{\text{eig}}^2) + NN_{\text{Lan}}N_{\text{eig}}),$$

where  $N_{\text{iter}}$  denotes the number of performed iterations to achieve a sparse Laplacian matrix.

**Sparse Laplacian Matrix Design based on  $p$ -Nearest Neighbor Graph:** In contrast to adaptive thresholding-based graph construction, computing a  $p$ -nearest neighbor graph results in considerable cost. In addition to eigen-decomposition and sorting operations, the algorithm finds  $p$ -nearest neighbors which is of complexity  $N^2 \log N$  flam [5] in each iteration. Therefore, the overall computational cost of sparse Laplacian matrix design using  $p$ -nearest graph is written in terms of flam as follows

$$N_{\text{piter}}(N(N_{\text{Lan}}^2 - N_{\text{eig}}^2) + NN_{\text{Lan}}N_{\text{eig}} + N^2 \log N).$$

### C. Step 2: Estimating Vector $\mathbf{v}$

1) *Step 2.1: Computing Candidate Block Sizes:* The estimation of candidate block size matrix can mainly be attributed to changepoint detection which is a widely researched topic in the literature and there are variety of different alternatives for changepoint detection, e.g. binary segmentation (BS) or optimal partitioning (OP) approaches. In [8], the computational cost of BS and OP

are indicated as  $O(N \log N)$  and  $O(N^2)$ , respectively. Then, a computationally efficient the pruned exact linear time (PELT) method has been provided. The complexity of the PELT method is  $O(N)$  (under certain conditions) which can be reach  $O(N^2)$  in the worst-case [8].

### 2) Step 2.2: Estimating Matrix of Similarity Coefficients:

#### Step 2.2.1: Estimating Target Similarity Coefficients

Since the eigen-decomposition of  $2 \times 2$  matrix does not require a considerable time, the computational complexity of plane-based piece wise linear fitting algorithm in [2] mainly depends on covariance matrix and the mean vector estimation.

First, let consider the covariance matrix computation. For two random vectors, the covariance function includes  $N$  executions where each execution includes two addition and one multiplication. Therefore, it can be said that calculation of covariance for two random vectors requires  $2N\text{fladd} + N\text{flmlt} + 1\text{fldiv}$ . As vector  $\mathbf{v}$  fitting generates covariance matrix of dimension  $2 \times 2$ , our covariance matrix computation necessitates  $6N\text{fladd} + 3N\text{flmlt} + 3\text{fldiv}$ .

After computing covariance matrix, the mean operator including  $N - 1$  additions and a division is executed two times for two vectors. Thus, mean vector computation mainly requires  $2(N - 1)$  fladd + 2 fldiv and total piece-wise linear fitting complexity results in  $8N - 2$  fladd +  $3N$  flmlt + 5 fldiv.

#### Step 2.2.2: Estimating Undesired Similarity Coefficients

The undesired similarity coefficients' estimation consists of two consecutive steps. For every candidate size vector  $\mathbf{n}_r = [N_{r_1}, N_{r_2}, \dots, N_{r_{K_{\text{cand}}}}] \in \mathbb{Z}_+^{K_{\text{cand}}}$  the proposed method first computes shifted vector whose complexity principally depends on vector of increase computation. To compute a vector of increase associated with group similarity between block  $i$  and  $j$ , the method executes  $N_{r_i}$  times where each execution includes  $N_{r_j} - 1$  addition. This means that the vector of increase associated with group similarity between block  $i$  and  $j$  results in  $N_{r_i}(N_{r_j} - 1)$  fladd. Further, the algorithm finds median of computed vector which is of dimension  $N_{r_i} \times 1$ . To compute the median, the vector can be sorted in  $O(N_{r_i} \sqrt{\log N_{r_i}})$  complexity using [6]. When size of the  $j$ th block  $N_{r_j}$  is sufficiently large valued, the vector of increase computation dominates median operation. Therefore, computing an undesired similarity coefficient corresponds to group similarity between block  $i$  and  $j$  takes minimally  $N_{r_i}(N_{r_j} - 1)$  fladd and that can be written for  $i = 2, \dots, K_{\text{cand}}$  and  $j = 1, \dots, i - 1$  as follows

$$\sum_{i=2}^{K_{\text{cand}}} \sum_{j=1}^{i-1} N_{r_i}(N_{r_j} - 1) \text{ fladd}.$$

To summarize, estimating the similarity coefficients matrix  $\hat{\mathbf{W}}_{\text{sim}}^{(r)}$  and the vector  $\hat{\mathbf{v}}^{(r)} \in \mathbb{R}^N$  associated with a candidate block size vector  $\mathbf{n}_r \in \mathbb{Z}_+^{K_{\text{cand}}}$  requires minimally

$$K_{\text{cand}}(8N - 2 \text{ fladd} + 3N \text{ flmlt} + 5 \text{ fldiv}) \\ + \sum_{i=2}^{K_{\text{cand}}} \sum_{j=1}^{i-1} N_{r_i}(N_{r_j} - 1) \text{ fladd}.$$

To compute all possible  $\hat{\mathbf{W}}_{\text{sim}}^{(r)} \in \mathbb{R}^{K_{\text{cand}} \times K_{\text{cand}}}$  and  $\hat{\mathbf{v}}^{(r)} \in \mathbb{R}^N$  correspond to  $\mathbf{N}^{(K_{\text{cand}})} = [\mathbf{n}_1, \mathbf{n}_2, \dots, \mathbf{n}_\zeta]^\top \in \mathbb{Z}_+^{\zeta \times K_{\text{cand}}}$  for  $K_{\text{cand}} = K_{\text{min}}, \dots, K_{\text{max}}$ , the proposed method requires

$$\zeta \left( K_{\text{cand}}(8N - 2 \text{ fladd} + 3N \text{ flmlt} + 5 \text{ fldiv}) \right. \\ \left. + \sum_{i=2}^{K_{\text{cand}}} \sum_{j=1}^{i-1} N_{r_i}(N_{r_j} - 1) \text{ fladd} \right).$$

When the number of candidate block size vectors increases, the complexity of these numerous operations is significantly larger than changepoint detection using PELT method. Thus, its computational cost can be ignored in vector  $\mathbf{v}$  estimation.

## XI. EXPERIMENTAL SETTING

### A. Parameter Definition

#### 1) FRS-BDR for Unknown Number of Blocks:

Eigen-decomposition function: the generalized eigen-decomposition

Minimum number of blocks ( $K_{\text{min}}$ ): 2

Maximum number of blocks ( $K_{\text{max}}$ ):  $2 \times K$

Minimum number of nodes in the blocks ( $N_{\text{min}}$ ):  $\frac{N}{K_{\text{max}}}$

Maximum number of changepoints ( $N_{\text{cmax}}$ ):  $2 \times (K_{\text{max}} - 1)$

Sparse Laplacian matrix design algorithm:  $p$ -nearest graph (For details, see Algorithm 4 in accompanying material.)

#### 2) FRS-BDR for Known Number of Blocks:

Eigen-decomposition function : the generalized eigen-decomposition

Minimum number of nodes in the blocks ( $N_{\text{min}}$ ):  $\frac{N}{2 \times K}$

Maximum number of changepoints  $N_{\text{cmax}}$ :  $2 \times (K - 1)$

Sparse Laplacian matrix design algorithm :  $p$ -nearest graph (For details, see Algorithm 4 in accompanying material.)

#### 3) Spectral Clustering:

Laplacian matrix :  $\mathbf{L} = \mathbf{D} - \mathbf{W}$

Partitioning method :  $K$ -means

Eigen-decomposition function : the generalized eigen-decomposition

### B. Evaluation Metrics

In the following, the different clustering performance evaluation metrics are detailed.

► Average clustering accuracy ( $\bar{c}_{\text{acc}}$ ) is measured by

$$\bar{c}_{\text{acc}} = \frac{1}{NN_E} \sum_{m=1}^{N_E} \sum_{n=1}^N \mathbb{1}_{\{\hat{c}_n = c_n\}},$$

where

$$\mathbb{1}_{\{\hat{c}_n = c_n\}} = \begin{cases} 1, & \text{if } \hat{c}_n = c_n \\ 0, & \text{otherwise} \end{cases},$$

$N$  is the number of observations,  $N_E$  is the total number of experiments,  $c_n$  and  $\hat{c}_n$  are the estimated and ground truth labels for the  $n$ th observation, respectively.

► The empirical probability of detection  $p_{\text{det}}$  is used to analyze cluster enumeration performance as follows

$$p_{\text{det}} = \frac{1}{N_E} \sum_{m=1}^{N_E} \mathbb{1}_{\{\hat{K}=K\}},$$

where  $\hat{K}$  denotes the number of clusters estimate and  $\mathbb{1}_{\{\hat{K}=K\}}$  is the indicator function.

► Modularity (mod) is a metric that evaluates the quality of partition. The modularity score tends to one if a vertex has more edges within the assigned community. As in [9] and [10], mod is calculated by

$$\text{mod} = \frac{1}{2g} \sum_{m,n}^N \left[ w_{m,n} - \frac{d_m d_n}{2g} \right] \delta(c_m, c_n)$$

Here,  $d_m = \sum_{n=1}^N w_{m,n}$  is the overall edge weight attached to vertex  $m$ ,  $g = \frac{1}{2} \sum_{m,n} w_{m,n}$  and the function  $\delta(c_m, c_n)$  equals one if  $c_m = c_n$  and is zero otherwise.

► Conductance (cond) evaluates quality of partition in terms of the fraction of edges that points outside the community. Therefore, a small-valued conductance score means good partitioning performance and it can be calculated as [11]

$$\text{cond} = \frac{\sum_{m,n}^N w_{m,n} \mathbb{1}_{\{c_m \neq c_n\}}}{\sum_{m,n}^N w_{m,n}},$$

where  $w_{m,n}$  denotes the weight of the edge between the  $m$ th and the  $n$ th feature vector of  $\mathbf{X}$ , the function  $\mathbb{1}_{\{c_m \neq c_n\}}$  equals one if  $c_m \neq c_n$  and is zero otherwise.

## REFERENCES

- [1] J. R. Silvester, "Determinants of block matrices", *Math. Gazz.*, vol 84, pp. 460-467, 2000.
- [2] X. Yang, H. Yang, F. Zhang, L. Zhang, X. Fan, Q. Ye and L. Fu, "Piecewise linear regression based on plane clustering," *IEEE Access*, vol. 7, pp. 29845-29855, 2019.
- [3] G. W. Stewart, *Matrix Algorithms: Volume I Basic Decompositions*, Society for Industrial and Applied Mathematics, 1998.
- [4] G. W. Stewart, *Matrix Algorithms: Volume II Eigensystems*, Society for Industrial and Applied Mathematics, 2001.
- [5] D. Cai, X. He, W. V. Zhang and J. Han, "Regularized locality preserving indexing via spectral regression," in *Proc. 16th ACM Conf. Inf. Knowl. Manage.*, pp. 741-750, 2007.
- [6] Y. Han, "Sorting Real Numbers in  $O(n\sqrt{\log n})$  Time and Linear Space", *Algorithmica*, vol. 82, pp. 966-978, 2020.
- [7] G. W. Stewart, "A Krylov-Schur algorithm for large eigenproblems", *SIAM Journal on Matrix Analysis and Applications*, vol. 23, pp. 601-614, 2002.
- [8] R. Killick, P. Fearnhead and I. A. Eckley, "Optimal detection of changepoints with a linear computational cost," *J. Am. Stat. Assoc.*, vol. 107, pp. 1590-1598, 2012.
- [9] M. Girvan and M. E. J. Newman, "Community structure in social and biological networks," in *Proc. Natl. Acad. Sci.*, vol. 99, pp. 7821-7826, 2002.
- [10] M. E. J. Newman, "Modularity and community structure in networks," in *Proc. Natl. Acad. Sci.*, vol. 103, pp. 8577-8582, 2006.
- [11] J. J. Yang and J. Leskovec, "Defining and evaluating network communities based on groundtruth," *Knowl. Inf. Syst.*, vol. 42, pp. 181-213, 2015.

# Accompanying Material: Fast and Robust Sparsity-Aware Block Diagonal Representation

Aylin Taştan\*, Michael Muma†, and Abdelhak M. Zoubir‡

## STRUCTURE

The Accompanying Material for the paper Fast and Robust Sparsity-Aware Block Diagonal Representation (FRS-BDR) is organized as follows: In Appendix A and B, the theorems by reference to outlier effects on eigenvalues are proved based on the generalized and the standard eigen-decompositions, respectively. The theoretical analysis of the outlier effects on vector  $\mathbf{v}$  is the subject of Appendix C. Appendix D contains the auxiliary information that is used to analyse the effects of outliers on the eigenvalues and in Appendix E real-world data examples analyzing deviations from the theoretical analysis are given. Lastly, additional information on FRS-BDR, including visual summary, sparse Laplacian matrix analysis, algorithms and detailed experimental results, is provided.

## APPENDIX A: THE GENERALIZED EIGEN-DECOMPOSITION BASED EIGENVALUE ANALYSIS

### A.1 Outlier Effects on Target Eigenvalues: Proof of Theorem 1

Let  $\tilde{\mathbf{W}} \in \mathbb{R}^{(N+1) \times (N+1)}$  and  $\tilde{\mathbf{L}} \in \mathbb{R}^{(N+1) \times (N+1)}$ , respectively, denote a block zero-diagonal symmetric affinity matrix and associated Laplacian matrix for  $K$  blocks with an additional Type II outlier that is correlated with all blocks, i.e.,

$$\tilde{\mathbf{W}} = \begin{bmatrix} 0 & \tilde{w}_{\text{II},1} & \tilde{w}_{\text{II},1} & \dots & \tilde{w}_{\text{II},1} & \tilde{w}_{\text{II},2} & \tilde{w}_{\text{II},2} & \dots & \tilde{w}_{\text{II},2} & \dots & \tilde{w}_{\text{II},K} & \tilde{w}_{\text{II},K} & \dots & \tilde{w}_{\text{II},K} \\ \tilde{w}_{\text{II},1} & 0 & w_1 & \dots & w_1 & & & & & & & & & & \\ \tilde{w}_{\text{II},1} & w_1 & 0 & \dots & w_1 & & & & & & & & & & \\ \vdots & \vdots & \vdots & \ddots & \vdots & & & & & & & & & & \\ \tilde{w}_{\text{II},1} & w_1 & w_1 & \dots & 0 & & & & & & & & & & \\ \tilde{w}_{\text{II},2} & & & & & 0 & w_2 & \dots & w_2 & & & & & & \\ \tilde{w}_{\text{II},2} & & & & & w_2 & 0 & \dots & w_2 & & & & & & \\ \vdots & & & & & \vdots & \vdots & \ddots & \vdots & & & & & & \\ \tilde{w}_{\text{II},2} & & & & & w_2 & w_2 & \dots & 0 & & & & & & \\ \vdots & & & & & & & & & \ddots & & & & & \\ \tilde{w}_{\text{II},K} & & & & & & & & & & 0 & w_K & \dots & w_K & \\ \tilde{w}_{\text{II},K} & & & & & & & & & & w_K & 0 & \dots & w_K & \\ \vdots & & & & & & & & & & \vdots & \vdots & \ddots & \vdots & \\ \tilde{w}_{\text{II},K} & & & & & & & & & & \dots & w_K & w_K & \dots & 0 \end{bmatrix}$$

and

$$\tilde{\mathbf{L}} = \begin{bmatrix} \tilde{d}_{\text{II}} & -\tilde{w}_{\text{II},1} & -\tilde{w}_{\text{II},1} & \dots & -\tilde{w}_{\text{II},1} & -\tilde{w}_{\text{II},2} & -\tilde{w}_{\text{II},2} & \dots & -\tilde{w}_{\text{II},2} & \dots & -\tilde{w}_{\text{II},K} & -\tilde{w}_{\text{II},K} & \dots & -\tilde{w}_{\text{II},K} \\ -\tilde{w}_{\text{II},1} & \tilde{d}_1 & -w_1 & \dots & -w_1 & & & & & & & & & & \\ -\tilde{w}_{\text{II},1} & -w_1 & \tilde{d}_1 & \dots & -w_1 & & & & & & & & & & \\ \vdots & \vdots & \vdots & \ddots & \vdots & & & & & & & & & & \\ -\tilde{w}_{\text{II},1} & -w_1 & -w_1 & \dots & \tilde{d}_1 & & & & & & & & & & \\ -\tilde{w}_{\text{II},2} & & & & & \tilde{d}_2 & -w_2 & \dots & -w_2 & & & & & & \\ -\tilde{w}_{\text{II},2} & & & & & -w_2 & \tilde{d}_2 & \dots & -w_2 & & & & & & \\ \vdots & & & & & \vdots & \vdots & \ddots & \vdots & & & & & & \\ -\tilde{w}_{\text{II},2} & & & & & -w_2 & -w_2 & \dots & \tilde{d}_2 & & & & & & \\ \vdots & & & & & & & & & \ddots & & & & & \\ -\tilde{w}_{\text{II},K} & & & & & & & & & & \tilde{d}_K & -w_K & \dots & -w_K & \\ -\tilde{w}_{\text{II},K} & & & & & & & & & & -w_K & \tilde{d}_K & \dots & -w_K & \\ \vdots & & & & & & & & & & \vdots & \vdots & \ddots & \vdots & \\ -\tilde{w}_{\text{II},K} & & & & & & & & & & \dots & -w_K & -w_K & \dots & \tilde{d}_K \end{bmatrix}$$

\*The author was with the Signal Processing Group, Technische Universität Darmstadt, Darmstadt, Germany and is now with the Pattern Recognition Group, University of Bern, Bern, Switzerland (e-mail: a.tastan@spg.tu-darmstadt.de; aylin.tastan@unibe.ch).

†The author is with the Robust Data Science Group, Technische Universität Darmstadt, Darmstadt, Germany (e-mail: michael.muma@tu-darmstadt.de).

‡The author is with the Signal Processing Group, Technische Universität Darmstadt, Darmstadt, Germany (e-mail: zoubir@spg.tu-darmstadt.de).



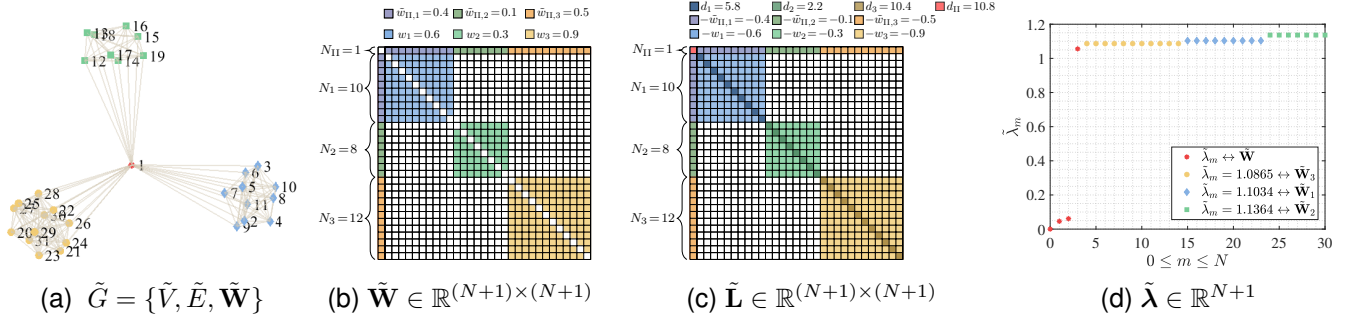


Fig. 1: Exemplary plot of Theorem 1 ( $\mathbf{n} = [1, 10, 8, 12]^T \in \mathbb{R}^{K+1}$ ,  $N + 1 = 31$ ,  $K = 3$ ).

To simplify the determinant of the first matrix, it transformed into a lower diagonal matrix by applying the following Gaussian elimination steps

$$\begin{aligned} \frac{N_1 \tilde{w}_{\Pi,1} z_1^{-1}}{-N_1 w_1 z_1^{-1} + 1} R_2 + R_1 &\rightarrow R_1 \\ \frac{N_2 \tilde{w}_{\Pi,2} z_2^{-1}}{-N_2 w_2 z_2^{-1} + 1} R_3 + R_1 &\rightarrow R_1 \\ &\vdots \\ \frac{N_K \tilde{w}_{\Pi,K} z_K^{-1}}{-N_K w_K z_K^{-1} + 1} R_{K+1} + R_1 &\rightarrow R_1 \end{aligned}$$

where  $R_K$  denotes  $K$ th row. Then, the simplified determinant yields

$$0 = c_{\Pi} (-N_1 w_1 z_1^{-1} + 1) (-N_2 w_2 z_2^{-1} + 1) \dots (-N_K w_K z_K^{-1} + 1) z_{\Pi} z_1^{N_1} z_2^{N_2} \dots z_K^{N_K}$$

where

$$c_{\Pi} = \left( 1 - \frac{N_1 \tilde{w}_{\Pi,1}^2 z_1^{-1} z_{\Pi}^{-1}}{-N_1 w_1 z_1^{-1} + 1} - \frac{N_2 \tilde{w}_{\Pi,2}^2 z_2^{-1} z_{\Pi}^{-1}}{-N_2 w_2 z_2^{-1} + 1} - \dots - \frac{N_K \tilde{w}_{\Pi,K}^2 z_K^{-1} z_{\Pi}^{-1}}{-N_K w_K z_K^{-1} + 1} \right).$$

For  $z_{\Pi} = \sum_{j=1}^K N_j \tilde{w}_{\Pi,j} - \tilde{\lambda} \sum_{j=1}^K N_j \tilde{w}_{\Pi,j}$  and  $z_j = N_j w_j + \tilde{w}_{\Pi,j} - \tilde{\lambda} ((N_j - 1)w_j + \tilde{w}_{\Pi,j})$  such that  $j = 1, \dots, K$  the determinant yields

$$\begin{aligned} 0 &= (-N_1 w_1 z_1^{-1} + 1) (-N_2 w_2 z_2^{-1} + 1) \dots (-N_K w_K z_K^{-1} + 1) z_{\Pi} z_1^{N_1} z_2^{N_2} \dots z_K^{N_K} z_{\Pi}^{-1} \\ &\quad \left( z_{\Pi} - \frac{N_1 \tilde{w}_{\Pi,1}^2 z_1^{-1}}{-N_1 w_1 z_1^{-1} + 1} - \frac{N_2 \tilde{w}_{\Pi,2}^2 z_2^{-1}}{-N_2 w_2 z_2^{-1} + 1} - \dots - \frac{N_K \tilde{w}_{\Pi,K}^2 z_K^{-1}}{-N_K w_K z_K^{-1} + 1} \right) \\ 0 &= (\tilde{w}_{\Pi,1} - \tilde{\lambda} \tilde{d}_1) (\tilde{w}_{\Pi,2} - \tilde{\lambda} \tilde{d}_2) \dots (\tilde{w}_{\Pi,K} - \tilde{\lambda} \tilde{d}_K) (N_1 w_1 + \tilde{w}_{\Pi,1} - \tilde{\lambda} \tilde{d}_1)^{N_1-1} (N_2 w_2 + \tilde{w}_{\Pi,2} - \tilde{\lambda} \tilde{d}_2)^{N_2-1} \dots (N_K w_K + \tilde{w}_{\Pi,K} - \tilde{\lambda} \tilde{d}_K)^{N_K-1} \\ &\quad \left( \sum_{j=1}^K N_j \tilde{w}_{\Pi,j} - \tilde{\lambda} \tilde{d}_{\Pi} - \frac{N_1 \tilde{w}_{\Pi,1}^2}{\tilde{w}_{\Pi,1} - \tilde{\lambda} \tilde{d}_1} - \frac{N_2 \tilde{w}_{\Pi,2}^2}{\tilde{w}_{\Pi,2} - \tilde{\lambda} \tilde{d}_2} - \dots - \frac{N_K \tilde{w}_{\Pi,K}^2}{\tilde{w}_{\Pi,K} - \tilde{\lambda} \tilde{d}_K} \right) \\ 0 &= (\tilde{w}_{\Pi,1} - \tilde{\lambda} \tilde{d}_1) (\tilde{w}_{\Pi,2} - \tilde{\lambda} \tilde{d}_2) \dots (\tilde{w}_{\Pi,K} - \tilde{\lambda} \tilde{d}_K) (N_1 w_1 + \tilde{w}_{\Pi,1} - \tilde{\lambda} \tilde{d}_1)^{N_1-1} (N_2 w_2 + \tilde{w}_{\Pi,2} - \tilde{\lambda} \tilde{d}_2)^{N_2-1} \dots (N_K w_K + \tilde{w}_{\Pi,K} - \tilde{\lambda} \tilde{d}_K)^{N_K-1} \\ &\quad \left( N_1 \tilde{w}_{\Pi,1} - \frac{N_1 \tilde{w}_{\Pi,1}^2}{\tilde{w}_{\Pi,1} - \tilde{\lambda} \tilde{d}_1} + N_2 \tilde{w}_{\Pi,2} - \frac{N_2 \tilde{w}_{\Pi,2}^2}{\tilde{w}_{\Pi,2} - \tilde{\lambda} \tilde{d}_2} - \dots + N_K \tilde{w}_{\Pi,K} - \frac{N_K \tilde{w}_{\Pi,K}^2}{\tilde{w}_{\Pi,K} - \tilde{\lambda} \tilde{d}_K} - \tilde{\lambda} \tilde{d}_{\Pi} \right) \\ 0 &= (\tilde{w}_{\Pi,1} - \tilde{\lambda} \tilde{d}_1) (\tilde{w}_{\Pi,2} - \tilde{\lambda} \tilde{d}_2) \dots (\tilde{w}_{\Pi,K} - \tilde{\lambda} \tilde{d}_K) (N_1 w_1 + \tilde{w}_{\Pi,1} - \tilde{\lambda} \tilde{d}_1)^{N_1-1} (N_2 w_2 + \tilde{w}_{\Pi,2} - \tilde{\lambda} \tilde{d}_2)^{N_2-1} \dots (N_K w_K + \tilde{w}_{\Pi,K} - \tilde{\lambda} \tilde{d}_K)^{N_K-1} \\ &\quad \left( -\frac{N_1 \tilde{w}_{\Pi,1} \tilde{\lambda} \tilde{d}_1}{\tilde{w}_{\Pi,1} - \tilde{\lambda} \tilde{d}_1} - \frac{N_2 \tilde{w}_{\Pi,2} \tilde{\lambda} \tilde{d}_2}{\tilde{w}_{\Pi,2} - \tilde{\lambda} \tilde{d}_2} - \dots - \frac{N_K \tilde{w}_{\Pi,K} \tilde{\lambda} \tilde{d}_K}{\tilde{w}_{\Pi,K} - \tilde{\lambda} \tilde{d}_K} - \tilde{\lambda} \tilde{d}_{\Pi} \right) \\ 0 &= \tilde{\lambda} (N_1 w_1 + \tilde{w}_{\Pi,1} - \tilde{\lambda} \tilde{d}_1)^{N_1-1} (N_2 w_2 + \tilde{w}_{\Pi,2} - \tilde{\lambda} \tilde{d}_2)^{N_2-1} \dots (N_K w_K + \tilde{w}_{\Pi,K} - \tilde{\lambda} \tilde{d}_K)^{N_K-1} (\tilde{w}_{\Pi,1} - \tilde{\lambda} \tilde{d}_1) (\tilde{w}_{\Pi,2} - \tilde{\lambda} \tilde{d}_2) \dots (\tilde{w}_{\Pi,K} - \tilde{\lambda} \tilde{d}_K) \\ &\quad \left( -\frac{N_1 \tilde{w}_{\Pi,1} \tilde{d}_1}{\tilde{w}_{\Pi,1} - \tilde{\lambda} \tilde{d}_1} - \frac{N_2 \tilde{w}_{\Pi,2} \tilde{d}_2}{\tilde{w}_{\Pi,2} - \tilde{\lambda} \tilde{d}_2} - \dots - \frac{N_K \tilde{w}_{\Pi,K} \tilde{d}_K}{\tilde{w}_{\Pi,K} - \tilde{\lambda} \tilde{d}_K} - \tilde{d}_{\Pi} \right) \end{aligned}$$

Now,  $N + 1 - K$  number of eigenvalues can be written as

$$\left\{ \begin{array}{l} N_1 - 1 \text{ elements of } \tilde{\lambda} \text{ equal to } \frac{N_1 w_1 + \tilde{w}_{\text{II},1}}{\tilde{d}_1} \\ N_2 - 1 \text{ elements of } \tilde{\lambda} \text{ equal to } \frac{N_2 w_2 + \tilde{w}_{\text{II},2}}{\tilde{d}_2} \\ \vdots \\ N_K - 1 \text{ elements of } \tilde{\lambda} \text{ equal to } \frac{N_K w_K + \tilde{w}_{\text{II},K}}{\tilde{d}_K} \\ \text{the smallest element of } \tilde{\lambda} \text{ equal to zero} \end{array} \right.$$

and the remaining  $K$  number of eigenvalues are roots of the equation

$$0 = (\tilde{w}_{\text{II},1} - \tilde{\lambda}\tilde{d}_1)(\tilde{w}_{\text{II},2} - \tilde{\lambda}\tilde{d}_2)\dots(\tilde{w}_{\text{II},K} - \tilde{\lambda}\tilde{d}_K) \left( -\frac{N_1\tilde{w}_{\text{II},1}\tilde{d}_1}{\tilde{w}_{\text{II},1} - \tilde{\lambda}\tilde{d}_1} - \frac{N_2\tilde{w}_{\text{II},2}\tilde{d}_2}{\tilde{w}_{\text{II},2} - \tilde{\lambda}\tilde{d}_2} \dots - \frac{N_K\tilde{w}_{\text{II},K}\tilde{d}_K}{\tilde{w}_{\text{II},K} - \tilde{\lambda}\tilde{d}_K} - \tilde{d}_{\text{II}} \right)$$

$$0 = \prod_{j=1}^K (\tilde{w}_{\text{II},j} - \tilde{\lambda}\tilde{d}_j) \left( -\sum_{j=1}^K \frac{N_j\tilde{w}_{\text{II},j}\tilde{d}_j}{\tilde{w}_{\text{II},j} - \tilde{\lambda}\tilde{d}_j} - \tilde{d}_{\text{II}} \right).$$

□

### A.2 Outlier Effects on Target Eigenvalues: Proof of Theorem 2

Let  $\tilde{\mathbf{W}} \in \mathbb{R}^{N \times N}$  and  $\tilde{\mathbf{L}} \in \mathbb{R}^{N \times N}$  denote  $K$  block zero diagonal affinity matrix and associated Laplacian in which  $i$ th block has similarity with remaining  $K - 1$  number of blocks. For simplicity, let  $i = 1$ , i.e.

$$\tilde{\mathbf{W}} = \begin{bmatrix} 0 & w_1 & \dots & w_1 & \tilde{w}_{1,2} & \dots & \tilde{w}_{1,2} & \dots & \tilde{w}_{1,K} & \dots & \tilde{w}_{1,K} \\ w_1 & 0 & \dots & w_1 & \tilde{w}_{1,2} & \dots & \tilde{w}_{1,2} & \dots & \tilde{w}_{1,K} & \dots & \tilde{w}_{1,K} \\ \vdots & \vdots & \ddots & \vdots & \vdots & \ddots & \vdots & \ddots & \vdots & \ddots & \vdots \\ w_1 & w_1 & \dots & 0 & \tilde{w}_{1,2} & \dots & \tilde{w}_{1,2} & \dots & \tilde{w}_{1,K} & \dots & \tilde{w}_{1,K} \\ \tilde{w}_{1,2} & \dots & \tilde{w}_{1,2} & 0 & w_2 & \dots & w_2 & \dots & \dots & \dots & \dots \\ \tilde{w}_{1,2} & \dots & \tilde{w}_{1,2} & w_2 & 0 & \dots & w_2 & \dots & \dots & \dots & \dots \\ \vdots & \dots & \vdots & \vdots & \vdots & \ddots & \vdots & \ddots & \vdots & \ddots & \vdots \\ \tilde{w}_{1,2} & \dots & \tilde{w}_{1,2} & w_2 & w_2 & \dots & 0 & \dots & \dots & \dots & \dots \\ \vdots & \dots & \vdots & \vdots & \vdots & \ddots & \vdots & \ddots & \vdots & \ddots & \vdots \\ \tilde{w}_{1,K} & \dots & \tilde{w}_{1,K} & \dots & \dots & \dots & 0 & w_K & \dots & w_K & \dots \\ \tilde{w}_{1,K} & \dots & \tilde{w}_{1,K} & \dots & \dots & \dots & w_K & 0 & \dots & w_K & \dots \\ \vdots & \dots & \vdots & \dots & \dots & \dots & \vdots & \vdots & \ddots & \vdots & \dots \\ \tilde{w}_{1,K} & \dots & \tilde{w}_{1,K} & \dots & \dots & \dots & w_K & w_K & \dots & 0 & \dots \end{bmatrix}$$

and

$$\tilde{\mathbf{L}} = \begin{bmatrix} \tilde{d}_1 & -w_1 & \dots & -w_1 & -\tilde{w}_{1,2} & \dots & -\tilde{w}_{1,2} & \dots & -\tilde{w}_{1,K} & \dots & -\tilde{w}_{1,K} \\ -w_1 & \tilde{d}_1 & \dots & -w_1 & -\tilde{w}_{1,2} & \dots & -\tilde{w}_{1,2} & \dots & -\tilde{w}_{1,K} & \dots & -\tilde{w}_{1,K} \\ \vdots & \vdots & \ddots & \vdots & \vdots & \ddots & \vdots & \ddots & \vdots & \ddots & \vdots \\ -w_1 & -w_1 & \dots & \tilde{d}_1 & -\tilde{w}_{1,2} & \dots & -\tilde{w}_{1,2} & \dots & -\tilde{w}_{1,K} & \dots & -\tilde{w}_{1,K} \\ -\tilde{w}_{1,2} & \dots & -\tilde{w}_{1,2} & \tilde{d}_2 & -w_2 & \dots & -w_2 & \dots & \dots & \dots & \dots \\ -\tilde{w}_{1,2} & \dots & -\tilde{w}_{1,2} & -w_2 & \tilde{d}_2 & \dots & -w_2 & \dots & \dots & \dots & \dots \\ \vdots & \dots & \vdots & \vdots & \vdots & \ddots & \vdots & \ddots & \vdots & \ddots & \vdots \\ -\tilde{w}_{1,2} & \dots & -\tilde{w}_{1,2} & -w_2 & -w_2 & \dots & \tilde{d}_2 & \dots & \dots & \dots & \dots \\ \vdots & \dots & \vdots & \vdots & \vdots & \ddots & \vdots & \ddots & \vdots & \ddots & \vdots \\ -\tilde{w}_{1,K} & \dots & -\tilde{w}_{1,K} & \dots & \dots & \dots & \tilde{d}_K & -w_K & \dots & -w_K & \dots \\ -\tilde{w}_{1,K} & \dots & -\tilde{w}_{1,K} & \dots & \dots & \dots & -w_K & \tilde{d}_K & \dots & -w_K & \dots \\ \vdots & \dots & \vdots & \dots & \dots & \dots & \vdots & \vdots & \ddots & \vdots & \dots \\ -\tilde{w}_{1,K} & \dots & -\tilde{w}_{1,K} & \dots & \dots & \dots & -w_K & -w_K & \dots & \tilde{d}_K & \dots \end{bmatrix}$$





To simplify the determinant of the first matrix, it transformed into a lower diagonal matrix by applying the following Gaussian elimination steps

$$\begin{aligned} & \frac{N_2 \tilde{w}_{1,2} z_2^{-1}}{-N_2 w_2 z_2^{-1} + 1} R_2 + R_1 \rightarrow R_1 \\ & \frac{N_3 \tilde{w}_{1,3} z_3^{-1}}{-N_3 w_3 z_3^{-1} + 1} R_3 + R_1 \rightarrow R_1 \\ & \vdots \\ & \frac{N_K \tilde{w}_{1,K} z_K^{-1}}{-N_K w_K z_K^{-1} + 1} R_K + R_1 \rightarrow R_1 \end{aligned}$$

where  $R_K$  denotes  $K$ th row. Then, the simplified determinant yields

$$0 = \det(\mathbf{H}) \begin{vmatrix} c_1 & 0 & 0 & \dots & 0 \\ -N_1 \tilde{w}_{1,2} z_1^{-1} & -N_2 w_2 z_2^{-1} + 1 & 0 & \dots & 0 \\ -N_1 \tilde{w}_{1,3} z_1^{-1} & 0 & -N_3 w_3 z_3^{-1} + 1 & \dots & 0 \\ \vdots & \vdots & \vdots & \ddots & \vdots \\ -N_1 \tilde{w}_{1,K} z_1^{-1} & 0 & \dots & \dots & -N_K w_K z_K^{-1} + 1 \end{vmatrix}$$

where  $c_1$  equals to

$$c_1 = -N_1 w_1 z_1^{-1} + 1 - \frac{N_2 \tilde{w}_{1,2} z_2^{-1} N_1 \tilde{w}_{1,2} z_1^{-1}}{-N_2 w_2 z_2^{-1} + 1} - \dots - \frac{N_K \tilde{w}_{1,K} z_K^{-1} N_1 \tilde{w}_{1,K} z_1^{-1}}{-N_K w_K z_K^{-1} + 1}.$$

For  $z_1 = N_1 w_1 + \sum_{j=2}^K N_j \tilde{w}_{1,j} - \tilde{\lambda}((N_1 - 1)w_1 + \sum_{j=2}^K N_j \tilde{w}_{1,j})$  and  $z_j = N_j w_j + N_1 \tilde{w}_{1,j} - \tilde{\lambda}((N_j - 1)w_j + N_1 \tilde{w}_{1,j})$  with  $j = 2, \dots, K$ , the determinant  $\det(\tilde{\mathbf{L}} - \tilde{\lambda} \tilde{\mathbf{D}}) = 0$  yields

$$0 = z_1^{N_1} z_2^{N_2} \dots z_K^{N_K} (-N_2 w_2 z_2^{-1} + 1) \dots (-N_K w_K z_K^{-1} + 1) c_1$$

$$0 = z_1^{N_1} z_2^{N_2 - 1} \dots z_K^{N_K - 1} (-N_2 w_2 + z_2) \dots (-N_K w_K + z_K) c_1$$

$$0 = z_1^{N_1} z_2^{N_2 - 1} \dots z_K^{N_K - 1} (-N_2 w_2 + z_2) \dots (-N_K w_K + z_K) z_1^{-1} \left( -N_1 w_1 + z_1 - \frac{N_1 N_2 \tilde{w}_{1,2}^2 z_2^{-1}}{-N_2 w_2 z_2^{-1} + 1} - \dots - \frac{N_1 N_K \tilde{w}_{1,K}^2 z_K^{-1}}{-N_K w_K z_K^{-1} + 1} \right)$$

$$0 = z_1^{N_1 - 1} z_2^{N_2 - 1} \dots z_K^{N_K - 1} (-N_2 w_2 + z_2) \dots (-N_K w_K + z_K) \left( -N_1 w_1 + z_1 - \frac{N_1 N_2 \tilde{w}_{1,2}^2}{z_2 - N_2 w_2} - \dots - \frac{N_1 N_K \tilde{w}_{1,K}^2}{z_K - N_K w_K} \right)$$

$$0 = \left( N_1 w_1 + \sum_{j=2}^K N_j \tilde{w}_{1,j} - \tilde{\lambda} \tilde{d}_1 \right)^{N_1 - 1} \left( N_2 w_2 + N_1 \tilde{w}_{1,2} - \tilde{\lambda} \tilde{d}_2 \right)^{N_2 - 1} \dots \left( N_K w_K + N_1 \tilde{w}_{1,K} - \tilde{\lambda} \tilde{d}_K \right)^{N_K - 1}$$

$$\left( N_1 \tilde{w}_{1,2} - \tilde{\lambda} \tilde{d}_2 \right) \dots \left( N_1 \tilde{w}_{1,K} - \tilde{\lambda} \tilde{d}_K \right) \left( \sum_{j=2}^K N_j \tilde{w}_{1,j} - \tilde{\lambda} \tilde{d}_1 - \frac{N_1 N_2 \tilde{w}_{1,2}^2}{N_1 \tilde{w}_{1,2} - \tilde{\lambda} \tilde{d}_2} - \dots - \frac{N_1 N_K \tilde{w}_{1,K}^2}{N_1 \tilde{w}_{1,K} - \tilde{\lambda} \tilde{d}_K} \right)$$

$$0 = \left( N_1 w_1 + \sum_{j=2}^K N_j \tilde{w}_{1,j} - \tilde{\lambda} \tilde{d}_1 \right)^{N_1 - 1} \left( N_2 w_2 + N_1 \tilde{w}_{1,2} - \tilde{\lambda} \tilde{d}_2 \right)^{N_2 - 1} \dots \left( N_K w_K + N_1 \tilde{w}_{1,K} - \tilde{\lambda} \tilde{d}_K \right)^{N_K - 1}$$

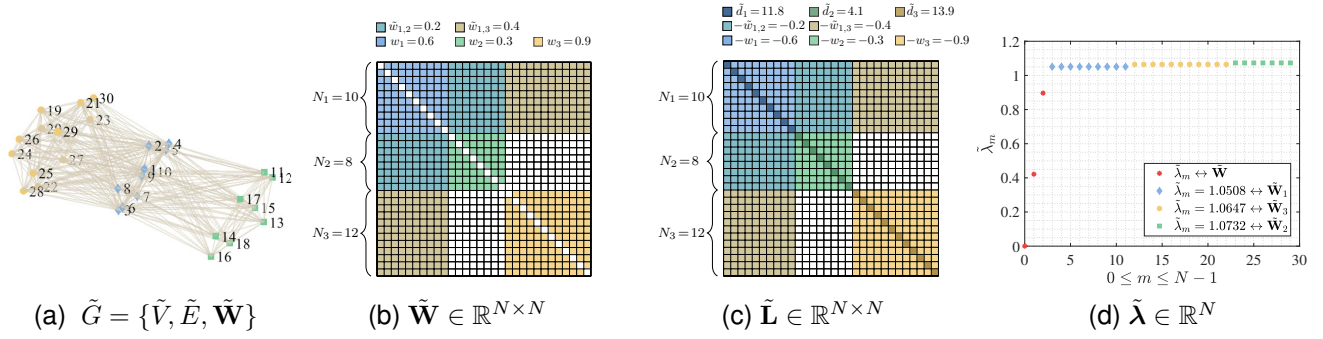
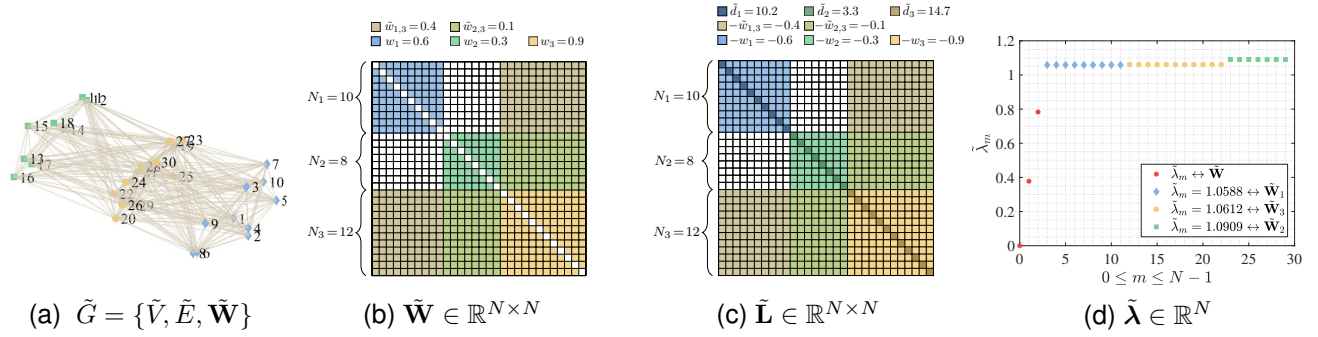
$$\left( N_1 \tilde{w}_{1,2} - \tilde{\lambda} \tilde{d}_2 \right) \dots \left( N_1 \tilde{w}_{1,K} - \tilde{\lambda} \tilde{d}_K \right) \left( N_2 \tilde{w}_{1,2} - \frac{N_1 N_2 \tilde{w}_{1,2}^2}{N_1 \tilde{w}_{1,2} - \tilde{\lambda} \tilde{d}_2} + \dots + N_K \tilde{w}_{1,K} - \frac{N_1 N_K \tilde{w}_{1,K}^2}{N_1 \tilde{w}_{1,K} - \tilde{\lambda} \tilde{d}_K} - \tilde{\lambda} \tilde{d}_1 \right)$$

$$0 = \left( N_1 w_1 + \sum_{j=2}^K N_j \tilde{w}_{1,j} - \tilde{\lambda} \tilde{d}_1 \right)^{N_1 - 1} \left( N_2 w_2 + N_1 \tilde{w}_{1,2} - \tilde{\lambda} \tilde{d}_2 \right)^{N_2 - 1} \dots \left( N_K w_K + N_1 \tilde{w}_{1,K} - \tilde{\lambda} \tilde{d}_K \right)^{N_K - 1}$$

$$\left( N_1 \tilde{w}_{1,2} - \tilde{\lambda} \tilde{d}_2 \right) \dots \left( N_1 \tilde{w}_{1,K} - \tilde{\lambda} \tilde{d}_K \right) \left( -\frac{\tilde{\lambda} \tilde{d}_2 N_2 \tilde{w}_{1,2}}{N_1 \tilde{w}_{1,2} - \tilde{\lambda} \tilde{d}_2} \dots - \frac{\tilde{\lambda} \tilde{d}_K N_K \tilde{w}_{1,K}}{N_1 \tilde{w}_{1,K} - \tilde{\lambda} \tilde{d}_K} - \tilde{\lambda} \tilde{d}_1 \right)$$

$$0 = \tilde{\lambda} \left( N_1 w_1 + \sum_{j=2}^K N_j \tilde{w}_{1,j} - \tilde{\lambda} \tilde{d}_1 \right)^{N_1 - 1} \left( N_2 w_2 + N_1 \tilde{w}_{1,2} - \tilde{\lambda} \tilde{d}_2 \right)^{N_2 - 1} \dots \left( N_K w_K + N_1 \tilde{w}_{1,K} - \tilde{\lambda} \tilde{d}_K \right)^{N_K - 1}$$

$$\left( N_1 \tilde{w}_{1,2} - \tilde{\lambda} \tilde{d}_2 \right) \dots \left( N_1 \tilde{w}_{1,K} - \tilde{\lambda} \tilde{d}_K \right) \left( -\frac{\tilde{d}_2 N_2 \tilde{w}_{1,2}}{N_1 \tilde{w}_{1,2} - \tilde{\lambda} \tilde{d}_2} \dots - \frac{\tilde{d}_K N_K \tilde{w}_{1,K}}{N_1 \tilde{w}_{1,K} - \tilde{\lambda} \tilde{d}_K} - \tilde{d}_1 \right)$$


 Fig. 2: Exemplary plot of Theorem 2 ( $\mathbf{n} = [10, 8, 12]^\top \in \mathbb{R}^K$ ,  $N = 30$ ,  $K = 3$ ,  $i = 1$ ).

 Fig. 3: Exemplary plot of Theorem 2 ( $\mathbf{n} = [10, 8, 12]^\top \in \mathbb{R}^K$ ,  $N = 30$ ,  $K = 3$ ,  $i = K$ ).

Based on this,  $N + 1 - K$  number of eigenvalues are

$$\left\{ \begin{array}{l} N_i - 1 \text{ elements of } \tilde{\lambda} \text{ equal to } \frac{N_i w_i + \sum_{\substack{j=1 \\ j \neq i}}^K N_j \tilde{w}_{i,j}}{\tilde{d}_i} \\ N_j - 1 \text{ elements of } \tilde{\lambda} \text{ equal to } \frac{N_j w_j + N_i \tilde{w}_{i,j}}{\tilde{d}_j} \\ \vdots \\ N_K - 1 \text{ elements of } \tilde{\lambda} \text{ equal to } \frac{N_K w_K + N_i \tilde{w}_{i,K}}{\tilde{d}_K} \\ \text{the smallest element of } \tilde{\lambda} \text{ equal to zero} \end{array} \right.$$

and the remaining  $K - 1$  eigenvalues are roots of the equation

$$0 = (N_1 \tilde{w}_{1,2} - \tilde{\lambda} \tilde{d}_2) \dots (N_1 \tilde{w}_{1,K} - \tilde{\lambda} \tilde{d}_K) \left( -\frac{\tilde{d}_2 N_2 \tilde{w}_{1,2}}{N_1 \tilde{w}_{1,2} - \tilde{\lambda} \tilde{d}_2} \dots - \frac{\tilde{d}_K N_K \tilde{w}_{1,K}}{N_1 \tilde{w}_{1,K} - \tilde{\lambda} \tilde{d}_K} - \tilde{d}_1 \right)$$

$$0 = \prod_{\substack{j=1 \\ j \neq i}}^K (N_i \tilde{w}_{i,j} - \tilde{\lambda} \tilde{d}_j) \left( -\sum_{\substack{j=1 \\ j \neq i}}^K \frac{\tilde{d}_j N_j \tilde{w}_{i,j}}{N_i \tilde{w}_{i,j} - \tilde{\lambda} \tilde{d}_j} - \tilde{d}_i \right)$$

where  $i = 1$  and  $j = 2, \dots, K$ . □

## APPENDIX B: THE STANDARD EIGEN-DECOMPOSITION BASED EIGENVALUE ANALYSIS

## B.1 Outlier Effects on Target Eigenvalues

**Theorem. 1.S.** Let  $\tilde{\mathbf{W}} \in \mathbb{R}^{(N+1) \times (N+1)}$  define a symmetric affinity matrix, that is equal to  $\mathbf{W}$ , except for an additional Type II outlier that shares similarity coefficients with  $K$  blocks where  $\tilde{w}_{\text{II},K} > 0$  denotes the similarity coefficient between the outlier  $\circ_{\text{II}}$  and the  $K$ th block. Then, for the associated corrupted Laplacian matrix  $\tilde{\mathbf{L}} \in \mathbb{R}^{(N+1) \times (N+1)}$  with eigenvalues  $\tilde{\lambda} \in \mathbb{R}^{N+1}$ , it holds that

$$\begin{cases} N_1 - 1 \text{ elements of } \tilde{\lambda} \text{ equal to } N_1 w_1 + \tilde{w}_{\text{II},1} \\ N_2 - 1 \text{ elements of } \tilde{\lambda} \text{ equal to } N_2 w_2 + \tilde{w}_{\text{II},2} \\ \vdots \\ N_K - 1 \text{ elements of } \tilde{\lambda} \text{ equal to } N_K w_K + \tilde{w}_{\text{II},K} \\ \text{the smallest element of } \tilde{\lambda} \text{ equal to zero} \end{cases}$$

and the remaining  $K$  eigenvalues are the roots of

$$\prod_{j=1}^K (\tilde{w}_{\text{II},j} - \tilde{\lambda}) \left( - \sum_{j=1}^K \frac{N_j \tilde{w}_{\text{II},j}}{\tilde{w}_{\text{II},j} - \tilde{\lambda}} - 1 \right) = 0.$$

where  $\tilde{\lambda} \in \tilde{\lambda}$ .

*Proof.* Let  $\tilde{\mathbf{W}} \in \mathbb{R}^{(N+1) \times (N+1)}$  and  $\tilde{\mathbf{L}} \in \mathbb{R}^{(N+1) \times (N+1)}$ , respectively, denote a block zero-diagonal symmetric affinity matrix and associated Laplacian matrix for  $K$  blocks with an additional Type II outlier that is correlated with all blocks, i.e.,

$$\tilde{\mathbf{W}} = \begin{bmatrix} 0 & \tilde{w}_{\text{II},1} & \tilde{w}_{\text{II},1} & \dots & \tilde{w}_{\text{II},1} & \tilde{w}_{\text{II},2} & \tilde{w}_{\text{II},2} & \dots & \tilde{w}_{\text{II},2} & \dots & \tilde{w}_{\text{II},K} & \tilde{w}_{\text{II},K} & \dots & \tilde{w}_{\text{II},K} \\ \tilde{w}_{\text{II},1} & 0 & w_1 & \dots & w_1 & & & & & & & & & & \\ \tilde{w}_{\text{II},1} & w_1 & 0 & \dots & w_1 & & & & & & & & & & \\ \vdots & \vdots & \vdots & \ddots & \vdots & & & & & & & & & & \\ \tilde{w}_{\text{II},1} & w_1 & w_1 & \dots & 0 & & & & & & & & & & \\ \tilde{w}_{\text{II},2} & & & & 0 & w_2 & \dots & w_2 & & & & & & & \\ \tilde{w}_{\text{II},2} & & & & w_2 & 0 & \dots & w_2 & & & & & & & \\ \vdots & & & & \vdots & \vdots & \ddots & \vdots & & & & & & & \\ \tilde{w}_{\text{II},2} & & & & w_2 & w_2 & \dots & 0 & & & & & & & \\ \vdots & & & & \vdots & \vdots & \ddots & \vdots & & & & & & & \\ \tilde{w}_{\text{II},K} & & & & & & & \dots & 0 & w_K & \dots & w_K & & & \\ \tilde{w}_{\text{II},K} & & & & & & & & w_K & 0 & \dots & w_K & & & \\ \vdots & & & & & & & & \vdots & \vdots & \ddots & \vdots & & & \\ \vdots & & & & & & & & \vdots & \vdots & \ddots & \vdots & & & \\ \tilde{w}_{\text{II},K} & & & & & & & & \dots & w_K & w_K & \dots & 0 & & \end{bmatrix}$$

and

$$\tilde{\mathbf{L}} = \begin{bmatrix} \tilde{d}_{\text{II}} & -\tilde{w}_{\text{II},1} & -\tilde{w}_{\text{II},1} & \dots & -\tilde{w}_{\text{II},1} & -\tilde{w}_{\text{II},2} & -\tilde{w}_{\text{II},2} & \dots & -\tilde{w}_{\text{II},2} & \dots & -\tilde{w}_{\text{II},K} & -\tilde{w}_{\text{II},K} & \dots & -\tilde{w}_{\text{II},K} \\ -\tilde{w}_{\text{II},1} & \tilde{d}_1 & -w_1 & \dots & -w_1 & & & & & & & & & & \\ -\tilde{w}_{\text{II},1} & -w_1 & \tilde{d}_1 & \dots & -w_1 & & & & & & & & & & \\ \vdots & \vdots & \vdots & \ddots & \vdots & & & & & & & & & & \\ -\tilde{w}_{\text{II},1} & -w_1 & -w_1 & \dots & \tilde{d}_1 & & & & & & & & & & \\ -\tilde{w}_{\text{II},2} & & & & \tilde{d}_2 & -w_2 & \dots & -w_2 & & & & & & & \\ -\tilde{w}_{\text{II},2} & & & & -w_2 & \tilde{d}_2 & \dots & -w_2 & & & & & & & \\ \vdots & & & & \vdots & \vdots & \ddots & \vdots & & & & & & & \\ -\tilde{w}_{\text{II},2} & & & & -w_2 & -w_2 & \dots & \tilde{d}_2 & & & & & & & \\ \vdots & & & & \vdots & \vdots & \ddots & \vdots & & & & & & & \\ -\tilde{w}_{\text{II},K} & & & & & & & \dots & \tilde{d}_K & -w_K & \dots & -w_K & & & \\ -\tilde{w}_{\text{II},K} & & & & & & & & -w_K & \tilde{d}_K & \dots & -w_K & & & \\ \vdots & & & & & & & & \vdots & \vdots & \ddots & \vdots & & & \\ -\tilde{w}_{\text{II},K} & & & & & & & & \dots & -w_K & -w_K & \dots & \tilde{d}_K & & \end{bmatrix}$$

where  $\tilde{d}_{\text{II}} = \sum_{j=1}^K N_j \tilde{w}_{\text{II},j}$  and  $\tilde{d}_j = (N_j - 1)w_j + \tilde{w}_{\text{II},j}$ . To compute the eigenvalues of the Laplacian matrix  $\tilde{\mathbf{L}}$ ,  $\det(\tilde{\mathbf{L}} - \tilde{\lambda}\mathbf{I}) = 0$  is considered which can equivalently be written in matrix form as follows



To simplify the determinant of the first matrix, it transformed into a lower diagonal matrix by applying the following Gaussian elimination steps

$$\begin{aligned} & \frac{N_1 \tilde{w}_{\text{II},1} (z_1 - \tilde{\lambda})^{-1}}{-N_1 w_1 (z_1 - \tilde{\lambda})^{-1} + 1} R_2 + R_1 \rightarrow R_1 \\ & \frac{N_2 \tilde{w}_{\text{II},2} (z_2 - \tilde{\lambda})^{-1}}{-N_2 w_2 (z_2 - \tilde{\lambda})^{-1} + 1} R_3 + R_1 \rightarrow R_1 \\ & \vdots \\ & \frac{N_K \tilde{w}_{\text{II},K} (z_K - \tilde{\lambda})^{-1}}{-N_K w_K (z_K - \tilde{\lambda})^{-1} + 1} R_{K+1} + R_1 \rightarrow R_1 \end{aligned}$$

where  $R_K$  denotes  $K$ th row. Then, the simplified determinant yields

$$0 = c_{\text{II}} (-N_1 w_1 (z_1 - \tilde{\lambda})^{-1} + 1) (-N_2 w_2 (z_2 - \tilde{\lambda})^{-1} + 1) \dots (-N_K w_K (z_K - \tilde{\lambda})^{-1} + 1) (z_{\text{II}} - \tilde{\lambda}) (z_1 - \tilde{\lambda})^{N_1} (z_2 - \tilde{\lambda})^{N_2} \dots (z_K - \tilde{\lambda})^{N_K}$$

where

$$c_{\text{II}} = \left( 1 - \frac{N_1 \tilde{w}_{\text{II},1} (z_1 - \tilde{\lambda})^{-1} \tilde{w}_{\text{II},1} (z_{\text{II}} - \tilde{\lambda})^{-1}}{-N_1 w_1 (z_1 - \tilde{\lambda})^{-1} + 1} - \frac{N_2 \tilde{w}_{\text{II},2} (z_2 - \tilde{\lambda})^{-1} \tilde{w}_{\text{II},2} (z_{\text{II}} - \tilde{\lambda})^{-1}}{-N_2 w_2 (z_2 - \tilde{\lambda})^{-1} + 1} - \dots - \frac{N_K \tilde{w}_{\text{II},K} (z_K - \tilde{\lambda})^{-1} \tilde{w}_{\text{II},K} (z_{\text{II}} - \tilde{\lambda})^{-1}}{-N_K w_K (z_K - \tilde{\lambda})^{-1} + 1} \right).$$

For  $z_{\text{II}} = \sum_{j=1}^K N_j \tilde{w}_{\text{II},j}$  and  $z_j = N_j w_j + \tilde{w}_{\text{II},j}$  such that  $j = 1, \dots, K$  the determinant yields

$$\begin{aligned} 0 &= (-N_1 w_1 (z_1 - \tilde{\lambda})^{-1} + 1) (-N_2 w_2 (z_2 - \tilde{\lambda})^{-1} + 1) \dots (-N_K w_K (z_K - \tilde{\lambda})^{-1} + 1) (z_{\text{II}} - \tilde{\lambda}) (z_1 - \tilde{\lambda})^{N_1} (z_2 - \tilde{\lambda})^{N_2} \dots (z_K - \tilde{\lambda})^{N_K} \\ & \quad (z_{\text{II}} - \tilde{\lambda})^{-1} \left( z_{\text{II}} - \tilde{\lambda} - \frac{N_1 \tilde{w}_{\text{II},1} (z_1 - \tilde{\lambda})^{-1} \tilde{w}_{\text{II},1}}{-N_1 w_1 (z_1 - \tilde{\lambda})^{-1} + 1} - \frac{N_2 \tilde{w}_{\text{II},2} (z_2 - \tilde{\lambda})^{-1} \tilde{w}_{\text{II},2}}{-N_2 w_2 (z_2 - \tilde{\lambda})^{-1} + 1} - \dots - \frac{N_K \tilde{w}_{\text{II},K} (z_K - \tilde{\lambda})^{-1} \tilde{w}_{\text{II},K}}{-N_K w_K (z_K - \tilde{\lambda})^{-1} + 1} \right) \\ 0 &= (\tilde{w}_{\text{II},1} - \tilde{\lambda}) (\tilde{w}_{\text{II},2} - \tilde{\lambda}) \dots (\tilde{w}_{\text{II},K} - \tilde{\lambda}) (N_1 w_1 + \tilde{w}_{\text{II},1} - \tilde{\lambda})^{N_1 - 1} (N_2 w_2 + \tilde{w}_{\text{II},2} - \tilde{\lambda})^{N_2 - 1} \dots (N_K w_K + \tilde{w}_{\text{II},K} - \tilde{\lambda})^{N_K - 1} \\ & \quad \left( \sum_{j=1}^K N_j \tilde{w}_{\text{II},j} - \tilde{\lambda} - \frac{N_1 \tilde{w}_{\text{II},1}^2}{\tilde{w}_{\text{II},1} - \tilde{\lambda}} - \frac{N_2 \tilde{w}_{\text{II},2}^2}{\tilde{w}_{\text{II},2} - \tilde{\lambda}} \dots - \frac{N_K \tilde{w}_{\text{II},K}^2}{\tilde{w}_{\text{II},K} - \tilde{\lambda}} \right) \\ 0 &= (\tilde{w}_{\text{II},1} - \tilde{\lambda}) (\tilde{w}_{\text{II},2} - \tilde{\lambda}) \dots (\tilde{w}_{\text{II},K} - \tilde{\lambda}) (N_1 w_1 + \tilde{w}_{\text{II},1} - \tilde{\lambda})^{N_1 - 1} (N_2 w_2 + \tilde{w}_{\text{II},2} - \tilde{\lambda})^{N_2 - 1} \dots (N_K w_K + \tilde{w}_{\text{II},K} - \tilde{\lambda})^{N_K - 1} \\ & \quad \left( N_1 \tilde{w}_{\text{II},1} - \frac{N_1 \tilde{w}_{\text{II},1}^2}{\tilde{w}_{\text{II},1} - \tilde{\lambda}} + N_2 \tilde{w}_{\text{II},2} - \frac{N_2 \tilde{w}_{\text{II},2}^2}{\tilde{w}_{\text{II},2} - \tilde{\lambda}} \dots + N_K \tilde{w}_{\text{II},K} - \frac{N_K \tilde{w}_{\text{II},K}^2}{\tilde{w}_{\text{II},K} - \tilde{\lambda}} - \tilde{\lambda} \right) \\ 0 &= (\tilde{w}_{\text{II},1} - \tilde{\lambda}) (\tilde{w}_{\text{II},2} - \tilde{\lambda}) \dots (\tilde{w}_{\text{II},K} - \tilde{\lambda}) (N_1 w_1 + \tilde{w}_{\text{II},1} - \tilde{\lambda})^{N_1 - 1} (N_2 w_2 + \tilde{w}_{\text{II},2} - \tilde{\lambda})^{N_2 - 1} \dots (N_K w_K + \tilde{w}_{\text{II},K} - \tilde{\lambda})^{N_K - 1} \\ & \quad \left( -\frac{N_1 \tilde{w}_{\text{II},1} \tilde{\lambda}}{\tilde{w}_{\text{II},1} - \tilde{\lambda}} - \frac{N_2 \tilde{w}_{\text{II},2} \tilde{\lambda}}{\tilde{w}_{\text{II},2} - \tilde{\lambda}} \dots - \frac{N_K \tilde{w}_{\text{II},K} \tilde{\lambda}}{\tilde{w}_{\text{II},K} - \tilde{\lambda}} - \tilde{\lambda} \right) \\ 0 &= (\tilde{w}_{\text{II},1} - \tilde{\lambda}) (\tilde{w}_{\text{II},2} - \tilde{\lambda}) \dots (\tilde{w}_{\text{II},K} - \tilde{\lambda}) (N_1 w_1 + \tilde{w}_{\text{II},1} - \tilde{\lambda})^{N_1 - 1} (N_2 w_2 + \tilde{w}_{\text{II},2} - \tilde{\lambda})^{N_2 - 1} \dots (N_K w_K + \tilde{w}_{\text{II},K} - \tilde{\lambda})^{N_K - 1} \tilde{\lambda} \\ & \quad \left( -\frac{N_1 \tilde{w}_{\text{II},1}}{\tilde{w}_{\text{II},1} - \tilde{\lambda}} - \frac{N_2 \tilde{w}_{\text{II},2}}{\tilde{w}_{\text{II},2} - \tilde{\lambda}} \dots - \frac{N_K \tilde{w}_{\text{II},K}}{\tilde{w}_{\text{II},K} - \tilde{\lambda}} - 1 \right) \end{aligned}$$

Now,  $N + 1 - K$  number of eigenvalues can be computed as

$$\left\{ \begin{array}{l} N_1 - 1 \text{ elements of } \tilde{\lambda} \text{ equal to } z_1 = N_1 w_1 + \tilde{w}_{\text{II},1} \\ N_2 - 1 \text{ elements of } \tilde{\lambda} \text{ equal to } z_2 = N_2 w_2 + \tilde{w}_{\text{II},2} \\ \vdots \\ N_K - 1 \text{ elements of } \tilde{\lambda} \text{ equal to } z_K = N_K w_K + \tilde{w}_{\text{II},K} \\ \text{the smallest element of } \tilde{\lambda} \text{ equal to zero} \end{array} \right.$$

and the remaining  $K$  number of eigenvalues are roots of the equation

$$\begin{aligned} 0 &= (\tilde{w}_{\text{II},1} - \tilde{\lambda}) (\tilde{w}_{\text{II},2} - \tilde{\lambda}) \dots (\tilde{w}_{\text{II},K} - \tilde{\lambda}) \left( -\frac{N_1 \tilde{w}_{\text{II},1}}{\tilde{w}_{\text{II},1} - \tilde{\lambda}} - \frac{N_2 \tilde{w}_{\text{II},2}}{\tilde{w}_{\text{II},2} - \tilde{\lambda}} \dots - \frac{N_K \tilde{w}_{\text{II},K}}{\tilde{w}_{\text{II},K} - \tilde{\lambda}} - 1 \right) \\ 0 &= \prod_{j=1}^K (\tilde{w}_{\text{II},j} - \tilde{\lambda}) \left( -\sum_{j=1}^K \frac{N_j \tilde{w}_{\text{II},j}}{\tilde{w}_{\text{II},j} - \tilde{\lambda}} - 1 \right) \end{aligned}$$

□

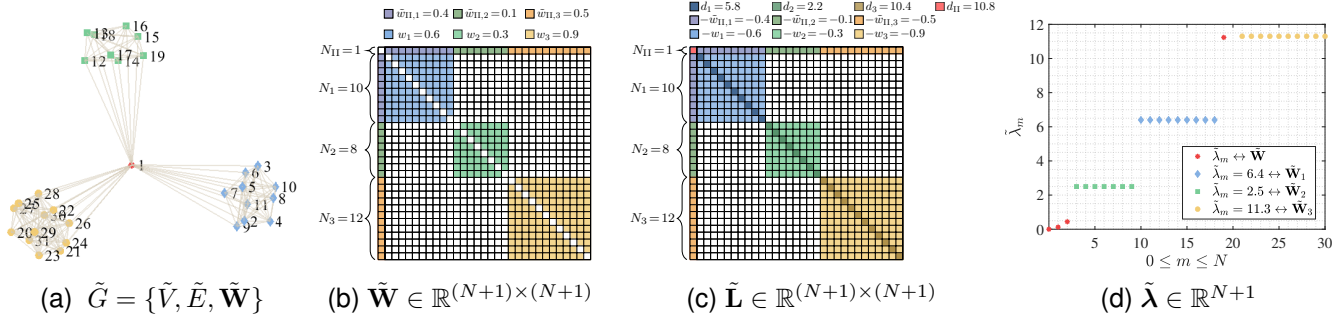


Fig. 4: Exemplary plot of Theorem 1.S. ( $\mathbf{n} = [1, 10, 8, 12]^\top \in \mathbb{R}^{K+1}$ ,  $N + 1 = 31$ ,  $K = 3$ ).

**Theorem. 2.S.** Let  $\tilde{W} \in \mathbb{R}^{N \times N}$  define an affinity matrix, that is equal to  $\mathbf{W}$ , except that block  $i$  has similarity with the remaining  $K - 1$  blocks with  $\tilde{w}_{i,j} = \tilde{w}_{j,i} > 0$  denoting the value around which the similarity coefficients between blocks  $i$  and  $j$  are concentrated for  $j = 1, \dots, K$  and  $i \neq j$ . Then, the eigenvalues  $\tilde{\lambda} \in \mathbb{R}^N$  of  $\tilde{L} \in \mathbb{R}^{N \times N}$  are as follows:

$$\left\{ \begin{array}{l} N_i - 1 \text{ elements of } \tilde{\lambda} \text{ equal to } N_i w_i + \sum_{\substack{j=1 \\ j \neq i}}^K N_j \tilde{w}_{i,j} \\ N_j - 1 \text{ elements of } \tilde{\lambda} \text{ equal to } N_j w_j + N_i \tilde{w}_{i,j} \\ \vdots \\ N_K - 1 \text{ elements of } \tilde{\lambda} \text{ equal to } N_K w_K + N_i \tilde{w}_{i,K} \\ \text{the smallest element of } \tilde{\lambda} \text{ equal to zero} \end{array} \right.$$

and the remaining  $K - 1$  eigenvalues in  $\tilde{\lambda}$  are the roots of

$$\prod_{\substack{j=1 \\ j \neq i}}^K (N_i \tilde{w}_{i,j} - \tilde{\lambda}) \left( \sum_{\substack{j=1 \\ j \neq i}}^K -\frac{N_j \tilde{w}_{i,j}}{N_i \tilde{w}_{i,j} - \tilde{\lambda}} - 1 \right) = 0$$

where  $\tilde{\lambda} \in \tilde{\lambda}$ .

*Proof.* Let  $\tilde{W} \in \mathbb{R}^{N \times N}$  and  $\tilde{L} \in \mathbb{R}^{N \times N}$  denote  $K$  block zero diagonal affinity matrix and associated Laplacian in which  $i$ th block has similarity with remaining  $K - 1$  number of blocks. For simplicity, let  $i = 1$ , i.e.

$$\tilde{W} = \begin{bmatrix} 0 & w_1 & \dots & w_1 & \tilde{w}_{1,2} & \dots & \tilde{w}_{1,2} & \dots & \tilde{w}_{1,K} & \dots & \tilde{w}_{1,K} \\ w_1 & 0 & \dots & w_1 & \tilde{w}_{1,2} & \dots & \tilde{w}_{1,2} & \dots & \tilde{w}_{1,K} & \dots & \tilde{w}_{1,K} \\ \vdots & \vdots & \ddots & \vdots & \vdots & \ddots & \vdots & \ddots & \vdots & \ddots & \vdots \\ w_1 & w_1 & \dots & 0 & \tilde{w}_{1,2} & \dots & \tilde{w}_{1,2} & \dots & \tilde{w}_{1,K} & \dots & \tilde{w}_{1,K} \\ \tilde{w}_{1,2} & \dots & \tilde{w}_{1,2} & 0 & w_2 & \dots & w_2 & \dots & \dots & \dots & \dots \\ \tilde{w}_{1,2} & \dots & \tilde{w}_{1,2} & w_2 & 0 & \dots & w_2 & \dots & \dots & \dots & \dots \\ \vdots & \vdots & \ddots & \vdots & \vdots & \ddots & \vdots & \ddots & \vdots & \ddots & \vdots \\ \tilde{w}_{1,2} & \dots & \tilde{w}_{1,2} & w_2 & w_2 & \dots & 0 & \dots & \dots & \dots & \dots \\ \vdots & \vdots & \ddots & \vdots & \vdots & \ddots & \vdots & \ddots & \vdots & \ddots & \vdots \\ \tilde{w}_{1,K} & \dots & \tilde{w}_{1,K} & \dots & \dots & \dots & 0 & w_K & \dots & w_K & \dots \\ \tilde{w}_{1,K} & \dots & \tilde{w}_{1,K} & \dots & \dots & \dots & w_K & 0 & \dots & w_K & \dots \\ \vdots & \vdots & \ddots & \vdots & \vdots & \ddots & \vdots & \ddots & \vdots & \ddots & \vdots \\ \tilde{w}_{1,K} & \dots & \tilde{w}_{1,K} & \dots & \dots & \dots & w_K & w_K & \dots & 0 & \dots \end{bmatrix}$$

and





where  $z_1 = N_1 w_1 + \sum_{j=2}^K N_j \tilde{w}_{1,j}$  and  $z_j = N_j w_j + N_1 \tilde{w}_{1,j}$  for  $j = 2, \dots, K$ . Using determinant properties of block matrices [2], it holds that

$$0 = \det(\mathbf{H}) \begin{vmatrix} -N_1 w_1 (z_1 - \tilde{\lambda})^{-1} + 1 & -N_2 \tilde{w}_{1,2} (z_2 - \tilde{\lambda})^{-1} & -N_3 \tilde{w}_{1,3} (z_3 - \tilde{\lambda})^{-1} & \dots & -N_K \tilde{w}_{1,K} (z_K - \tilde{\lambda})^{-1} \\ -N_1 \tilde{w}_{1,2} (z_1 - \tilde{\lambda})^{-1} & -N_2 w_2 (z_2 - \tilde{\lambda})^{-1} + 1 & 0 & \dots & 0 \\ -N_1 \tilde{w}_{1,3} (z_1 - \tilde{\lambda})^{-1} & 0 & -N_3 w_3 (z_3 - \tilde{\lambda})^{-1} + 1 & \dots & 0 \\ \vdots & \vdots & \vdots & \ddots & \vdots \\ -N_1 \tilde{w}_{1,K} (z_1 - \tilde{\lambda})^{-1} & 0 & \dots & \dots & -N_K w_K (z_K - \tilde{\lambda})^{-1} + 1 \end{vmatrix}.$$

To simplify the determinant of the first matrix, it transformed into a lower diagonal matrix by applying the following Gaussian elimination steps

$$\begin{aligned} & \frac{N_2 \tilde{w}_{1,2} (z_2 - \tilde{\lambda})^{-1}}{-N_2 w_2 (z_2 - \tilde{\lambda})^{-1} + 1} R_2 + R_1 \rightarrow R_1 \\ & \frac{N_3 \tilde{w}_{1,3} (z_3 - \tilde{\lambda})^{-1}}{-N_3 w_3 (z_3 - \tilde{\lambda})^{-1} + 1} R_3 + R_1 \rightarrow R_1 \\ & \vdots \\ & \frac{N_K \tilde{w}_{1,K} (z_K - \tilde{\lambda})^{-1}}{-N_K w_K (z_K - \tilde{\lambda})^{-1} + 1} R_K + R_1 \rightarrow R_1 \end{aligned}$$

where  $R_K$  denotes  $K$ th row. Then, the simplified determinant yields

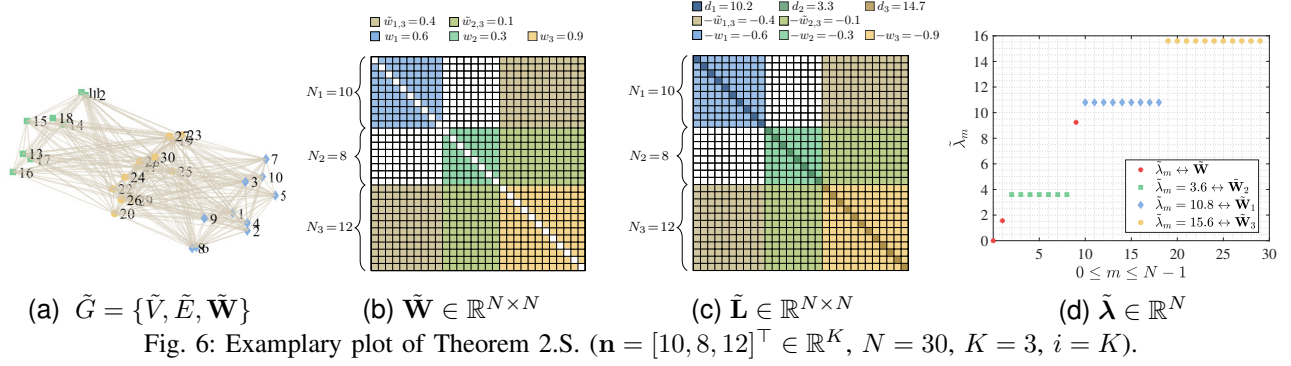
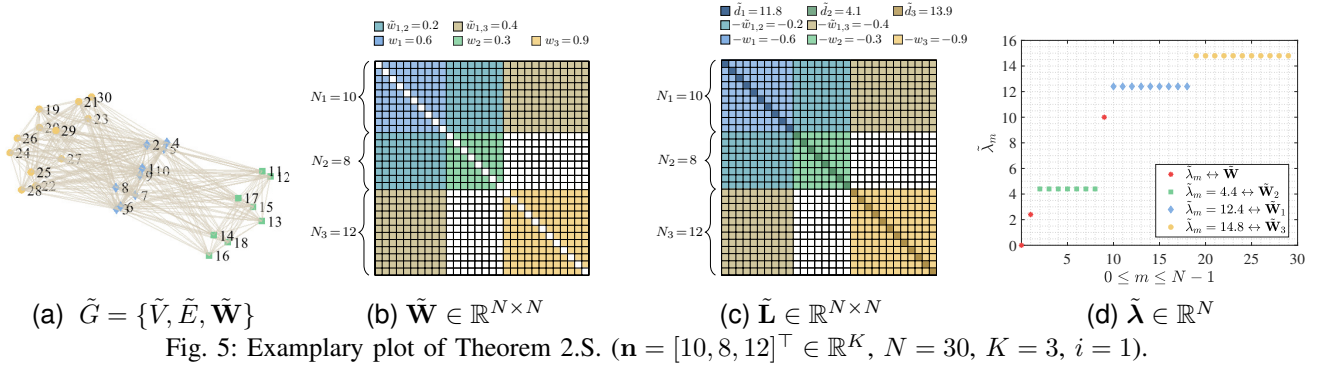
$$0 = \det(\mathbf{H}) \begin{vmatrix} c_1 & 0 & 0 & \dots & 0 \\ -N_1 \tilde{w}_{1,2} (z_1 - \tilde{\lambda})^{-1} & -N_2 w_2 (z_2 - \tilde{\lambda})^{-1} + 1 & 0 & \dots & 0 \\ -N_1 \tilde{w}_{1,3} (z_1 - \tilde{\lambda})^{-1} & 0 & -N_3 w_3 (z_3 - \tilde{\lambda})^{-1} + 1 & \dots & 0 \\ \vdots & \vdots & \vdots & \ddots & \vdots \\ -N_1 \tilde{w}_{1,K} (z_1 - \tilde{\lambda})^{-1} & 0 & \dots & \dots & -N_K w_K (z_K - \tilde{\lambda})^{-1} + 1 \end{vmatrix}$$

where  $c_1$  equals to

$$c_1 = -N_1 w_1 (z_1 - \tilde{\lambda})^{-1} + 1 - \frac{N_2 \tilde{w}_{1,2} (z_2 - \tilde{\lambda})^{-1} N_1 \tilde{w}_{1,2} (z_1 - \tilde{\lambda})^{-1}}{-N_2 w_2 (z_2 - \tilde{\lambda})^{-1} + 1} - \dots - \frac{N_K \tilde{w}_{1,K} (z_K - \tilde{\lambda})^{-1} N_1 \tilde{w}_{1,K} (z_1 - \tilde{\lambda})^{-1}}{-N_K w_K (z_K - \tilde{\lambda})^{-1} + 1}.$$

For  $z_1 = N_1 w_1 + \sum_{j=2}^K N_j \tilde{w}_{1,j}$  and  $z_j = N_j w_j + N_1 \tilde{w}_{1,j}$  such that  $j = 2, \dots, K$ , the determinant  $\det(\tilde{\mathbf{L}} - \tilde{\lambda} \mathbf{I}) = 0$  yields

$$\begin{aligned} 0 &= (z_1 - \tilde{\lambda})^{N_1} (z_2 - \tilde{\lambda})^{N_2} \dots (z_K - \tilde{\lambda})^{N_K} (-N_2 w_2 (z_2 - \tilde{\lambda})^{-1} + 1) \dots (-N_K w_K (z_K - \tilde{\lambda})^{-1} + 1) c_1 \\ 0 &= (z_1 - \tilde{\lambda})^{N_1} (-N_2 w_2 (z_2 - \tilde{\lambda})^{N_2 - 1} + (z_2 - \tilde{\lambda})^{N_2}) \dots (-N_K w_K (z_K - \tilde{\lambda})^{N_K - 1} + (z_K - \tilde{\lambda})^{N_K}) c_1 \\ 0 &= (z_1 - \tilde{\lambda})^{N_1} (z_2 - \tilde{\lambda})^{N_2 - 1} \dots (z_K - \tilde{\lambda})^{N_K - 1} (-N_2 w_2 + z_2 - \tilde{\lambda}) \dots (-N_K w_K + z_K - \tilde{\lambda}) c_1 \\ 0 &= (z_1 - \tilde{\lambda})^{N_1} (z_2 - \tilde{\lambda})^{N_2 - 1} \dots (z_K - \tilde{\lambda})^{N_K - 1} (-N_2 w_2 + z_2 - \tilde{\lambda}) \dots (-N_K w_K + z_K - \tilde{\lambda}) \\ & \quad (z_1 - \tilde{\lambda})^{-1} \left( -N_1 w_1 + z_1 - \tilde{\lambda} - \frac{N_2 \tilde{w}_{1,2} (z_2 - \tilde{\lambda})^{-1} N_1 \tilde{w}_{1,2}}{-N_2 w_2 (z_2 - \tilde{\lambda})^{-1} + 1} - \dots - \frac{N_K \tilde{w}_{1,K} (z_K - \tilde{\lambda})^{-1} N_1 \tilde{w}_{1,K}}{-N_K w_K (z_K - \tilde{\lambda})^{-1} + 1} \right) \\ 0 &= (z_1 - \tilde{\lambda})^{N_1 - 1} (z_2 - \tilde{\lambda})^{N_2 - 1} \dots (z_K - \tilde{\lambda})^{N_K - 1} (-N_2 w_2 + z_2 - \tilde{\lambda}) \dots (-N_K w_K + z_K - \tilde{\lambda}) \\ & \quad \left( -N_1 w_1 + z_1 - \tilde{\lambda} - \frac{N_2 \tilde{w}_{1,2} (z_2 - \tilde{\lambda})^{-1} N_1 \tilde{w}_{1,2}}{-N_2 w_2 (z_2 - \tilde{\lambda})^{-1} + 1} - \dots - \frac{N_K \tilde{w}_{1,K} (z_K - \tilde{\lambda})^{-1} N_1 \tilde{w}_{1,K}}{-N_K w_K (z_K - \tilde{\lambda})^{-1} + 1} \right) \\ 0 &= \left( N_1 w_1 + \sum_{j=2}^K N_j \tilde{w}_{1,j} - \tilde{\lambda} \right)^{N_1 - 1} \left( N_2 w_2 + N_1 \tilde{w}_{1,2} - \tilde{\lambda} \right)^{N_2 - 1} \dots \left( N_K w_K + N_1 \tilde{w}_{1,K} - \tilde{\lambda} \right)^{N_K - 1} (N_1 \tilde{w}_{1,2} - \tilde{\lambda}) \dots (N_1 \tilde{w}_{1,K} - \tilde{\lambda}) \\ & \quad \left( \sum_{j=2}^K N_j \tilde{w}_{1,j} - \tilde{\lambda} - \frac{N_1 N_2 \tilde{w}_{1,2}^2}{N_1 \tilde{w}_{1,2} - \tilde{\lambda}} - \dots - \frac{N_1 N_K \tilde{w}_{1,K}^2}{N_1 \tilde{w}_{1,K} - \tilde{\lambda}} \right) \\ 0 &= \left( N_1 w_1 + \sum_{j=2}^K N_j \tilde{w}_{1,j} - \tilde{\lambda} \right)^{N_1 - 1} \left( N_2 w_2 + N_1 \tilde{w}_{1,2} - \tilde{\lambda} \right)^{N_2 - 1} \dots \left( N_K w_K + N_1 \tilde{w}_{1,K} - \tilde{\lambda} \right)^{N_K - 1} (N_1 \tilde{w}_{1,2} - \tilde{\lambda}) \dots (N_1 \tilde{w}_{1,K} - \tilde{\lambda}) \\ & \quad \left( -\frac{N_2 \tilde{w}_{1,2} \tilde{\lambda}}{N_1 \tilde{w}_{1,2} - \tilde{\lambda}} \dots - \frac{N_K \tilde{w}_{1,K} \tilde{\lambda}}{N_1 \tilde{w}_{1,K} - \tilde{\lambda}} - \tilde{\lambda} \right) \\ 0 &= \left( N_1 w_1 + \sum_{j=2}^K N_j \tilde{w}_{1,j} - \tilde{\lambda} \right)^{N_1 - 1} \left( N_2 w_2 + N_1 \tilde{w}_{1,2} - \tilde{\lambda} \right)^{N_2 - 1} \dots \left( N_K w_K + N_1 \tilde{w}_{1,K} - \tilde{\lambda} \right)^{N_K - 1} (N_1 \tilde{w}_{1,2} - \tilde{\lambda}) \dots (N_1 \tilde{w}_{1,K} - \tilde{\lambda}) \tilde{\lambda} \\ & \quad \left( -\frac{N_2 \tilde{w}_{1,2}}{N_1 \tilde{w}_{1,2} - \tilde{\lambda}} \dots - \frac{N_K \tilde{w}_{1,K}}{N_1 \tilde{w}_{1,K} - \tilde{\lambda}} - 1 \right) \end{aligned}$$



Based on this,  $N + 1 - K$  number of eigenvalues are

$$\left\{ \begin{array}{l} N_1 - 1 \text{ elements of } \tilde{\lambda} \text{ equal to } N_1 w_1 + \sum_{j=2}^K N_j \tilde{w}_{1,j} \\ N_2 - 1 \text{ elements of } \tilde{\lambda} \text{ equal to } N_2 w_2 + N_1 \tilde{w}_{1,2} \\ \vdots \\ N_K - 1 \text{ elements of } \tilde{\lambda} \text{ equal to } N_K w_K + N_1 \tilde{w}_{1,K} \\ \text{the smallest element of } \tilde{\lambda} \text{ equal to zero} \end{array} \right.$$

and additionally  $K - 1$  number of eigenvalues are roots of the following equation

$$(N_1 \tilde{w}_{1,2} - \tilde{\lambda}) \dots (N_1 \tilde{w}_{1,K} - \tilde{\lambda}) \left( -\frac{N_2 \tilde{w}_{1,2}}{N_1 \tilde{w}_{1,2} - \tilde{\lambda}} \dots -\frac{N_K \tilde{w}_{1,K}}{N_1 \tilde{w}_{1,K} - \tilde{\lambda}} - 1 \right) = \prod_{j=2}^K (N_1 \tilde{w}_{1,j} - \tilde{\lambda}) \left( -\sum_{j=2}^K \frac{N_j \tilde{w}_{1,j}}{N_1 \tilde{w}_{1,j} - \tilde{\lambda}} - 1 \right) = 0$$

where  $i = 1$ . □



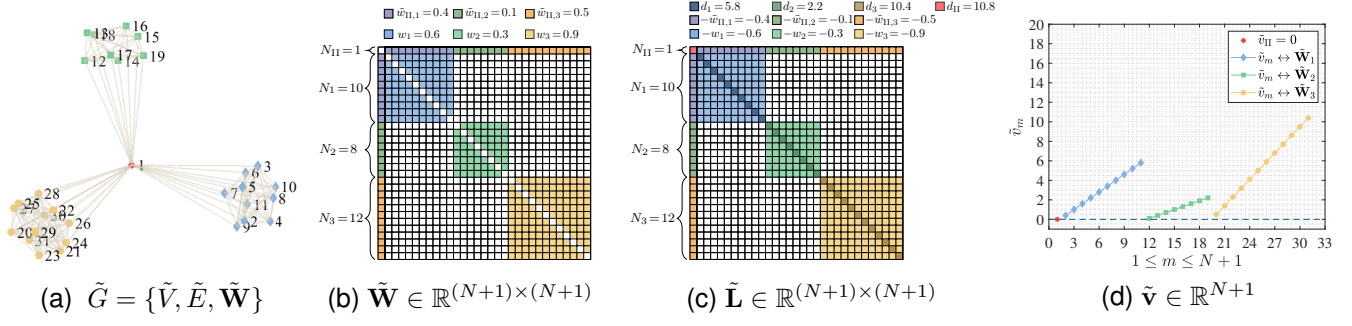


Fig. 7: Exemplary plot of Theorem 3 ( $\mathbf{n} = [1, 10, 8, 12]^\top \in \mathbb{R}^{K+1}$ ,  $N + 1 = 31$ ,  $K = 3$ ,  $m_{\text{II}} = 1$ ).

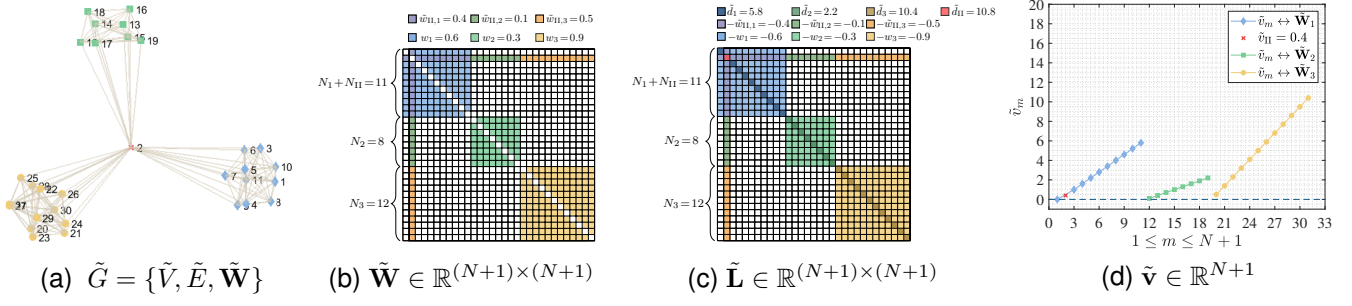


Fig. 8: Exemplary plot of Theorem 3 ( $\mathbf{n} = [1, 1, 9, 8, 12]^\top \in \mathbb{R}^{K+2}$ ,  $N + 1 = 31$ ,  $K = 3$ ,  $m_{\text{II}} = 2$ ).

Then, for each position of the outlier such that  $0 < m_{\text{II}} \leq N + 1$ ,  $m_{\text{II}} \in \mathbb{Z}^+$ , the vector  $\tilde{v}$  is computed as

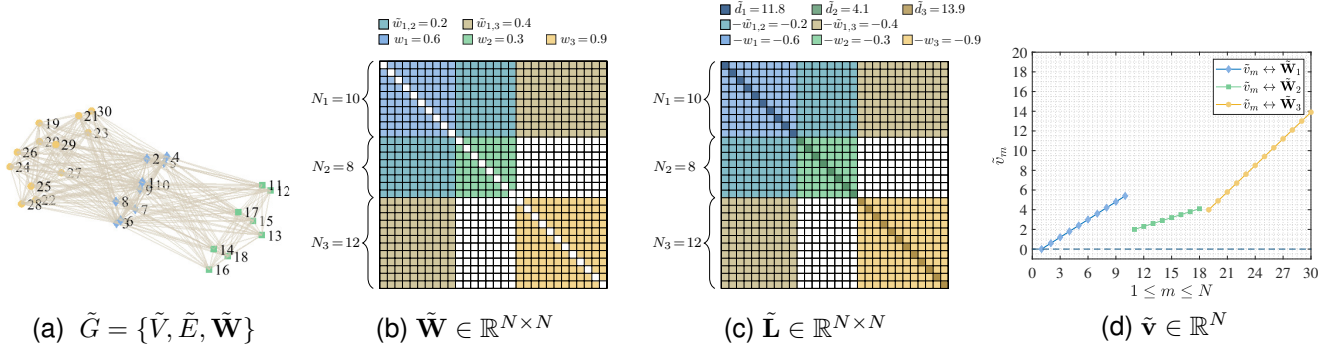
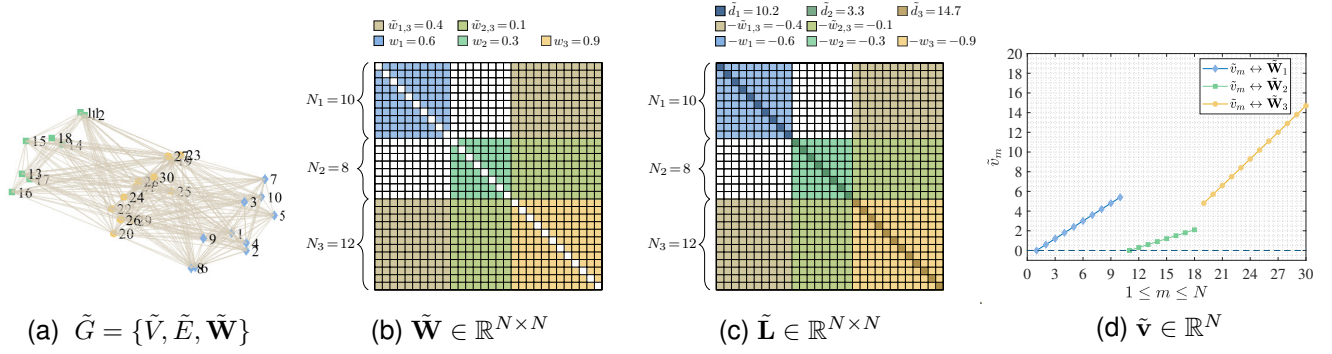
$$\begin{aligned} \tilde{\mathbf{v}}_{(m_{\text{II}}=1)} &= \underbrace{\begin{bmatrix} 0 \\ \tilde{w}_{\text{II},1}, \tilde{w}_{\text{II},1} + w_1, \dots, \tilde{w}_{\text{II},1} + (N_1 - 1)w_1, \tilde{w}_{\text{II},2}, \tilde{w}_{\text{II},2} + w_2, \dots, \tilde{w}_{\text{II},2} + (N_2 - 1)w_2, \dots, \tilde{w}_{\text{II},K}, \tilde{w}_{\text{II},K} + w_K, \dots, \tilde{w}_{\text{II},K} + (N_K - 1)w_K \end{bmatrix}}_{\tilde{\mathbf{v}}_{\text{II}} \in \mathbb{R}} \\ &= \underbrace{\begin{bmatrix} 0 \\ \tilde{w}_{\text{II},1}, \tilde{w}_{\text{II},1} + w_1, \dots, \tilde{w}_{\text{II},1} + (N_1 - 1)w_1 \end{bmatrix}}_{\tilde{\mathbf{v}}_1 \in \mathbb{R}^{N_1}} \underbrace{\begin{bmatrix} \tilde{w}_{\text{II},2}, \tilde{w}_{\text{II},2} + w_2, \dots, \tilde{w}_{\text{II},2} + (N_2 - 1)w_2 \end{bmatrix}}_{\tilde{\mathbf{v}}_2 \in \mathbb{R}^{N_2}} \underbrace{\begin{bmatrix} \tilde{w}_{\text{II},K}, \tilde{w}_{\text{II},K} + w_K, \dots, \tilde{w}_{\text{II},K} + (N_K - 1)w_K \end{bmatrix}}_{\tilde{\mathbf{v}}_K \in \mathbb{R}^{N_K}} \\ \vdots \\ \tilde{\mathbf{v}}_{(m_{\text{II}}=\ell_2-1)} &= \underbrace{\begin{bmatrix} 0, w_1, \dots, (N_1 - 1)w_1 \end{bmatrix}}_{\tilde{\mathbf{v}}_1 \in \mathbb{R}^{N_1}} \underbrace{\begin{bmatrix} N_1 \tilde{w}_{\text{II},1}, \tilde{w}_{\text{II},2}, \tilde{w}_{\text{II},2} + w_2, \dots, \tilde{w}_{\text{II},2} + (N_2 - 1)w_2 \end{bmatrix}}_{\tilde{\mathbf{v}}_{\text{II}} \in \mathbb{R}} \underbrace{\begin{bmatrix} \tilde{w}_{\text{II},K}, \tilde{w}_{\text{II},K} + w_K, \dots, \tilde{w}_{\text{II},K} + (N_K - 1)w_K \end{bmatrix}}_{\tilde{\mathbf{v}}_K \in \mathbb{R}^{N_K}} \\ \vdots \\ \tilde{\mathbf{v}}_{(m_{\text{II}}=N+1)} &= \underbrace{\begin{bmatrix} 0, w_1, \dots, (N_1 - 1)w_1 \end{bmatrix}}_{\tilde{\mathbf{v}}_1 \in \mathbb{R}^{N_1}} \underbrace{\begin{bmatrix} 0, w_2, \dots, (N_2 - 1)w_2 \end{bmatrix}}_{\tilde{\mathbf{v}}_2 \in \mathbb{R}^{N_2}} \underbrace{\begin{bmatrix} 0, w_K, \dots, (N_K - 1)w_K \end{bmatrix}}_{\tilde{\mathbf{v}}_K \in \mathbb{R}^{N_K}} \underbrace{\sum_{j=1}^K N_j \tilde{w}_{\text{II},j}}_{\tilde{\mathbf{v}}_{\text{II}} \in \mathbb{R}} \end{aligned}$$

As it can be seen, the components, whose indexes are valued between the outlier index and the largest index of the  $j$ th block such that  $m_{\text{II}} < m \leq u_j$ , increase by  $\tilde{w}_{\text{II},j}$  in the corrupted vector  $\tilde{v} \in \mathbb{R}^{N+1}$ . Further, the component associated with the outlier is valued as follows

$$\tilde{v}_{\text{II}} = \begin{cases} 0 & \text{if } 0 < m_{\text{II}} < \ell_1 \\ (m_{\text{II}} - \ell_1) \tilde{w}_{\text{II},1} & \text{if } \ell_1 < m_{\text{II}} < \ell_2 \\ \vdots & \vdots \\ \sum_{j=1}^{K-1} N_j \tilde{w}_{\text{II},j} + (m_{\text{II}} - \ell_K) \tilde{w}_{\text{II},K} & \text{if } \ell_K < m_{\text{II}} \leq N + 1 \end{cases},$$

where  $\ell_j$  denotes the lowest index of the  $j$ th block for  $j = 1, \dots, K$ .  $\square$



Fig. 11: Exemplary plot of Theorem 4 ( $\mathbf{n} = [10, 8, 12]^\top \in \mathbb{R}^K$ ,  $N = 30$ ,  $K = 3$ ,  $i = 1$ ).Fig. 12: Exemplary plot of Theorem 4 ( $\mathbf{n} = [10, 8, 12]^\top \in \mathbb{R}^K$ ,  $N = 30$ ,  $K = 3$ ,  $i = K$ ).

Then, for each position of the block  $i$  such that  $i = 1, \dots, K$ , the vector  $\tilde{v} \in \mathbb{R}^N$  is computed as

$$\tilde{v}_{(i=1)} = \underbrace{[0, w_1, \dots, (N_1 - 1)w_1]}_{\tilde{v}_1 \in \mathbb{R}^{N_1}} \underbrace{, N_1 \tilde{w}_{1,2}, w_2 + N_1 \tilde{w}_{1,2}, \dots, (N_2 - 1)w_2 + N_1 \tilde{w}_{1,2}}_{\tilde{v}_2 \in \mathbb{R}^{N_2}} \underbrace{, \dots, N_1 \tilde{w}_{1,K}, w_K + N_1 \tilde{w}_{1,K}, \dots, (N_K - 1)w_K + N_1 \tilde{w}_{1,K}}_{\tilde{v}_K \in \mathbb{R}^{N_K}}$$

$$\vdots$$

$$\tilde{v}_{(i=K)} = \underbrace{[0, w_1, \dots, (N_1 - 1)w_1]}_{\tilde{v}_1 \in \mathbb{R}^{N_1}} \underbrace{, 0, w_2, \dots, (N_2 - 1)w_2, \dots}_{\tilde{v}_2 \in \mathbb{R}^{N_2}} \underbrace{, \sum_{j=1}^{K-1} N_j \tilde{w}_{K,j}, w_K + \sum_{j=1}^{K-1} N_j \tilde{w}_{K,j}, \dots, (N_K - 1)w_K + \sum_{j=1}^{K-1} N_j \tilde{w}_{K,j}}_{\tilde{v}_K \in \mathbb{R}^{N_K}}.$$

Herein, the components associated with the blocks  $j > i$  are increase by  $N_i \tilde{w}_{i,j}$  while remain the same on the contrary. Further, if  $2 \leq i \leq K$  the components associated with the block  $i$  increase by  $\sum_{j=1}^{i-1} N_j \tilde{w}_{i,j}$  and remain the same otherwise.

In more details, starting from the  $i+1$ th block undesired similarity blocks are located only on the lower triangular side. Therefore, summing upper triangular part of the Laplacian matrix results in an increase by  $N_i \tilde{w}_{i,j}$  in these blocks. Additionally, for the  $i$ th block  $i - 1$  number of undesired similarity blocks are located on the lower triangular side which results in an increase by  $\sum_{j=1}^{i-1} N_j \tilde{w}_{i,j}$ .

□

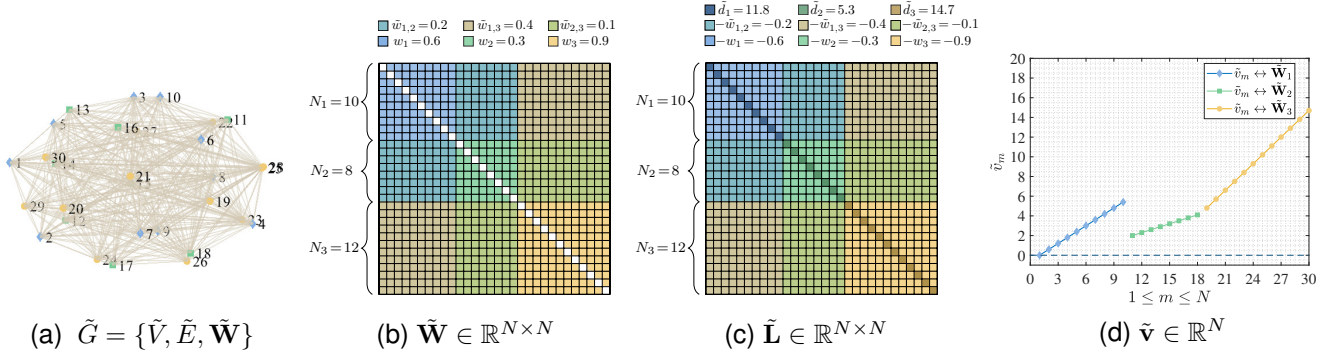


Fig. 13: Exemplary plot of Corollary 4.1 ( $\mathbf{n} = [10, 8, 12]^\top \in \mathbb{R}^K$ ,  $N = 30$ ,  $K = 3$ ).

### Proof of Corollary 4.1:

Let  $\tilde{L} \in \mathbb{R}^{N \times N}$  a corrupted Laplacian matrix, that is identical to  $L \in \mathbb{R}^{N \times N}$  except that each block  $i = 1, \dots, K$  has non-zero similarity coefficients with the remaining  $K - 1$  blocks, i.e.

$$\tilde{L} = \begin{bmatrix} \tilde{d}_1 & -w_1 & \dots & -w_1 & -\tilde{w}_{1,2} & -\tilde{w}_{1,2} & \dots & -\tilde{w}_{1,2} & \dots & -\tilde{w}_{1,K} & -\tilde{w}_{1,K} & \dots & -\tilde{w}_{1,K} \\ -w_1 & \tilde{d}_1 & \dots & -w_1 & -\tilde{w}_{1,2} & -\tilde{w}_{1,2} & \dots & -\tilde{w}_{1,2} & \dots & -\tilde{w}_{1,K} & -\tilde{w}_{1,K} & \dots & -\tilde{w}_{1,K} \\ \vdots & \vdots & \ddots & \vdots & \vdots & \vdots & \ddots & \vdots & \vdots & \vdots & \vdots & \ddots & \vdots \\ -w_1 & -w_1 & \dots & \tilde{d}_1 & -\tilde{w}_{1,2} & -\tilde{w}_{1,2} & \dots & -\tilde{w}_{1,2} & \dots & -\tilde{w}_{1,K} & -\tilde{w}_{1,K} & \dots & -\tilde{w}_{1,K} \\ -\tilde{w}_{1,2} & -\tilde{w}_{1,2} & \dots & -\tilde{w}_{1,2} & \tilde{d}_2 & -w_2 & \dots & -w_2 & \dots & -\tilde{w}_{2,K} & -\tilde{w}_{2,K} & \dots & -\tilde{w}_{2,K} \\ -\tilde{w}_{1,2} & -\tilde{w}_{1,2} & \dots & -\tilde{w}_{1,2} & -w_2 & \tilde{d}_2 & \dots & -w_2 & \dots & -\tilde{w}_{2,K} & -\tilde{w}_{2,K} & \dots & -\tilde{w}_{2,K} \\ \vdots & \vdots & \ddots & \vdots & \vdots & \vdots & \ddots & \vdots & \vdots & \vdots & \vdots & \ddots & \vdots \\ -\tilde{w}_{1,2} & -\tilde{w}_{1,2} & \dots & -\tilde{w}_{1,2} & -w_2 & -w_2 & \dots & \tilde{d}_2 & \dots & -\tilde{w}_{2,K} & -\tilde{w}_{2,K} & \dots & -\tilde{w}_{2,K} \\ \vdots & \vdots & \ddots & \vdots & \vdots & \vdots & \ddots & \vdots & \ddots & \vdots & \vdots & \ddots & \vdots \\ -\tilde{w}_{1,K} & -\tilde{w}_{1,K} & \dots & -\tilde{w}_{1,K} & -\tilde{w}_{2,K} & -\tilde{w}_{2,K} & \dots & -\tilde{w}_{2,K} & \dots & \tilde{d}_K & -w_K & \dots & -w_K \\ -\tilde{w}_{1,K} & -\tilde{w}_{1,K} & \dots & -\tilde{w}_{1,K} & -\tilde{w}_{2,K} & -\tilde{w}_{2,K} & \dots & -\tilde{w}_{2,K} & \dots & -w_K & \tilde{d}_K & \dots & -w_K \\ \vdots & \vdots & \ddots & \vdots & \vdots & \vdots & \ddots & \vdots & \vdots & \vdots & \vdots & \ddots & \vdots \\ -\tilde{w}_{1,K} & -\tilde{w}_{1,K} & \dots & -\tilde{w}_{1,K} & -\tilde{w}_{2,K} & -\tilde{w}_{2,K} & \dots & -\tilde{w}_{2,K} & \dots & -w_K & -w_K & \dots & \tilde{d}_K \end{bmatrix}.$$

Then, the vector  $\tilde{v}$  associated with  $\tilde{L}$  yields

$$\tilde{v} = \underbrace{[0, w_1, \dots, (N_1 - 1)w_1]}_{\tilde{v}_1 \in \mathbb{R}^{N_1}}, \underbrace{[N_1 \tilde{w}_{1,2}, w_2 + N_1 \tilde{w}_{1,2}, \dots, (N_2 - 1)w_2 + N_1 \tilde{w}_{1,2}, \dots]}_{\tilde{v}_2 \in \mathbb{R}^{N_2}}, \underbrace{\left[ \sum_{i=1}^{K-1} N_i \tilde{w}_{i,K}, w_K + \sum_{i=1}^{K-1} N_i \tilde{w}_{i,K}, \dots, (N_K - 1)w_K + \sum_{i=1}^{K-1} N_i \tilde{w}_{i,K} \right]}_{\tilde{v}_K \in \mathbb{R}^{N_K}}$$

which concludes the proof that the vector  $\tilde{v}$  is piece-wise linear function in the following form

$$\tilde{v}_m = \tilde{f}(m) = \begin{cases} (m - \ell_1)w_1 & \text{if } \ell_1 \leq m \leq u_1 \\ (u_1 - \ell_1 + 1)\tilde{w}_{1,2} + (m - \ell_2)w_2 & \text{if } \ell_2 \leq m \leq u_2 \\ \vdots \\ \sum_{i=1}^{K-1} (u_i - \ell_i + 1)\tilde{w}_{i,K} + (m - \ell_K)w_K & \text{if } \ell_K \leq m \leq u_K \end{cases}$$

where  $\ell_1=1$ ,  $u_1=N_1$ ,  $\ell_i=\sum_{k=1}^{i-1} N_k + 1$  and  $u_i=\sum_{k=1}^i N_k$  for  $i=2, \dots, K$ .  $\square$

## APPENDIX D: THE GENERALIZED MATRIX DETERMINANT LEMMA

Let  $\mathbf{M} \in \mathbb{R}^{2N \times 2N}$  be a block matrix that can be shown as

$$\begin{bmatrix} \mathbf{H} & \mathbf{U} \\ -\mathbf{V}^\top & \mathbf{I} \end{bmatrix}$$

where  $\mathbf{I} \in \mathbb{R}^{N \times N}$  is the identity matrix and  $\mathbf{H}, \mathbf{U}, \mathbf{V} \in \mathbb{R}^{N \times N}$ . Using determinant properties of block matrices with non-commuting blocks [2], for  $-\mathbf{V}^\top \mathbf{I} = \mathbf{I}(-\mathbf{V}^\top)$  the determinant of  $\mathbf{M}$  can be written as follows

$$\det(\mathbf{M}) = \det(\mathbf{H}\mathbf{I} - \mathbf{U}(-\mathbf{V}^\top)) = \det(\mathbf{H} + \mathbf{U}\mathbf{V}^\top).$$

Now, the next step is to simplify the determinant  $\det(\mathbf{H} + \mathbf{U}\mathbf{V}^\top)$  by computing a block diagonal matrix using Gaussian elimination. First, the entry under  $\mathbf{H}$  is eliminated as follows

$$\begin{bmatrix} \mathbf{I} & \mathbf{0} \\ \mathbf{V}^\top \mathbf{H}^\dagger & \mathbf{I} \end{bmatrix} \begin{bmatrix} \mathbf{H} & \mathbf{U} \\ -\mathbf{V}^\top & \mathbf{I} \end{bmatrix} = \begin{bmatrix} \mathbf{H} & \mathbf{U} \\ \mathbf{0} & \mathbf{V}^\top \mathbf{H}^\dagger \mathbf{U} + \mathbf{I} \end{bmatrix}.$$

Then, the entry above  $\mathbf{I}$  is eliminated as

$$\begin{bmatrix} \mathbf{H} & \mathbf{U} \\ -\mathbf{V}^\top & \mathbf{I} \end{bmatrix} \begin{bmatrix} \mathbf{I} & -\mathbf{H}^\dagger \mathbf{U} \\ \mathbf{0} & \mathbf{I} \end{bmatrix} = \begin{bmatrix} \mathbf{H} & \mathbf{0} \\ -\mathbf{V}^\top & \mathbf{V}^\top \mathbf{H}^\dagger \mathbf{U} + \mathbf{I} \end{bmatrix}.$$

Combining these two operations leads to

$$\begin{bmatrix} \mathbf{I} & \mathbf{0} \\ \mathbf{V}^\top \mathbf{H}^\dagger & \mathbf{I} \end{bmatrix} \begin{bmatrix} \mathbf{H} & \mathbf{U} \\ -\mathbf{V}^\top & \mathbf{I} \end{bmatrix} \begin{bmatrix} \mathbf{I} & -\mathbf{H}^\dagger \mathbf{U} \\ \mathbf{0} & \mathbf{I} \end{bmatrix} = \begin{bmatrix} \mathbf{H} & \mathbf{0} \\ \mathbf{0} & \mathbf{V}^\top \mathbf{H}^\dagger \mathbf{U} + \mathbf{I} \end{bmatrix}.$$

Consequently, the determinant yields

$$\det \left( \begin{bmatrix} \mathbf{I} & \mathbf{0} \\ \mathbf{V}^\top \mathbf{H}^\dagger & \mathbf{I} \end{bmatrix} \begin{bmatrix} \mathbf{H} & \mathbf{U} \\ -\mathbf{V}^\top & \mathbf{I} \end{bmatrix} \begin{bmatrix} \mathbf{I} & -\mathbf{H}^\dagger \mathbf{U} \\ \mathbf{0} & \mathbf{I} \end{bmatrix} \right) = \det \left( \begin{bmatrix} \mathbf{H} & \mathbf{0} \\ \mathbf{0} & \mathbf{V}^\top \mathbf{H}^\dagger \mathbf{U} + \mathbf{I} \end{bmatrix} \right).$$

$$\det(\mathbf{H} + \mathbf{U}\mathbf{V}^\top) = \det(\mathbf{H})\det(\mathbf{I} + \mathbf{V}^\top \mathbf{H}^\dagger \mathbf{U})$$



APPENDIX E: REAL-WORLD DATA EXAMPLES

E.1 Type I Outliers' Occurrence Analysis

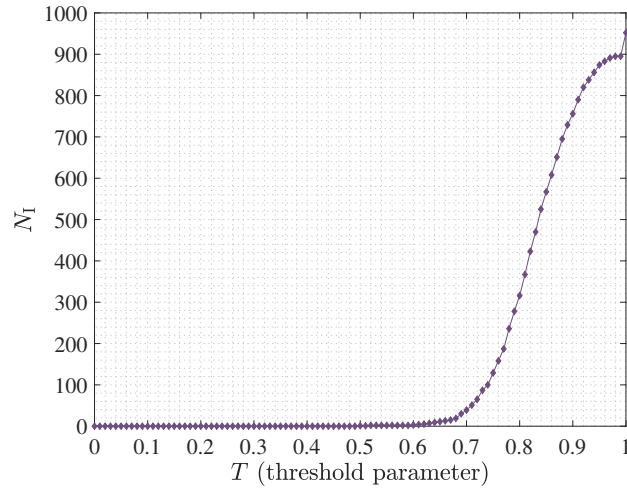


Fig. 14: Type I outliers' occurrence in MNIST [3] data base for increasing sparsity. An initial affinity matrix is defined by  $\mathbf{W} = \mathbf{X}^T \mathbf{X}$  and the example graphs are obtained by removing the edges whose corresponding edge weight is smaller than the defined threshold value  $T$ .

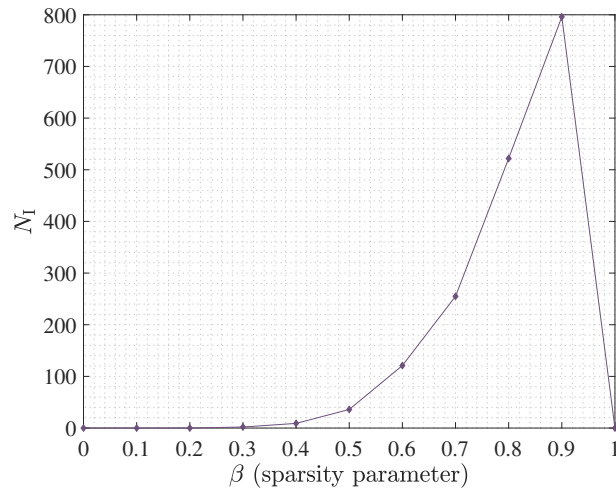


Fig. 15: Example of Type I outliers' occurrence in the MNIST [3] data base for an increasing sparsity level. Sparse affinity matrices are computed based on elastic net similarity measure for an increasing value of the penalty parameter  $\beta$ .

## E.2 Exemplary Deviations from the Target Vector $\mathbf{v}$

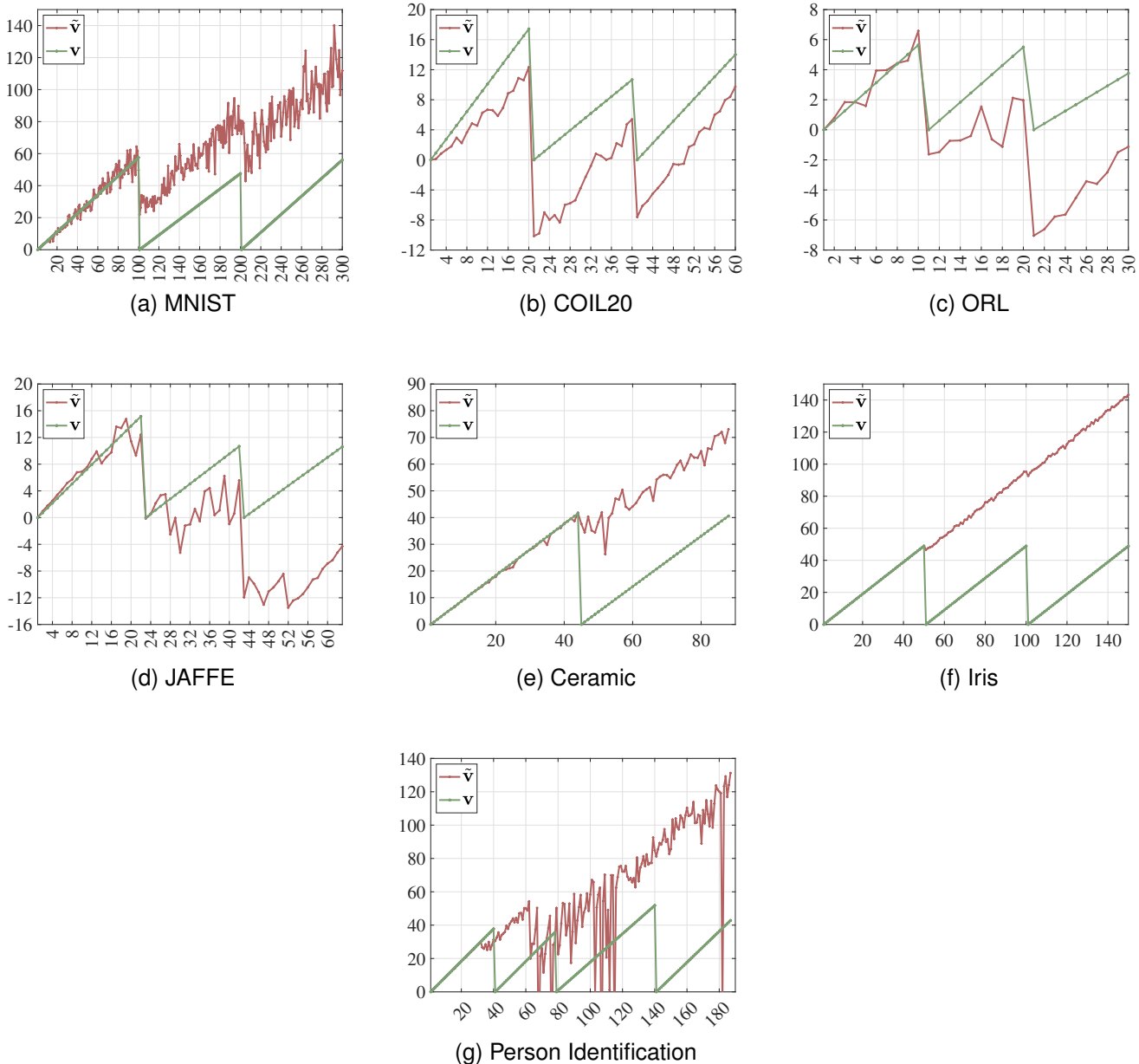


Fig. 16: Deviations from the ideal vector  $\mathbf{v}$  based on the initial affinity matrix structure, i.e.,  $\mathbf{W} = \mathbf{X}^\top \mathbf{X}$  for different data sets. The observed outlier effects are consistent with the derived theory.

The deviations from an “ideal” piece-wise linear function is related to the structure of the affinity matrix, e.g. if it produces an internally dense cluster structure, and if it includes Type I and Type II outliers and/or group similarity. This means that the chosen similarity measure and the determined level of sparsity will have a direct impact on the deviations from an “ideal” piece-wise linear function. Therefore, it is difficult to make general statements and the following discussion is based on examples from our own practice.

To analyze the assumed affinity matrix structure in Corollary 4.1 in comparison to the corrupted initial affinity matrix structure in real-world data sets, for every exemplary data set, we first compute the corrupted vector  $\tilde{\mathbf{v}}$  associated with the initial affinity matrix that is defined by  $\mathbf{W} = \mathbf{X}^\top \mathbf{X}$ . Similar to the theoretical analysis in Corollary 4.1, we consider deviations from the “ideal” piece-wise linear function  $\mathbf{v}$  that is computed by assuming that the similarity coefficients within the blocks are concentrated around the mean value. The obtained corrupted  $\tilde{\mathbf{v}}$  and that of the “ideal”  $\mathbf{v}$  structures are shown in Fig. 16 for different real-world data sets. As can be seen, undesired similarity coefficients between different blocks result in shifts from the “ideal” piece-wise linear functions starting from the second linear pieces, consistent with our theory in Corollary 4.1.

In particular, assumptions and findings of Corollary 4.1 hold in real-world data sets, especially, when the data sets include densely connected clusters of points, e.g. Ceramic [4] and Iris [5]. Additionally, corrupted data sets, e.g. Person Identification [6] whose corresponding affinity matrix is subject to Type I outliers and group similarity results in large deviations from the “ideal” piece-wise linear function with group similarity shifts and small-valued  $\tilde{\mathbf{v}}$  components corresponding to Type I outliers as it has been theoretically shown in Section IV of the FRS-BDR paper. Even though highly corrupted data sets generate large deviations from the assumed models in real-world scenarios, an appropriate block diagonal representation suppresses these outlier effects by providing an optimal level of sparsity as it is exemplified in Fig. 17.

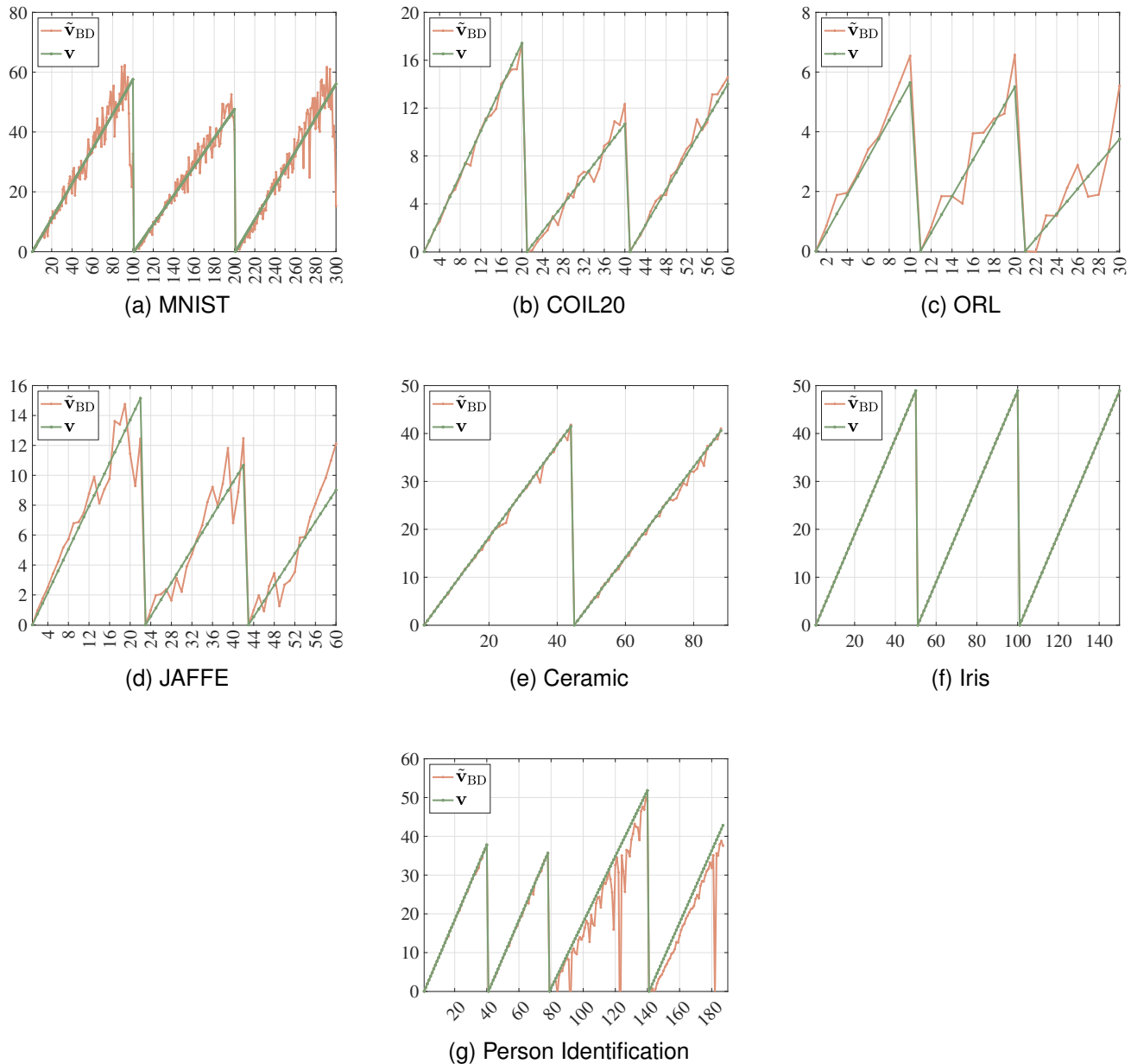


Fig. 17: Deviations from the ideal vector  $\mathbf{v}$  based on block diagonally structured affinity matrices for different data sets. After removing all between-cluster edges, the remaining deviations are from noisy or heterogeneously connected within-cluster edges.

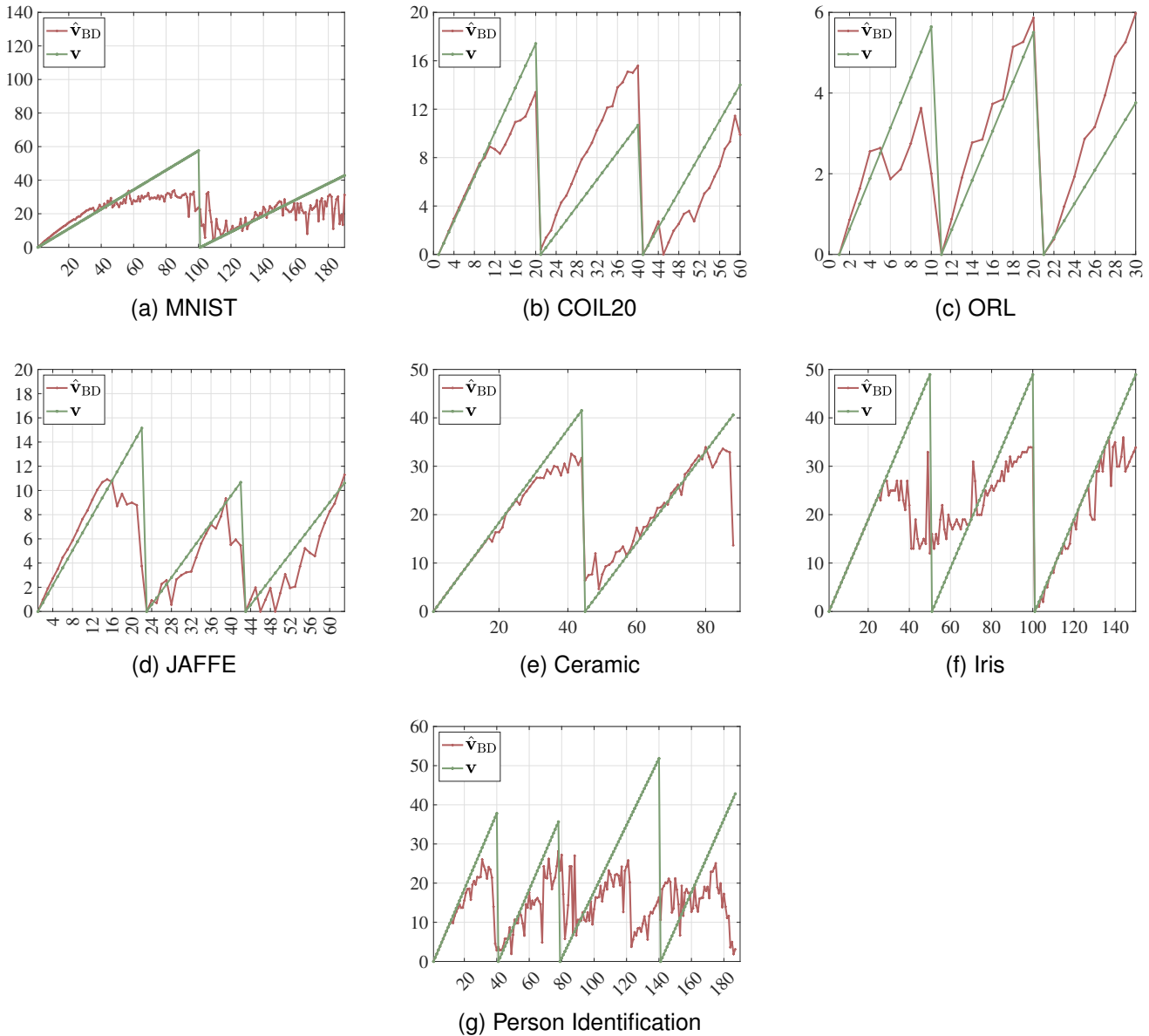
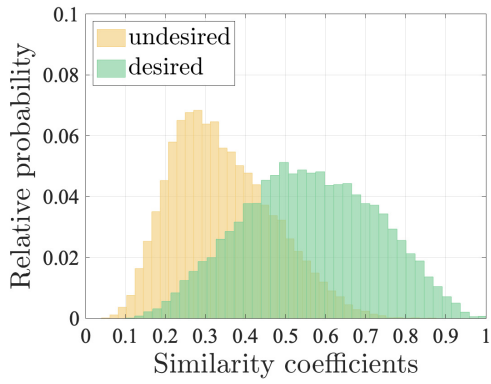


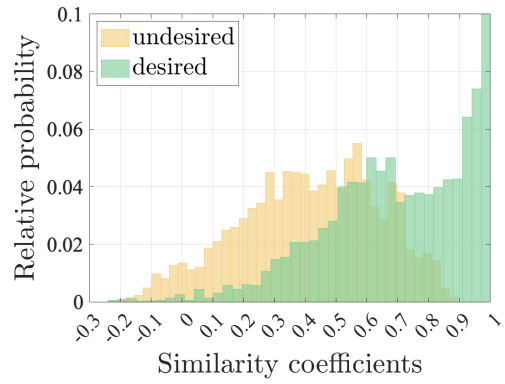
Fig. 18: Deviations from the ideal vector  $\mathbf{v}$  based on the estimated block diagonally structured affinity matrix for different data sets.

A further set of analysis illustrating the deviations from “ideal” piece-wise linear functions, “ideal”  $\mathbf{v}$  vectors and corresponding vector  $\hat{\mathbf{v}}_{\text{BD}}$  approximations, that represent the estimated FRS-BDR block diagonal affinity matrix structures, are provided in Fig. 18 for different data sets. As can be seen, heavily corrupted data sets, such as, Person Identification [6] result in large deviations from the “ideal” piece-wise linear function, while densely connected more easily separable clusters of points such as in the Ceramic [4] data set provide reasonably good approximations to the “ideal” structure. Although intra-cluster edges may result in large deviations from the determined “ideal” piece-wise linear functions in outlier-corrupted data sets, it is important to see that FRS-BDR algorithm removes the undesired edges between clusters in almost all cases, which is sufficient to obtain high clustering performance in these example. Another important point is that deviations from the “ideal” piece-wise linear function are considerably small for the FRS-BDR algorithm-based affinity matrix construction in comparison to the corrupted piece-wise linear function that has been shown in Fig. 16.

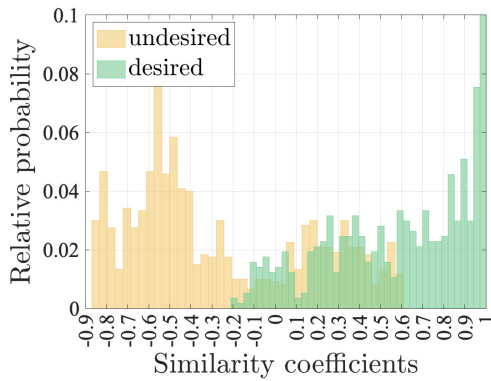
E.3 Similarity Coefficients' Analysis



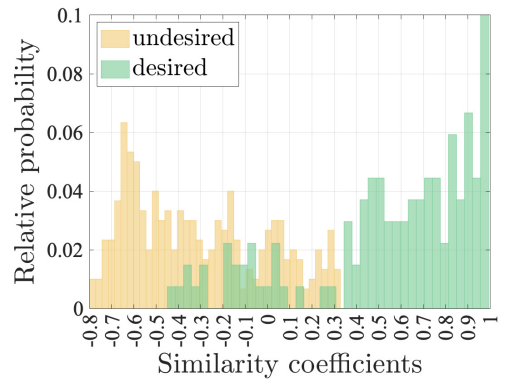
(a) MNIST



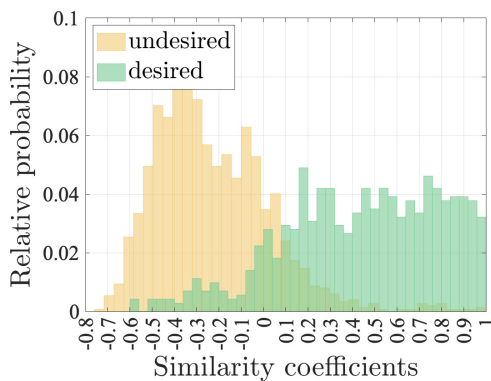
(b) USPS



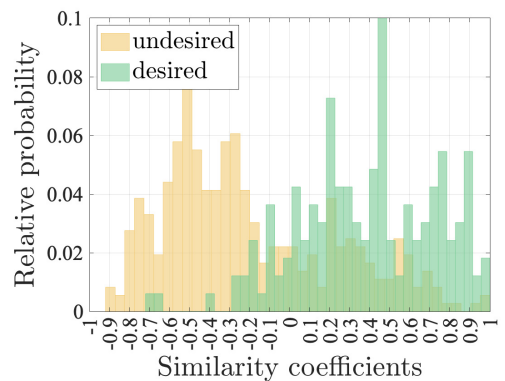
(c) COIL20



(d) ORL



(e) JAFFE

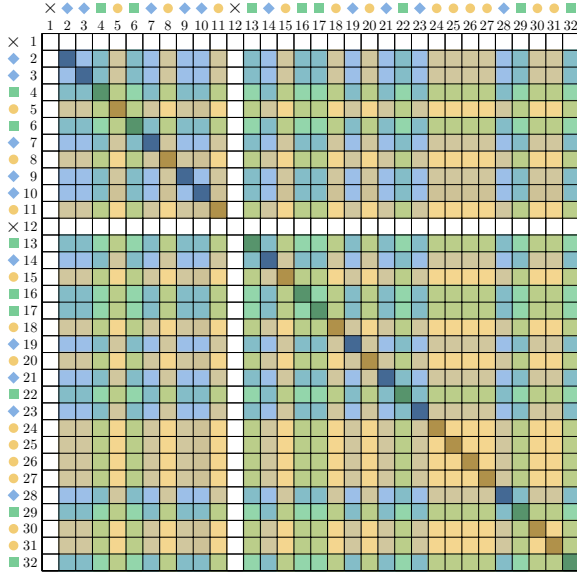


(f) YALE

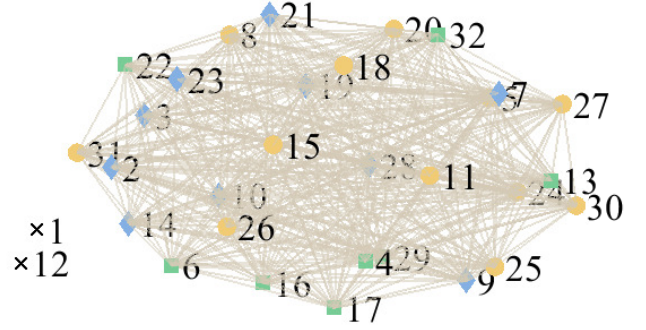
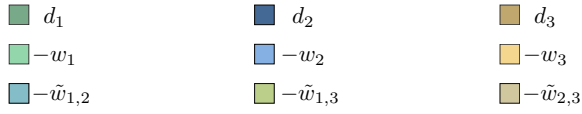
Fig. 19: Relative probability of similarity coefficients for different data sets.

APPENDIX F: ADDITIONAL INFORMATION FOR FRS-BDR

F.1 Visual Summary of FRS-BDR



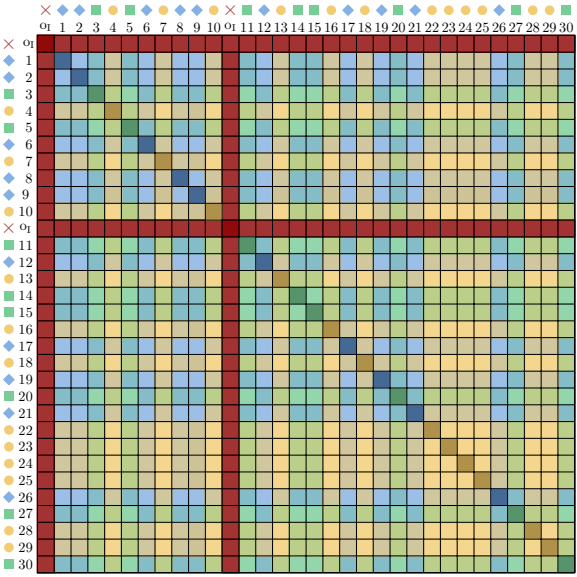
$$\mathbf{L} \in \mathbb{R}^{N \times N}$$



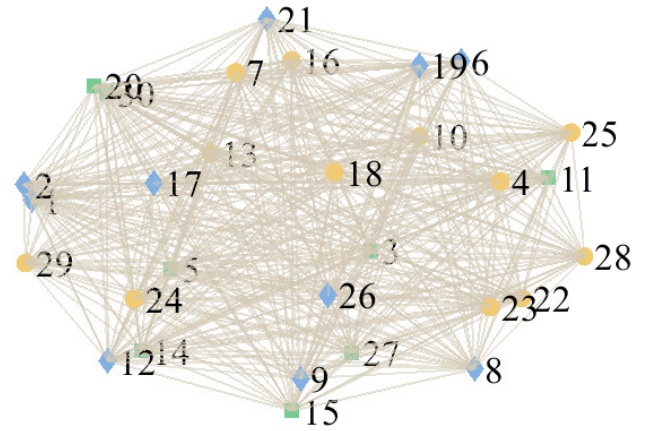
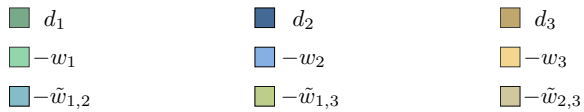
$$G = \{V, E, \mathbf{W}\}$$

$$\square d_1 = -w_1 = 0$$

(a) Initialization



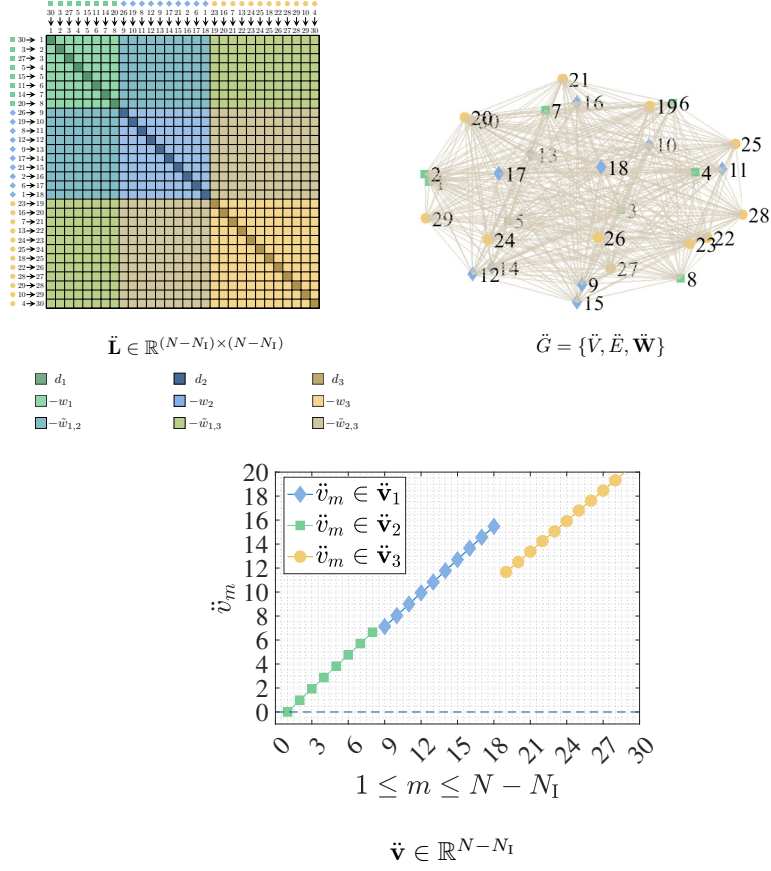
$$\hat{\mathbf{L}} \in \mathbb{R}^{(N-N_I) \times (N-N_I)}$$



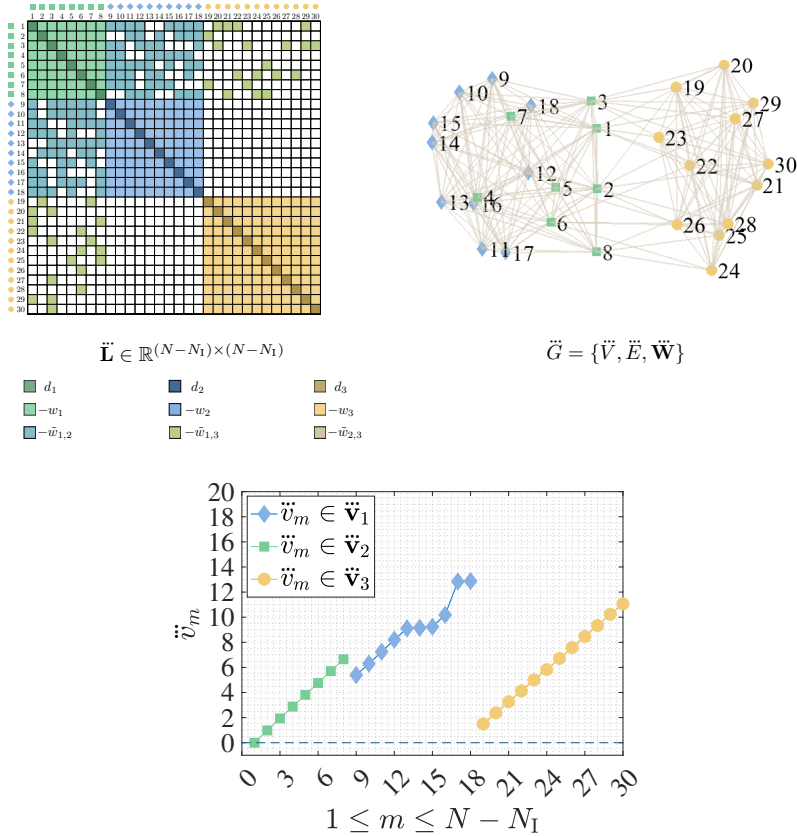
$$\hat{G} = \{\hat{V}, \hat{E}, \hat{\mathbf{W}}\}$$

$$\blacksquare d_1 = -w_1 \notin \hat{\mathbf{L}}$$

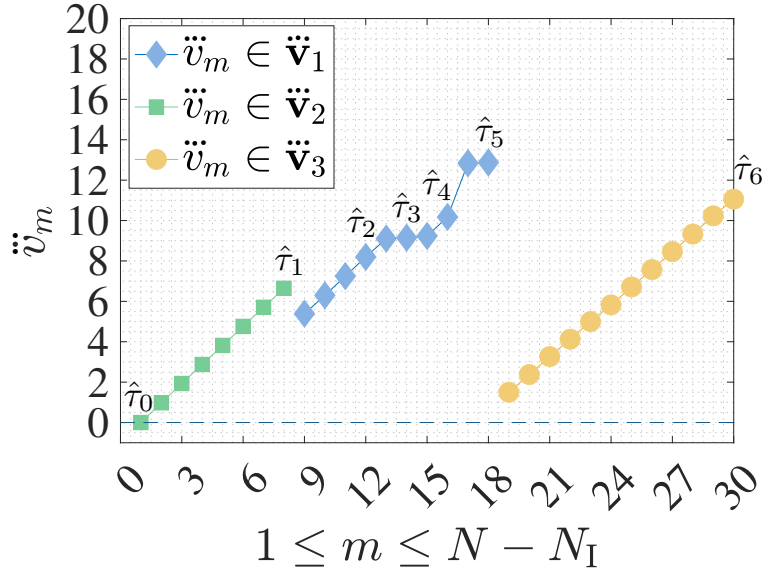
(b) Step 1.1: Type I Outlier Removal



(c) Step 1.2: Similarity-based Block Diagonal Ordering (sBDO)



(d) Step 1.3: Increase Sparsity for Excessive Group Similarity



$$(N_c = 2 \times K_{\text{cand}} = 2 \times 3 = 6)$$

$$\ddot{\mathbf{v}} \in \mathbb{R}^{N-N_I}$$

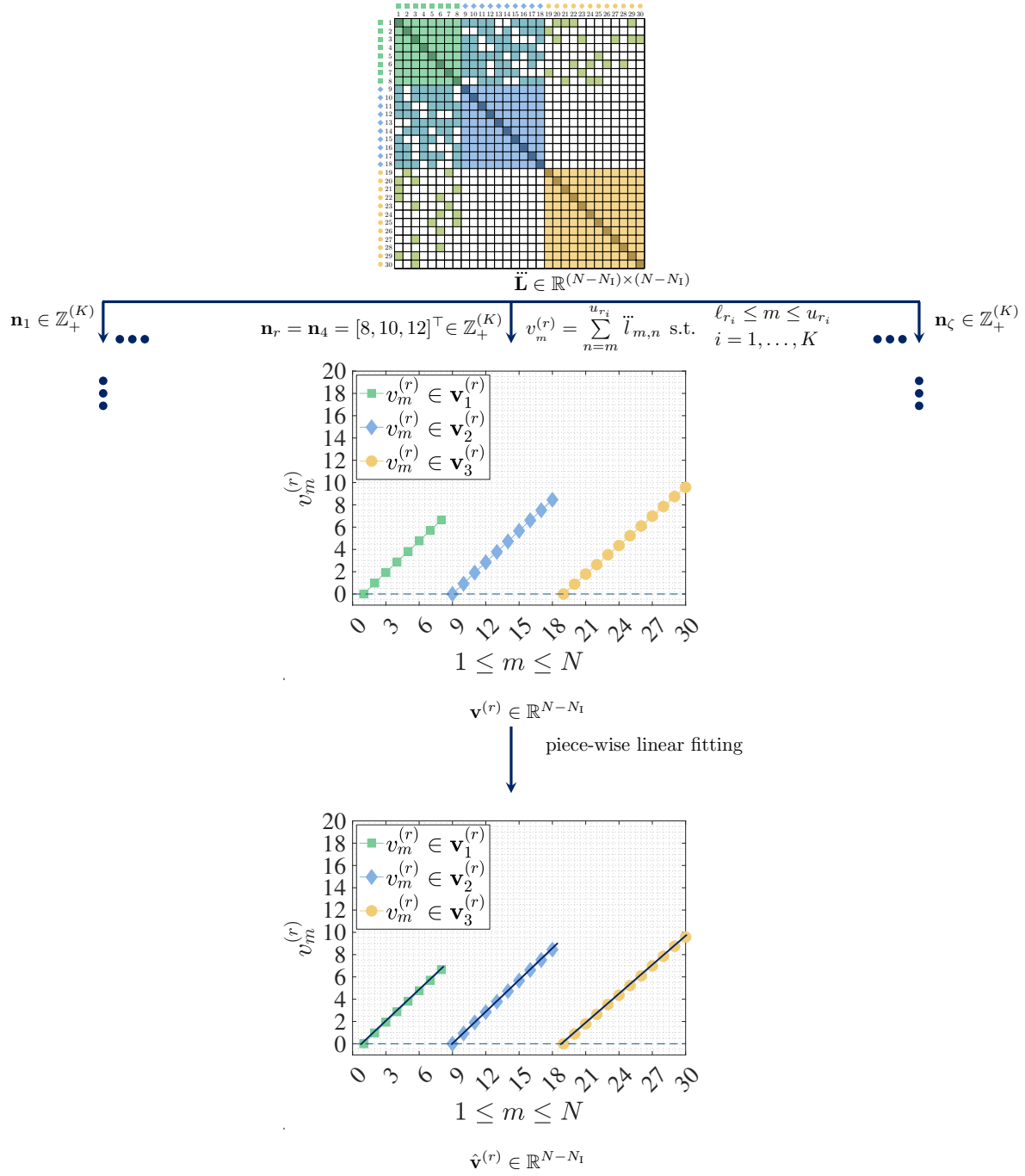
8	4	18	}	$\mathbf{n}_1$
8	6	16		$\mathbf{n}_2$
8	8	14		$\mathbf{n}_3$
8	10	12	}	$\mathbf{n}_4$
8	15	7		$\mathbf{n}_5$
12	2	16	}	$\mathbf{n}_6$
12	4	14		$\mathbf{n}_7$
12	6	12		$\mathbf{n}_8$
12	11	7	}	$\mathbf{n}_9$
14	2	14		$\mathbf{n}_{10}$
14	4	12		$\mathbf{n}_{11}$
14	9	7	}	$\mathbf{n}_{12}$
16	2	12		$\mathbf{n}_{13}$
16	7	7	}	$\mathbf{n}_{14}$
18	5	7		$\mathbf{n}_{15}$

$$\mathbf{N}^{(K)} = [\mathbf{n}_1, \mathbf{n}_2, \dots, \mathbf{n}_\zeta]^\top \in \mathbb{Z}_+^{\zeta \times K}$$

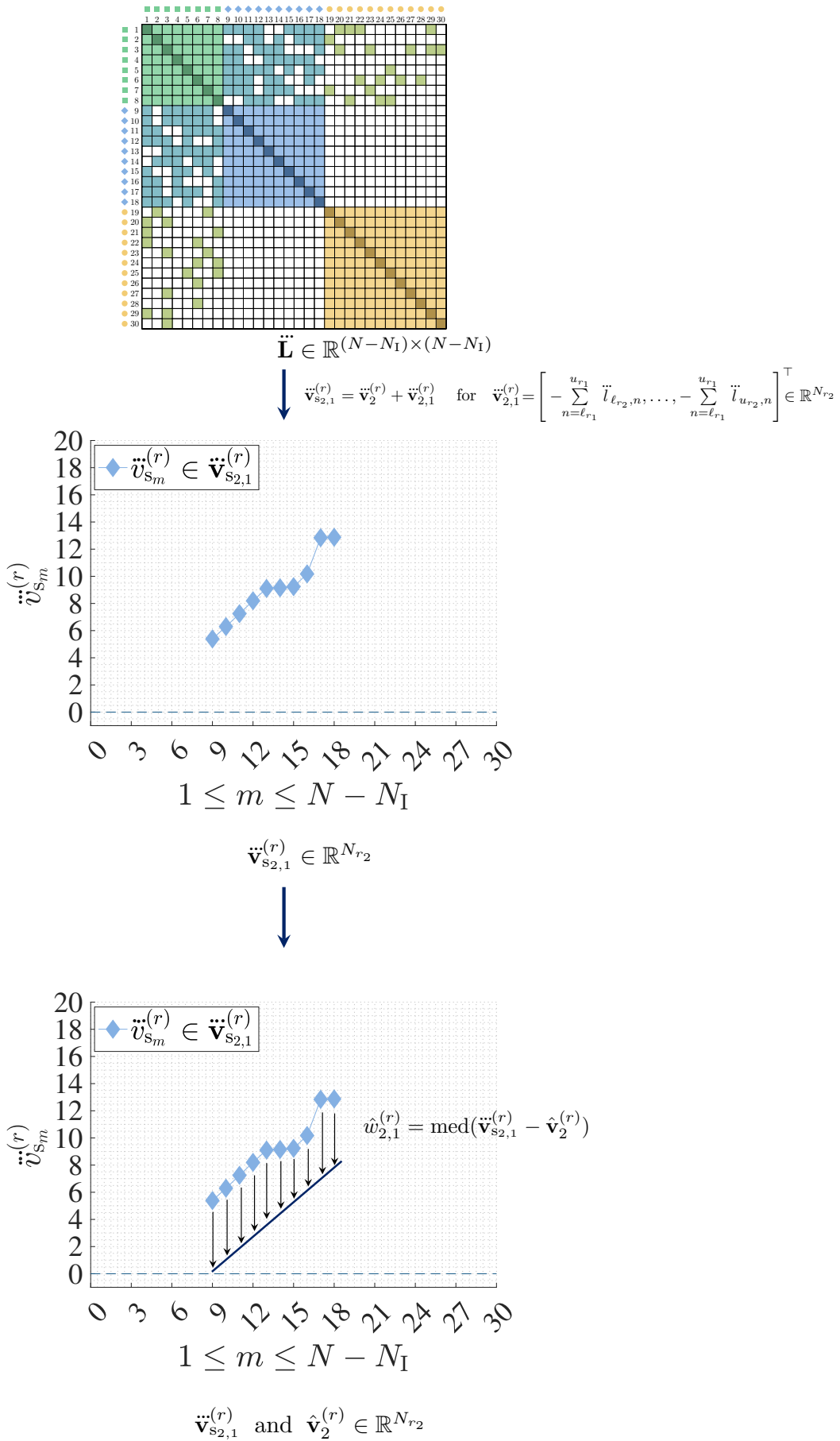
$$\zeta = \binom{N_c}{K-1} = \binom{6}{2} = 15$$

(e) Step 2.1: Compute Candidate Block Sizes

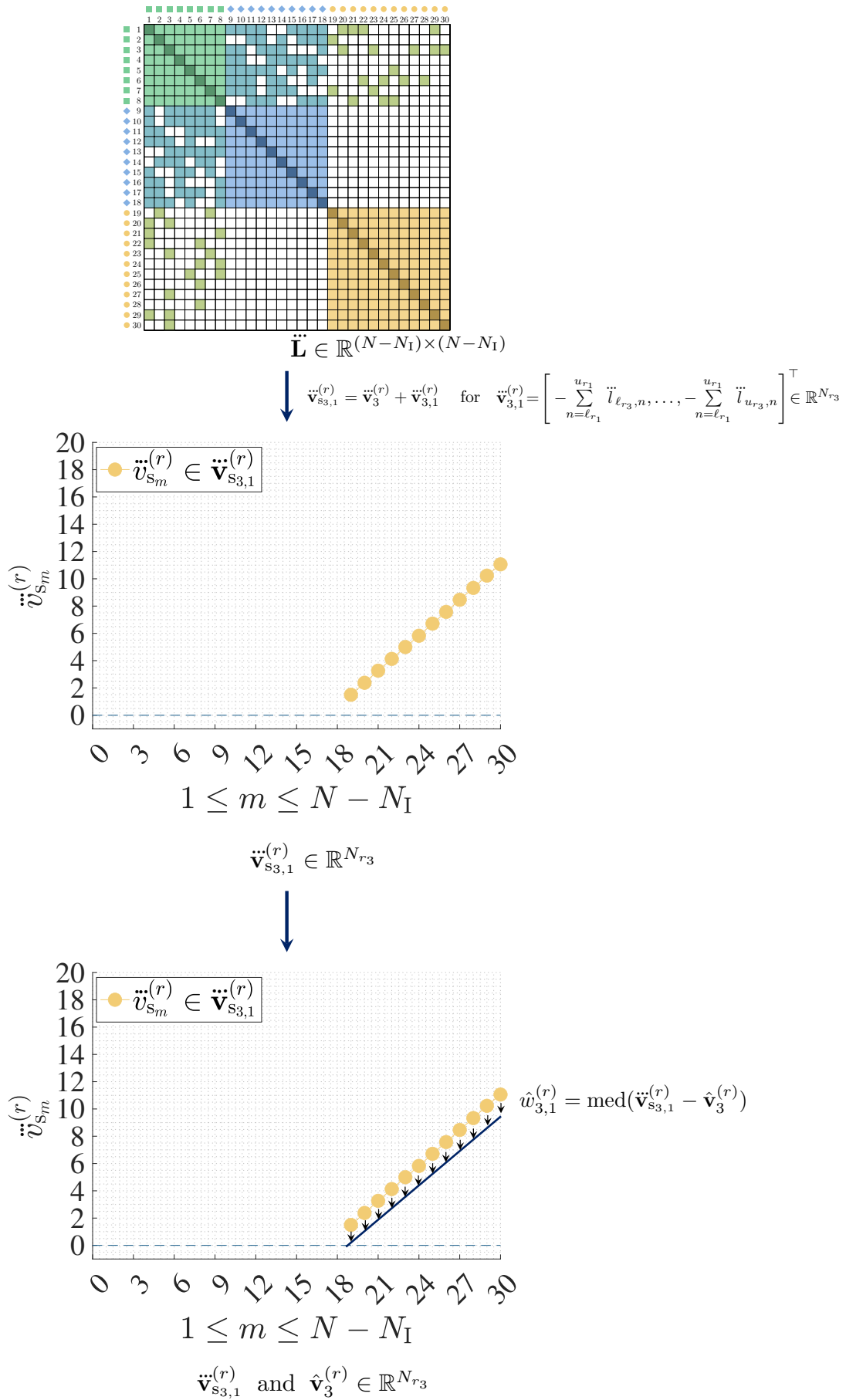




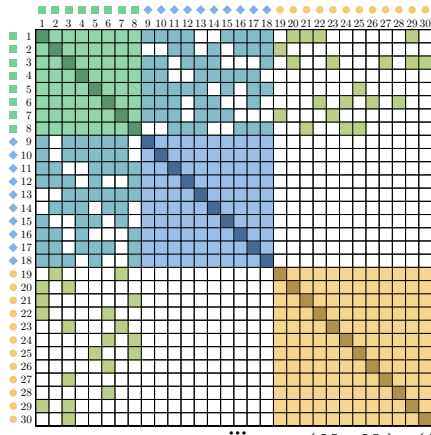
(f) Step 2.2.1: Estimate Target Similarity Coefficients  $\text{diag}(\mathbf{W}_{\text{sim}})$



(g) Step 2.2.2: Estimate Undesired Similarity Coefficients ( $i = 2, j = 1$ )

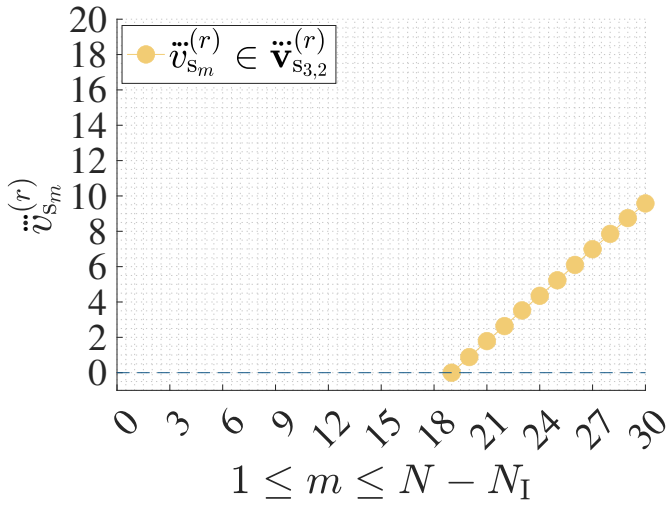


(h) Step 2.2.2: Estimate Undesired Similarity Coefficients ( $i = 3, j = 1$ )

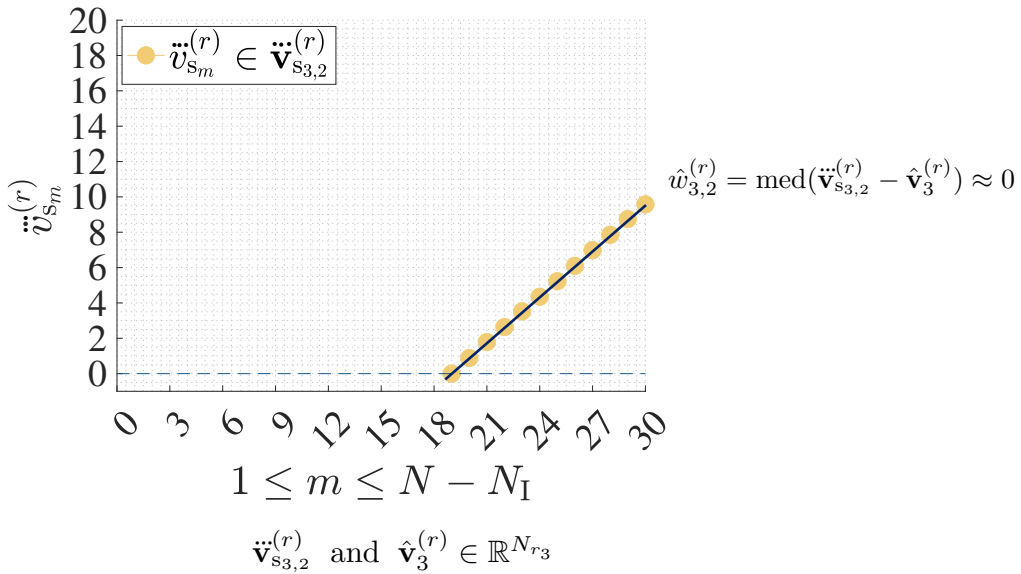


$$\tilde{\mathbf{L}} \in \mathbb{R}^{(N-N_I) \times (N-N_I)}$$

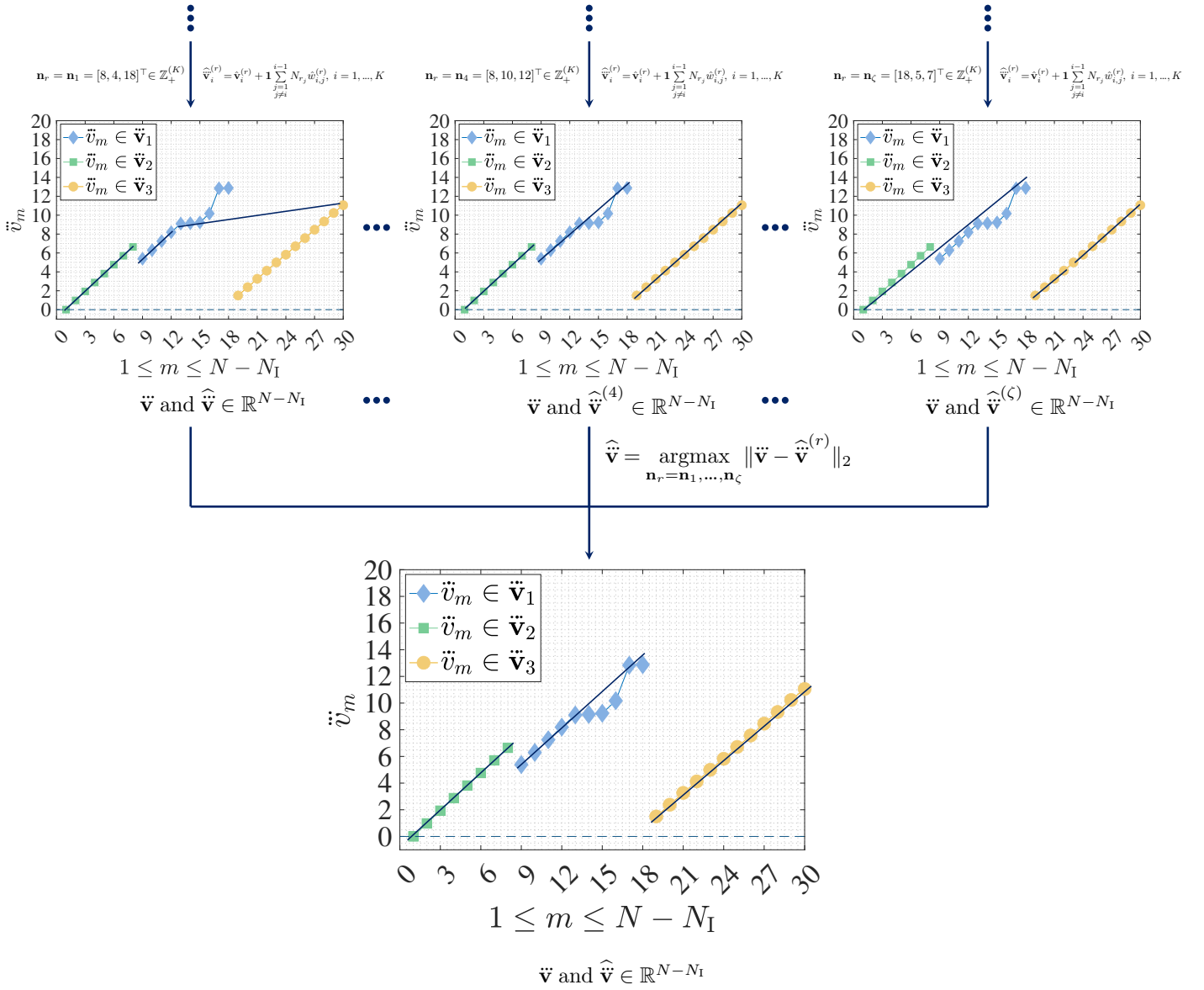
$$\downarrow \ddot{\mathbf{v}}_{s_{3,2}}^{(r)} = \ddot{\mathbf{v}}_3^{(r)} + \ddot{\mathbf{v}}_{3,2}^{(r)} \quad \text{for } \ddot{\mathbf{v}}_{3,2}^{(r)} = \left[ -\sum_{n=\ell_{r_2}}^{u_{r_2}} \ddot{l}_{\ell_{r_3},n}, \dots, -\sum_{n=\ell_{r_2}}^{u_{r_2}} \ddot{l}_{u_{r_3},n} \right]^T \in \mathbb{R}^{N_{r_3}}$$



$$\ddot{\mathbf{v}}_{s_{3,2}}^{(r)} \in \mathbb{R}^{N_{r_3}}$$



(i) Step 2.2.2: Estimate Undesired Similarity Coefficients ( $i = 3, j = 2$ )



(j) Step 2.3: Estimate Vector  $\tilde{\mathbf{v}}$

Fig. 20: Visual summary of FRS-BDR

## F.2 Sparse Laplacian Matrix Analysis

Step 1.3 of FRS-BDR determines a sparsity improved Laplacian matrix whose second smallest eigenvalue  $\lambda_1$  closes to zero. Considering eigenvalues of Laplacian matrix, that is associated with target block zero-diagonal symmetric affinity matrix,  $\lambda_1$  is definitely zero-valued. However, in real-world applications the distinct blocks may include negligibly small valued undesired similarity coefficients between different blocks. These coefficients result in an increase of  $\lambda_1$  and affect definition of "close to zero". Therefore, this section provides set of experiments for determining a sparse Laplacian matrix.

In Appendix A.2 it has been shown that multiple group similarity results in additional increase in the vector of eigenvalues. Therefore, for simplicity,  $\tilde{\mathbf{W}} \in \mathbb{R}^{N \times N}$  defining a  $K = 2$  block affinity matrix and associated Laplacian matrix  $\tilde{\mathbf{L}} \in \mathbb{R}^{N \times N}$  are considered in the experiments. In  $\tilde{\mathbf{W}} \in \mathbb{R}^{N \times N}$  each block  $\mathbf{W}_i, i = 1, 2$  is associated to a number  $N_i \in \mathbb{Z}_+ > 1$  of feature vectors and concentrated around a similarity constant  $w_i \in \mathbb{R}_+, i = 1, 2$  with negligibly small variations. Further,  $\tilde{w}_{i,j}$  denotes a constant around which the similarity coefficients between blocks  $i$  and  $j$  are concentrated, i.e.

$$\tilde{\mathbf{W}} = \begin{bmatrix} 0 & w_1 & \dots & w_1 & \tilde{w}_{1,2} & \dots & \tilde{w}_{1,2} \\ w_1 & 0 & \dots & w_1 & \tilde{w}_{1,2} & \dots & \tilde{w}_{1,2} \\ \vdots & \vdots & \ddots & \vdots & \vdots & \ddots & \vdots \\ w_1 & w_1 & \dots & 0 & \tilde{w}_{1,2} & \dots & \tilde{w}_{1,2} \\ \tilde{w}_{1,2} & \dots & \dots & \tilde{w}_{1,2} & 0 & w_2 & \dots & w_2 \\ \tilde{w}_{1,2} & \dots & \dots & \tilde{w}_{1,2} & w_2 & 0 & \dots & w_2 \\ \vdots & \vdots & \ddots & \vdots & \vdots & \vdots & \ddots & \vdots \\ \tilde{w}_{1,2} & \dots & \dots & \tilde{w}_{1,2} & w_2 & w_2 & \dots & 0 \end{bmatrix} \quad \text{and} \quad \tilde{\mathbf{L}} = \begin{bmatrix} \tilde{d}_1 & -w_1 & \dots & -w_1 & -\tilde{w}_{1,2} & \dots & -\tilde{w}_{1,2} \\ -w_1 & \tilde{d}_1 & \dots & -w_1 & -\tilde{w}_{1,2} & \dots & -\tilde{w}_{1,2} \\ \vdots & \vdots & \ddots & \vdots & \vdots & \ddots & \vdots \\ -w_1 & -w_1 & \dots & \tilde{d}_1 & -\tilde{w}_{1,2} & \dots & -\tilde{w}_{1,2} \\ -\tilde{w}_{1,2} & \dots & \dots & -\tilde{w}_{1,2} & \tilde{d}_2 & -w_2 & \dots & -w_2 \\ -\tilde{w}_{1,2} & \dots & \dots & -\tilde{w}_{1,2} & -w_2 & \tilde{d}_2 & \dots & -w_2 \\ \vdots & \vdots & \ddots & \vdots & \vdots & \vdots & \ddots & \vdots \\ -\tilde{w}_{1,2} & \dots & \dots & -\tilde{w}_{1,2} & -w_2 & -w_2 & \dots & \tilde{d}_2 \end{bmatrix},$$

where  $\tilde{d}_1 = (N_1 - 1)w_1 + N_2\tilde{w}_{1,2}$ ,  $\tilde{d}_2 = (N_2 - 1)w_2 + N_1\tilde{w}_{1,2}$  and  $w_i > \tilde{w}_{1,2}, i = 1, 2$ . According to the generalized eigen-decomposition, the second smallest eigenvalue  $\lambda_1$  of  $\tilde{\mathbf{L}}$  is

$$\lambda_1 = \frac{\tilde{d}_1 N_1 \tilde{w}_{1,2} + \tilde{d}_2 N_2 \tilde{w}_{1,2}}{\tilde{d}_1 \tilde{d}_2}.$$

Based on this, for  $\tilde{w}_{1,2} \rightarrow 1$  and  $w_i > \tilde{w}_{1,2}, i = 1, 2$ ,  $\lambda_1$  reaches its maximum value

$$\lambda_{1\max} = \frac{N_1 + N_2}{N_1 + N_2 - 1}$$

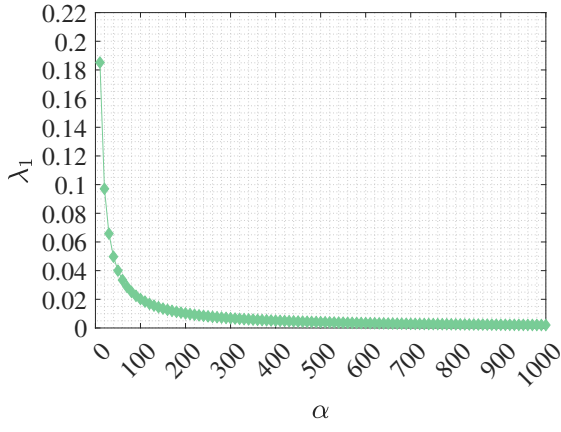
which tends to 1 for  $N_1 + N_2 \gg 1$ . Even though the maximum value of  $\lambda_1$  is explicit, its minimum value depends on different variables  $N_i, w_i$  and  $\tilde{w}_{i,j}$  for  $i = 1, 2, j = 1, 2$  and  $i \neq j$ . Therefore,  $\lambda_1$  is analyzed as a function of  $\alpha$  for different block size values in Fig. 21. Here,  $\alpha$  denotes the ratio between smallest target similarity coefficient  $w_{\min}$  and that of undesired  $\tilde{w}_{i,j}$  for  $i = 1, 2, j = 1, 2$  and  $i \neq j$ . As can be seen, the second smallest eigenvalue  $\lambda_1$  decreases to zero for  $w_1 \gg \tilde{w}_{1,2}$  and  $w_2 \gg \tilde{w}_{1,2}$ .

In contrast to generalized eigen-decomposition, the second smallest eigenvalue  $\lambda_1$  of  $\tilde{\mathbf{L}}$  associated to the standard eigen-decomposition does not affected by target similarity coefficients, i.e.

$$\lambda_1 = \tilde{w}_{1,2}(N_1 + N_2).$$

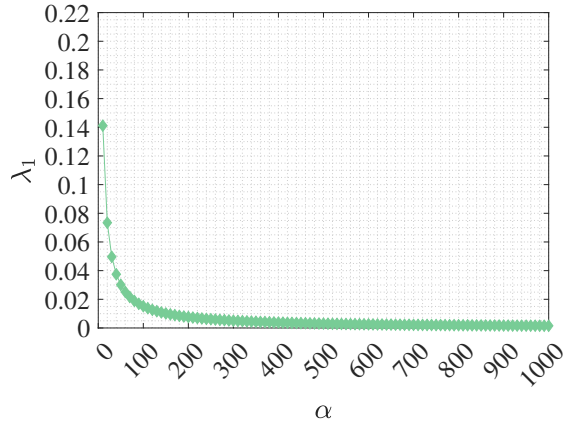
As  $N_i > 1, i = 1, 2$ ,  $\lambda_1$  can be reduced to zero for considerably small-valued undesired similarity coefficients. Therefore,  $\lambda_1$  is analyzed as a function of  $\tilde{w}_{1,2}$  for different block size values in Fig. 22. The figure implies that the value of undesired similarity coefficients is directly linked to closeness to zero. Therefore, the closeness to zero can be determined according to total sample size and desired value of undesired similarity.

To summarize, the eigenvalues based on generalized eigen-decomposition are less sensitive to block sizes which makes definition of close easier. As a result, based on the assumption that target similarity coefficients considerably larger valued than that of undesired coefficients, a selected  $\lambda_1$  value smaller than 0.05 might be sufficient to obtain sparse Laplacian matrices. In the proposed default setting, a Laplacian matrix is assumed to be sparse if its second smallest eigenvalue is valued by  $0 \leq \lambda_1 < 10^{-3}$ .



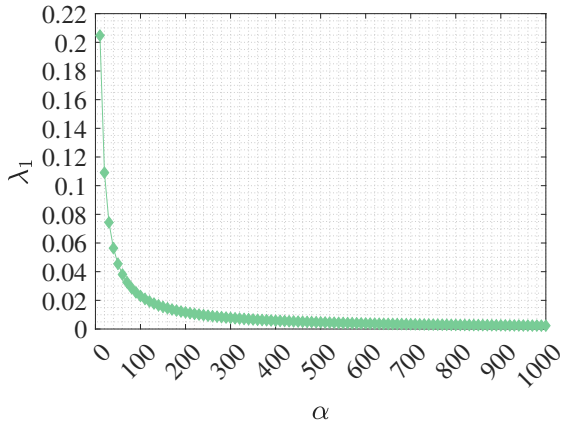
$$\mathbf{n} = [50, 50]^T \mathbb{Z}_+^2$$

$$\mathbf{w} = [0.6, 0.6]^T \mathbb{R}^2 \text{ and } w_1 = w_2 = \alpha \tilde{w}_{1,2}$$



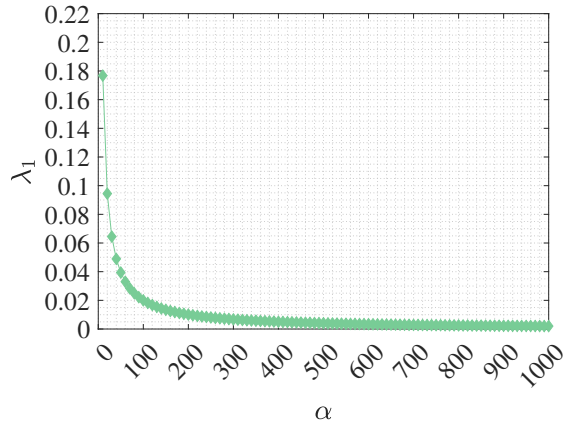
$$\mathbf{n} = [50, 50]^T \mathbb{Z}_+^2$$

$$\mathbf{w} = [0.6, 0.3]^T \mathbb{R}^2 \text{ and } w_1 = 2w_2 = 2\alpha \tilde{w}_{1,2}$$



$$\mathbf{n} = [50, 30]^T \mathbb{Z}_+^2$$

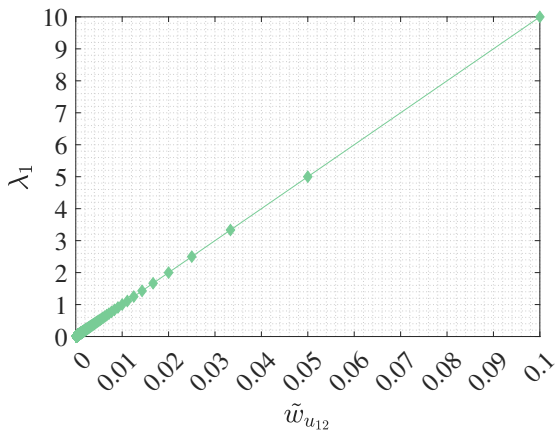
$$\mathbf{w} = [0.6, 0.6]^T \mathbb{R}^2 \text{ and } w_1 = w_2 = \alpha \tilde{w}_{1,2}$$



$$\mathbf{n} = [50, 30]^T \mathbb{Z}_+^2$$

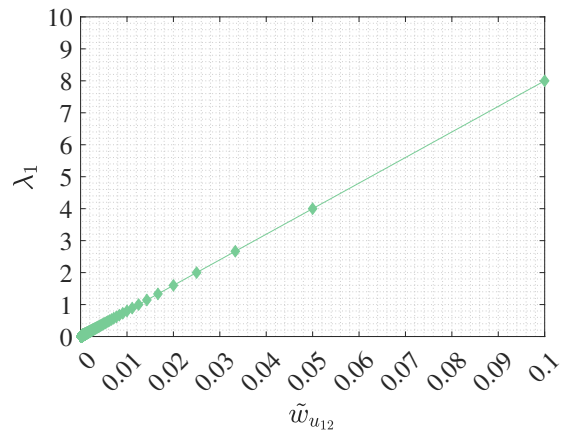
$$\mathbf{w} = [0.6, 0.3]^T \mathbb{R}^2 \text{ and } w_1 = 2w_2 = 2\alpha \tilde{w}_{1,2}$$

Fig. 21:  $\lambda_1$  for increasing values of  $\alpha$  associated with generalized eigen-decomposition



$$\mathbf{n} = [50, 50]^T \mathbb{Z}_+^2$$

$$\mathbf{w} = [0.6, 0.6]^T \mathbb{R}^2$$



$$\mathbf{n} = [50, 30]^T \mathbb{Z}_+^2$$

$$\mathbf{w} = [0.6, 0.6]^T \mathbb{R}^2$$

Fig. 22:  $\lambda_1$  for increasing values of  $\tilde{w}_{1,2}$  associated with standard eigen-decomposition

### F.3 Additional Algorithms

In this section, the design of sparse Laplacian matrix  $\ddot{\mathbf{L}}$  is detailed using different methods. In both algorithms, if the method does not provide any sparse Laplacian matrix  $\ddot{\mathbf{L}}$ , the sparsest nonnegative definite Laplacian matrix  $\ddot{\mathbf{L}}_{\text{alt}}$  is selected. The example algorithms have the same operational principle which can be further adapted to different graph construction methods.

---

#### Algorithm 1: Sparse Laplacian Matrix Design using Adaptive Thresholding

---

**Input:** a non-sparse affinity matrix  $\ddot{\mathbf{W}} \in \mathbb{R}^{(N-N_I) \times (N-N_I)}$ , initial threshold  $T_{\text{ini}}$  (optional, default is  $T_{\text{ini}} = 0.5$ ),  
 incrementation constant  $T_{\text{inc}}$  (optional, default is  $T_{\text{inc}} = 10^{-3}$ )

Set  $T = T_{\text{ini}}$

**while**  $T < 1$  **do**

Compute affinity matrix  $\ddot{\mathbf{W}}^{(T)}$  which is equal to  $\ddot{\mathbf{W}}$  except that the similarity coefficients smaller than  $T$  in  $\ddot{\mathbf{W}}^{(T)}$  are zero, i.e.  $\forall \ddot{w}_{mn}^{(T)} < T \in \ddot{\mathbf{W}}^{(T)}, \ddot{w}_{mn}^{(T)} = 0$  where  $m = 1, \dots, N - N_I, n = 1, \dots, N - N_I$  and  $m \neq n$

Based on obtained  $\ddot{\mathbf{W}}^{(T)}$ , compute  $\ddot{\mathbf{D}}^{(T)}$  and  $\ddot{\mathbf{L}}^{(T)}$  of dimension  $\mathbb{R}^{(N-N_I) \times (N-N_I)}$

Compute  $\ddot{\lambda}^{(T)} = [\ddot{\lambda}_0^{(T)}, \ddot{\lambda}_1^{(T)}, \dots, \ddot{\lambda}_{N-N_I-1}^{(T)}] \in \mathbb{R}^{N-N_I}$  in ascending order using Eq. (1) or Eq. (2)

**if**  $\ddot{\lambda}_1^{(T)} \cong 0$  (For detailed analysis, see Appendix F.2.) and  $\forall \ddot{\lambda}_m^{(T)} \in \ddot{\lambda}^{(T)}, \ddot{\lambda}_m^{(T)} \geq 0$  for  $m = 1, \dots, N - N_I - 1$  **then**

$\ddot{\mathbf{W}} = \ddot{\mathbf{W}}^{(T)}, \ddot{\mathbf{D}} = \ddot{\mathbf{D}}^{(T)}$  and  $\ddot{\mathbf{L}} = \ddot{\mathbf{L}}^{(T)}$

**break;**

**else if**  $\ddot{\lambda}_1^{(T)} \neq 0$  and  $\forall \ddot{\lambda}_m^{(T)} \in \ddot{\lambda}^{(T)}, \ddot{\lambda}_m^{(T)} \geq 0$  for  $m = 1, \dots, N - N_I - 1$  **then**

$\ddot{\mathbf{W}}_{\text{alt}} = \ddot{\mathbf{W}}^{(T)}, \ddot{\mathbf{D}}_{\text{alt}} = \ddot{\mathbf{D}}^{(T)}$  and  $\ddot{\mathbf{L}}_{\text{alt}} = \ddot{\mathbf{L}}^{(T)}$

$T \leftarrow T + T_{\text{inc}}$

**else**

$T \leftarrow T + T_{\text{inc}}$

**end if**

**end**

**if**  $\ddot{\mathbf{W}}$  does not exist **then**

**if**  $\ddot{\mathbf{W}}_{\text{alt}}$  exists **then**

$\ddot{\mathbf{W}} = \ddot{\mathbf{W}}_{\text{alt}}$

**else**

**error** : Please start with a smaller threshold

**end if**

**end if**

**Output:** Estimated sparse matrices  $\ddot{\mathbf{W}}, \ddot{\mathbf{D}}$  and  $\ddot{\mathbf{L}}$

---



---

#### Algorithm 2: Sparse Laplacian Matrix Design using $p$ -nearest Graph

---

**Input:** a non-sparse affinity matrix  $\ddot{\mathbf{W}} \in \mathbb{R}^{(N-N_I) \times (N-N_I)}$ , initial number of neighbors value  $p_{\text{ini}}$  (optional, default is  $p_{\text{ini}} = N - 2$ ),  
 decrease constant  $p_{\text{dec}}$  (optional, default is  $p_{\text{dec}} = 1$ ), minimum number of nodes in per  
 block  $N_{\text{min}}$  (optional, default is  $N_{\text{min}} \approx \frac{N}{K_{\text{max}}} \in \mathbb{Z}_+$ )

Set  $p = p_{\text{ini}}$

**while**  $p > N_{\text{min}}$  **do**

Construct affinity matrix  $\ddot{\mathbf{W}}^{(p)}$  using  $p$  nearest neighbors as in [7]

Based on obtained  $\ddot{\mathbf{W}}^{(p)}$ , compute  $\ddot{\mathbf{D}}^{(p)}$  and  $\ddot{\mathbf{L}}^{(p)}$  of dimension  $\mathbb{R}^{(N-N_I) \times (N-N_I)}$

Compute  $\ddot{\lambda}^{(p)} = [\ddot{\lambda}_0^{(p)}, \ddot{\lambda}_1^{(p)}, \dots, \ddot{\lambda}_{N-N_I-1}^{(p)}] \in \mathbb{R}^{N-N_I}$  in ascending order using Eq. (1) or Eq. (2)

**if**  $\ddot{\lambda}_1^{(p)} \cong 0$  (For detailed analysis, see Appendix F.2.) and  $\forall \ddot{\lambda}_m^{(p)} \in \ddot{\lambda}^{(p)}, \ddot{\lambda}_m^{(p)} \geq 0$  for  $m = 1, \dots, N - N_I - 1$  **then**

$\ddot{\mathbf{W}} = \ddot{\mathbf{W}}^{(p)}, \ddot{\mathbf{D}} = \ddot{\mathbf{D}}^{(p)}$  and  $\ddot{\mathbf{L}} = \ddot{\mathbf{L}}^{(p)}$

**break;**

**else if**  $\ddot{\lambda}_1^{(p)} \neq 0$  and  $\forall \ddot{\lambda}_m^{(p)} \in \ddot{\lambda}^{(p)}, \ddot{\lambda}_m^{(p)} \geq 0$  for  $m = 1, \dots, N - N_I - 1$  **then**

$\ddot{\mathbf{W}}_{\text{alt}} = \ddot{\mathbf{W}}^{(p)}, \ddot{\mathbf{D}}_{\text{alt}} = \ddot{\mathbf{D}}^{(p)}$  and  $\ddot{\mathbf{L}}_{\text{alt}} = \ddot{\mathbf{L}}^{(p)}$

$p \leftarrow p - p_{\text{dec}}$

**else**

$p \leftarrow p - p_{\text{dec}}$

**end if**

**end**

**if**  $\ddot{\mathbf{W}}$  does not exist **then**

**if**  $\ddot{\mathbf{W}}_{\text{alt}}$  exists **then**

$\ddot{\mathbf{W}} = \ddot{\mathbf{W}}_{\text{alt}}$

**else**

**error** : Please start with a greater  $p_{\text{ini}}$

**end if**

**end if**

**Output:** Estimated sparse matrices  $\ddot{\mathbf{W}}, \ddot{\mathbf{D}}$  and  $\ddot{\mathbf{L}}$

---



## F.4 Additional Experimental Results

### F.4.1 Handwritten Digit Clustering:

#### F.4.1.1 MNIST Data Set:

Subspace Clustering Performance for Different Block Diagonal Representation Methods														
Minimum-Maximum Clustering Accuracy ( $c_{accmin} - c_{accmax}$ ) for Different Regularization Parameters														
MNIST Data Set	$\mathbf{W}$	SSC	BD-SSC	LRR	BD-LRR	LSR	BDR-B	BDR-Z	RKLRR	IBDLR	FRPCAG	RSC	EBDR	FRS-BDR
2 subjects	87.1	50.5-82.6	50.5-90.3	51.0-89.2	51.1-89.9	51.5-86.8	50.9-91.8	51.0-89.8	50.5-91.6	50.5-92.2	91.2-95.1	53.7-60.1	85.5	89.7
3 subjects	72.0	33.9-37.5	33.8-76.1	34.2-74.8	34.3-72.5	34.9-71.8	34.4-67.6	34.4-67.7	33.9-70.0	33.9-79.0	62.3-79.7	39.7-45.1	68.6	79.6
5 subjects	60.9	20.6-25.1	20.4-63.7	21.0-62.4	21.1-62.5	20.6-60.8	23.0-48.6	20.5-54.4	20.6-59.2	20.6-65.4	52.5-61.7	28.8-31.7	52.3	67.5
8 subjects	53.4	13.1-18.0	12.9-56.0	13.7-50.6	13.7-52.4	13.8-53.7	13.9-37.6	13.3-46.0	13.1-50.1	13.1-57.7	50.0-56.5	20.6-23.2	42.3	59.3
10 subjects	51.2	10.7-16.9	10.4-52.7	11.2-45.6	11.2-50.8	11.6-50.1	10.9-33.5	10.8-45.4	10.6-44.1	10.5-53.4	48.5-57.2	16.8-24.2	38.9	57.6
Average	64.9	25.8-36.0	25.6-67.8	26.2-64.5	26.3-65.6	26.5-64.6	26.6-55.8	26.0-60.7	25.7-63.0	25.7-69.5	60.9-70.0	31.9-36.8	57.5	70.7

TABLE I: Subspace clustering performance of different block diagonal representation approaches on MNIST data set. The results are summarized for the similarity measure  $\mathbf{W} = \mathbf{X}^\top \mathbf{X}$ .

Detailed Computation time ( $t$ ) for FRS-BDR Method				
MNIST Data Set	Step 1.1	Step 1.2	Step 1.3	Step 2
2 subjects	0.007	0.064	0.194	0.004
3 subjects	0.011	0.171	0.602	0.007
5 subjects	0.033	1.106	3.262	0.018
8 subjects	0.096	5.045	15.797	0.018
10 subjects	0.164	10.053	35.965	0.017

TABLE II: Computation time performance of FRS-BDR method on MNIST data set. The results are summarized for the similarity measure  $\mathbf{W} = \mathbf{X}^\top \mathbf{X}$ .

Computation time ( $t$ ) for Different Block Diagonal Representation Methods														
Computation Time ( $t$ ) for Optimally Tuned Regularization Parameters														
MNIST Data Set	$\mathbf{W}$	SSC	BD-SSC	LRR	BD-LRR	LSR	BDR-B	BDR-Z	RKLRR	IBDLR	FRPCAG	RSC	EBDR	FRS-BDR
2 subjects	0.002	0.971	1.081	3.093	3.224	0.004	0.624	0.959	4.774	13.743	21.963	0.168	0.009	0.075
3 subjects	0.003	0.666	1.681	5.168	5.517	0.007	1.580	2.166	11.782	1.565	42.297	0.858	0.017	0.189
5 subjects	0.006	1.574	4.315	14.679	14.725	0.016	7.783	7.776	244.397	8.169	149.955	14.508	0.043	1.157
8 subjects	0.013	3.766	10.936	26.520	29.069	0.040	25.090	24.991	572.827	21.823	209.952	46.374	0.116	5.159
10 subjects	0.018	6.068	16.493	34.692	64.749	0.063	44.883	55.796	748.296	35.881	247.014	70.863	0.208	10.235
Average	0.008	2.609	6.901	16.830	23.457	0.026	15.992	18.338	316.415	16.236	134.236	26.554	0.079	3.363

TABLE III: Computation time performance of different block diagonal representation approaches on MNIST data set. The results are summarized for the similarity measure  $\mathbf{W} = \mathbf{X}^\top \mathbf{X}$  and sparsity assumed to be known for all sparse representation methods which means that computation time of FRS-BDR is detailed for Steps 1.1, 1.2 and 2.

Modularity Performance for Different Block Diagonal Representation Methods													
Modularity Performance corresponding to the Maximum Clustering Accuracy of Different Block Diagonal Representation Methods													
MNIST Data Set	$\mathbf{W}$	SSC	BD-SSC	LRR	BD-LRR	LSR	BDR-B	BDR-Z	RKLRR	IBDLR	EBDR	FRS-BDR	
2 subjects	0.0787	0.0328	0.2672	0	0	0.3110	0.3547	0.3583	0.1570	0.2016	0.3412	0.3334	
3 subjects	0.0730	0.0272	0.2830	0	0	0.4486	0.3053	0.4300	0.1538	0.2498	0.4141	0.4102	
5 subjects	0.0565	x	0.3147	0	0	0.4117	0.3524	0.5190	0.1288	0.2143	0.4696	0.4580	
8 subjects	0.0403	0.0668	0.2629	0	0	0.5548	0.3443	0.5324	0.0929	0.1552	0.4638	0.4780	
10 subjects	0.0346	0.0549	0.2259	0	0	0.3287	0.2738	0.4721	0.0846	0.1323	0.4634	0.4783	

TABLE IV: Modularity performance of different block diagonal representation approaches on the MNIST data set. The results are summarized for the similarity measure  $\mathbf{W} = \mathbf{X}^\top \mathbf{X}$ . All benchmark methods are 'oracle'-tuned, i.e., their tuning parameter is chosen such that maximal performance is achieved. 'x' denotes the failed results due to the generated unconnected graphs.

Modularity Performance for Different Block Diagonal Representation Methods													
Modularity Performance corresponding to the Minimum Clustering Accuracy of Different Block Diagonal Representation Methods													
MNIST Data Set	$\mathbf{W}$	SSC	BD-SSC	LRR	BD-LRR	LSR	BDR-B	BDR-Z	RKLRR	IBDLR	EBDR	FRS-BDR	
2 subjects	0.0787	x	0.0354	0	0	0.1466	0.1302	0.01966	x	x	0.3412	0.3334	
3 subjects	0.0730	x	0	0	0	0.0985	0.0764	0.0273	x	x	0.4141	0.4102	
5 subjects	0.0565	x	0	0	0	0.0203	0.0535	0.0186	x	x	0.4696	0.4580	
8 subjects	0.0403	x	-0.0003	0	0	0.0737	0.0117	0.0203	x	x	0.4638	0.4780	
10 subjects	0.0346	x	0	0	0	0.1659	0.0027	0.0212	x	x	0.4634	0.4783	

TABLE V: Modularity performance of different block diagonal representation approaches on the MNIST data set. The results are summarized for the similarity measure  $\mathbf{W} = \mathbf{X}^\top \mathbf{X}$ . All benchmark methods are 'oracle'-tuned, i.e., their tuning parameter is chosen such that minimal performance is obtained. 'x' denotes the failed results due to the generated unconnected graphs.

Conductance Performance for Different Block Diagonal Representation Methods												
MNIST Data Set	W	Conductance Performance corresponding to the Maximum Clustering Accuracy of Different Block Diagonal Representation Methods										
		SSC	BD-SSC	LRR	BD-LRR	LSR	BDR-B	BDR-Z	RKLRR	IBDLR	EBDR	FRS-BDR
2 subjects	0.4120	0.0113	0.0725	0.3331	0.1644	0.1796	0.0067	0.0656	0.3284	0.2854	0.0832	0.1569
3 subjects	0.5647	0.0054	0.0868	0.4609	0.2571	0.1862	0.1222	0.0890	0.4111	0.3844	0.1325	0.2387
5 subjects	0.7200	x	0.4666	0.7301	0.3747	0.3691	0.1728	0.1453	0.5902	0.5450	0.1831	0.3236
8 subjects	0.8169	0.0440	0.5985	0.8417	0.5438	0.3041	0.2686	0.1735	0.6645	0.7051	0.2722	0.3848
10 subjects	0.8509	0.0078	0.6613	0.8753	0.5919	0.5595	0.2232	0.1662	0.7063	0.7569	0.2960	0.4119

TABLE VI: Conductance performance of different block diagonal representation approaches on the MNIST data set. The results are summarized for the similarity measure  $\mathbf{W} = \mathbf{X}^\top \mathbf{X}$ . All benchmark methods are 'oracle'-tuned, i.e., their tuning parameter is chosen such that maximal performance is achieved. 'x' denotes the failed results due to the generated unconnected graphs.

Conductance Performance for Different Block Diagonal Representation Methods												
MNIST Data Set	W	Conductance Performance corresponding to the Minimum Clustering Accuracy of Different Block Diagonal Representation Methods										
		SSC	BD-SSC	LRR	BD-LRR	LSR	BDR-B	BDR-Z	RKLRR	IBDLR	EBDR	FRS-BDR
2 subjects	0.4120	x	0.0061	0	0	0	0.0316	0	x	x	0.0832	0.1569
3 subjects	0.5647	x	0.0133	0	0	0	0.1030	0	x	x	0.1325	0.2387
5 subjects	0.7200	x	0.0160	0	0	0	0.0779	0	x	x	0.1831	0.3236
8 subjects	0.8169	x	0.0783	0	0	0.0438	0.0030	0	x	x	0.2722	0.3848
10 subjects	0.8509	x	0.0179	0	0	0.1213	0	0	x	x	0.2960	0.4119

TABLE VII: Conductance performance of different block diagonal representation approaches on MNIST data set. The results are summarized for the similarity measure  $\mathbf{W} = \mathbf{X}^\top \mathbf{X}$ . All benchmark methods are 'oracle'-tuned, i.e., their tuning parameter is chosen such that minimal performance is obtained. 'x' denotes the failed results due to the generated unconnected graphs.

#### F.4.1.2 USPS Data Set:

Subspace Clustering Performance for Different Block Diagonal Representation Methods														
USPS Data Set	W	Minimum-Maximum Clustering Accuracy ( $e_{accmin} - e_{accmax}$ ) for Different Regularization Parameters												
		SSC	BD-SSC	LRR	BD-LRR	LSR	BDR-B	BDR-Z	RKLRR	IBDLR	FRPCAG	RSC	EBDR	FRS-BDR
2 subjects	87.6	51.0-69.5	54.3-90.6	52.1-74.3	52.2-85.9	56.0-88.6	51.1-93.0	51.1-93.1	51.0-92.9	51.0-93.2	77.3-88.9	51.3-65.3	87.0	92.6
3 subjects	70.4	34.4-55.0	36.8-77.4	35.5-68.7	35.5-69.4	38.3-71.9	36.5-85.1	34.7-85.6	34.4-80.7	34.4-86.6	65.0-78.6	37.7-48.8	77.2	87.5
5 subjects	61.1	21.2-44.4	24.7-66.9	21.6-45.7	22.1-54.6	23.1-63.9	22.4-74.5	21.2-76.0	21.2-65.0	21.2-76.8	67.1-73.3	28.1-33.7	63.3	77.3
8 subjects	50.7	13.7-35.7	18.1-59.4	14.4-44.2	14.5-46.1	15.3-58.7	13.8-69.2	14.7-68.4	13.7-60.1	13.7-70.7	66.0-70.2	21.2-24.2	52.4	65.2
10 subjects	49.4	11.0-41.4	10.6-56.0	11.8-46.2	12.2-39.8	13.8-52.0	12.2-68.6	14.8-68.2	11.0-57.8	11.2-69.8	56.2-70.4	17.1-23.4	47.4	59.8
Average	63.9	26.3-49.2	28.9-70.1	27.1-55.8	27.3-59.2	29.3-67.0	27.2-78.1	27.3-78.2	26.3-71.3	26.3-79.4	66.3-76.3	31.1-39.9	65.5	76.5

TABLE VIII: Subspace clustering performance of different block diagonal representation approaches on USPS data set. The results are summarized for the similarity measure  $\mathbf{W} = \mathbf{X}^\top \mathbf{X}$ .

Detailed Computation time ( $t$ ) for FRS-BDR Method				
USPS Data Set	Step 1.1	Step 1.2	Step 1.3	Step 2
2 subjects	0.003	0.015	0.049	0.002
3 subjects	0.004	0.034	0.154	0.003
5 subjects	0.007	0.108	0.401	0.005
8 subjects	0.019	0.464	1.689	0.004
10 subjects	0.032	1.110	3.444	0.119

TABLE IX: Computation time performance of FRS-BDR method on USPS data set. The results are summarized for the similarity measure  $\mathbf{W} = \mathbf{X}^\top \mathbf{X}$ .

Computation time ( $t$ ) for Different Block Diagonal Representation Methods														
USPS Data Set	W	Computation Time ( $t$ ) for Optimally Tuned Regularization Parameters												
		SSC	BD-SSC	LRR	BD-LRR	LSR	BDR-B	BDR-Z	RKLRR	IBDLR	FRPCAG	RSC	EBDR	FRS-BDR
2 subjects	0.001	0.096	0.108	0.561	0.587	0.001	0.260	0.256	0.561	3.971	1.461	0.060	0.006	0.020
3 subjects	0.001	0.228	0.252	1.239	1.115	0.001	0.607	0.606	2.358	0.952	5.346	0.231	0.008	0.041
5 subjects	0.001	0.631	0.632	2.639	2.509	0.002	1.757	1.781	5.302	1.962	8.373	1.542	0.011	0.120
8 subjects	0.003	1.429	2.011	4.106	4.286	0.006	4.837	5.095	11.177	4.579	19.560	9.288	0.028	0.487
10 subjects	0.003	2.260	2.929	4.257	4.713	0.008	7.127	7.664	14.232	8.551	15.804	22.698	0.050	1.261
Average	0.002	0.929	1.186	2.561	2.642	0.004	2.918	3.080	6.726	4.003	10.109	6.764	0.020	0.386

TABLE X: Computation time performance of different block diagonal representation approaches on USPS data set. The results are summarized for the similarity measure  $\mathbf{W} = \mathbf{X}^\top \mathbf{X}$  and sparsity assumed to be known for all sparse representation methods which means that computation time of FRS-BDR is detailed for Steps 1.1, 1.2 and 2.

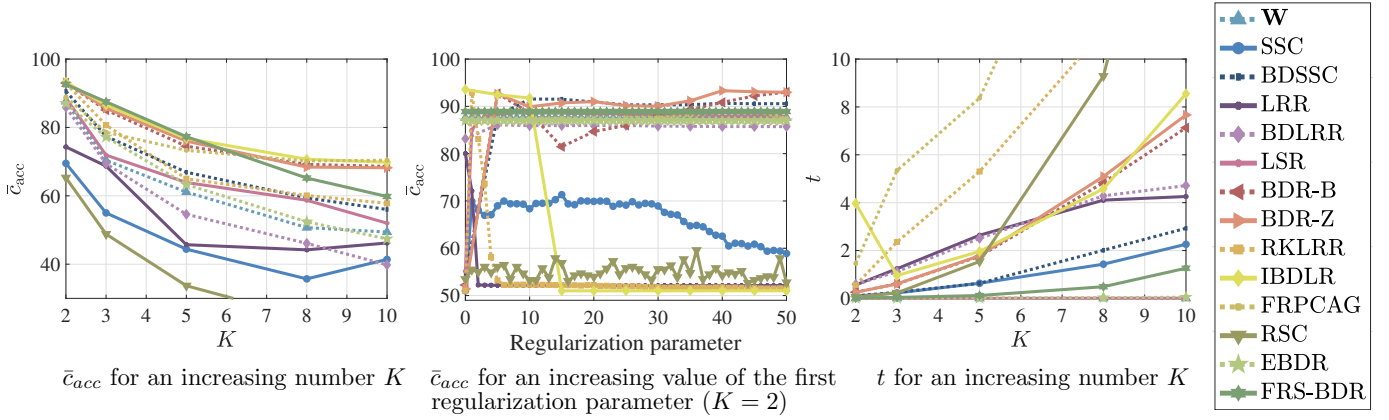


Fig. 23: Numerical results for USPS data set.

F.4.2 Object Clustering:  
F.4.2.1 COIL20 Data Set:

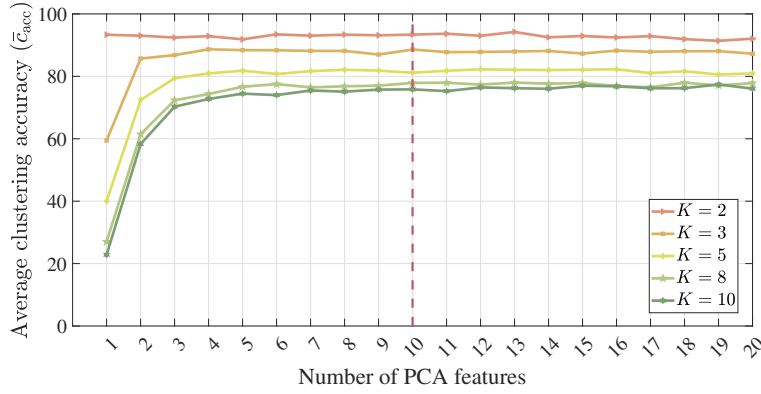


Fig. 24: Average clustering accuracy ( $\bar{c}_{acc}$ ) of FRS-BDR for increasing number of PCA features.

Subspace Clustering Performance for Different Block Diagonal Representation Methods														
Minimum-Maximum Clustering Accuracy ( $c_{accmin} - c_{accmax}$ ) for Different Regularization Parameters														
COIL20 Data Set	W	SSC	BD-SSC	LRR	BD-LRR	LSR	BDR-B	BDR-Z	RKLRR	IBDLR	FRPCAG	RSC	EBDR	FRS-BDR
2 subjects	68.9	52.5-86.6	54.5-65.9	57.1-64.9	60.8-63.6	58.0-61.8	54.3-95.9	53.3-95.6	52.5-72.9	52.5-69.7	90.6-91.6	55.6-60.7	95.8	93.1
3 subjects	42.3	36.0-83.3	39.3-54.9	66.7-68.1	58.2-67.1	44.1-47.3	38.2-89.1	37.8-88.8	36.2-66.0	35.9-72.1	83.9-87.8	42.3-45.8	90.1	88.1
5 subjects	26.4	23.0-80.6	26.2-57.6	64.0-76.5	65.1-76.4	34.3-37.0	25.3-83.3	27.1-83.1	23.1-73.6	22.8-75.4	72.5-79.7	31.1-33.8	80.9	82.5
8 subjects	17.3	15.6-75.6	18.2-63.3	56.3-73.4	64.0-73.4	25.2-28.0	18.0-75.6	21.9-75.6	15.5-71.3	15.5-74.2	67.1-73.4	24.7-26.1	72.4	77.3
10 subjects	14.6	13.1-72.5	15.6-65.3	54.2-72.9	63.7-73.0	20.6-24.9	15.3-74.5	20.0-74.2	13.1-72.0	13.0-73.4	65.6-71.3	22.2-24.2	69.1	75.9
Average	33.9	28.1-79.7	30.8-61.4	59.7-71.1	62.4-70.7	36.4-39.8	30.2-83.7	32.0-83.5	28.1-71.2	27.9-73.0	75.9-80.7	35.2-38.1	81.7	83.4

TABLE XI: Subspace clustering performance of different block diagonal representation approaches on COIL20 data set. The results are summarized for the similarity measure  $\mathbf{W} = \mathbf{X}^T \mathbf{X}$ .

Detailed Computation time ( $t$ ) for FRS-BDR Method				
COIL20 Data Set	Step 1.1	Step 1.2	Step 1.3	Step 2
2 subjects	0.002	0.004	0.014	0.002
3 subjects	0.003	0.007	0.029	0.003
5 subjects	0.006	0.014	0.071	0.007
8 subjects	0.019	0.039	0.192	0.098
10 subjects	0.032	0.064	0.319	0.206

TABLE XII: Computation time performance of FRS-BDR method on COIL20 data set. The results are summarized for the similarity measure  $\mathbf{W} = \mathbf{X}^T \mathbf{X}$ .

Computation time ( $t$ ) for Different Block Diagonal Representation Methods														
Computation Time ( $t$ ) for Optimally Tuned Regularization Parameters														
COIL20 Data Set	$\mathbf{W}$	SSC	BD-SSC	LRR	BD-LRR	LSR	BDR-B	BDR-Z	RKLRR	IBDLR	FRPCAG	RSC	EBDR	FRS-BDR
2 subjects	$3 \times 10^{-4}$	0.017	0.031	0.012	0.021	$3 \times 10^{-4}$	0.043	0.040	0.001	1.120	3.738	0.030	0.003	0.007
3 subjects	$3 \times 10^{-4}$	0.041	0.049	0.013	0.017	$2 \times 10^{-4}$	0.098	0.119	0.002	0.275	5.199	0.066	0.005	0.013
5 subjects	$4 \times 10^{-4}$	0.092	0.104	0.038	0.054	$3 \times 10^{-4}$	0.244	0.249	0.004	3.688	9.657	0.294	0.005	0.027
8 subjects	0.001	0.190	0.184	0.050	0.080	0.001	0.686	0.702	0.006	1.075	16.737	1.206	0.008	0.156
10 subjects	0.001	0.250	0.254	0.058	0.108	0.001	0.908	0.878	0.011	1.058	22.143	1.764	0.041	0.302
Average	$4 \times 10^{-4}$	0.118	0.124	0.034	0.056	$5 \times 10^{-4}$	0.396	0.397	0.005	1.443	11.495	0.672	0.012	0.101

TABLE XIII: Computation time performance of different block diagonal representation approaches on COIL20 data set. The results are summarized for the similarity measure  $\mathbf{W} = \mathbf{X}^\top \mathbf{X}$  and sparsity assumed to be known for all sparse representation methods which means that computation time of FRS-BDR is detailed for Steps 1.1, 1.2 and 2.

Modularity Performance for Different Block Diagonal Representation Methods													
Modularity Performance corresponding to the Maximum Clustering Accuracy of Different Block Diagonal Representation Methods													
COIL20 Data Set	$\mathbf{W}$	SSC	BD-SSC	LRR	BD-LRR	LSR	BDR-B	BDR-Z	RKLRR	IBDLR	EBDR	FRS-BDR	
2 subjects	0	0.3830	-1	0	0	1	0.4818	0.4611	0.1638	0.1906	0.4728	0.4116	
3 subjects	-0.69	0.5196	0.4726	0	0	1	0.6243	0.6106	0.1984	0.1773	0.6193	0.5720	
5 subjects	-1	0.6611	0.6648	0	0	1	0.7672	0.7482	0.2505	0.3196	0.7320	0.6638	
8 subjects	-0.13	0.7223	0.7556	0	0	1	0.8403	0.8261	0.2311	0.2333	0.7903	0.6829	
10 subjects	0.1496	0.7650	0.7611	0	0	1	0.8738	0.8592	0.2068	0.1888	0.8053	0.6756	

TABLE XIV: Modularity performance of different block diagonal representation approaches on the COIL20 data set. The results are summarized for the similarity measure  $\mathbf{W} = \mathbf{X}^\top \mathbf{X}$ . All benchmark methods are 'oracle'-tuned, i.e., their tuning parameter is chosen such that maximal performance is achieved.

Modularity Performance for Different Block Diagonal Representation Methods													
Modularity Performance corresponding to the Minimum Clustering Accuracy of Different Block Diagonal Representation Methods													
COIL20 Data Set	$\mathbf{W}$	SSC	BD-SSC	LRR	BD-LRR	LSR	BDR-B	BDR-Z	RKLRR	IBDLR	EBDR	FRS-BDR	
2 subjects	0	x	-1	0	0	1	0.0299	0.0100	x	x	0.4728	0.4116	
3 subjects	-0.69	x	-1	0	0	1	0.0281	0.0153	x	x	0.6193	0.5720	
5 subjects	-1	x	-0.0463	0	0	1	0.0473	0.0513	x	x	0.7320	0.6638	
8 subjects	-0.13	x	0.3647	0	0	1	0.0543	0.0740	x	x	0.7903	0.6829	
10 subjects	0.1496	x	0.1165	0	0	1	0.0492	0.1039	x	x	0.8053	0.6756	

TABLE XV: Modularity performance of different block diagonal representation approaches on the COIL20 data set. The results are summarized for the similarity measure  $\mathbf{W} = \mathbf{X}^\top \mathbf{X}$ . All benchmark methods are 'oracle'-tuned, i.e., their tuning parameter is chosen such that minimal performance is obtained. 'x' denotes the failed results due to the generated unconnected graphs.

Conductance Performance for Different Block Diagonal Representation Methods													
Conductance Performance corresponding to the Maximum Clustering Accuracy of Different Block Diagonal Representation Methods													
COIL20 Data Set	$\mathbf{W}$	SSC	BD-SSC	LRR	BD-LRR	LSR	BDR-B	BDR-Z	RKLRR	IBDLR	EBDR	FRS-BDR	
2 subjects	0	0.0481	0	0.3024	0.0072	0	0.0115	0.0202	0.2550	0.1892	0.0048	0.0054	
3 subjects	0.66	0.0809	0	0.0277	0.0276	0	0	0.0158	0.3802	0.4372	0.0104	0.03	
5 subjects	0.7300	0.0961	0.0127	0.0502	0.0501	0	0	0.0198	0.5176	0.4411	0.0214	0.0845	
8 subjects	0.5524	0.1113	0.0581	0.0935	0.0941	0	0.0076	0.0157	0.6253	0.6255	0.0292	0.1626	
10 subjects	0.6483	0.0953	0.1036	0.1274	0.1276	0	0.0037	0.0170	0.6797	0.6674	0.0485	0.1967	

TABLE XVI: Conductance performance of different block diagonal representation approaches on the COIL20 data set. The results are summarized for the similarity measure  $\mathbf{W} = \mathbf{X}^\top \mathbf{X}$ . All benchmark methods are 'oracle'-tuned, i.e., their tuning parameter is chosen such that maximal performance is achieved.

Conductance Performance for Different Block Diagonal Representation Methods													
Conductance Performance corresponding to the Minimum Clustering Accuracy of Different Block Diagonal Representation Methods													
COIL20 Data Set	$\mathbf{W}$	SSC	BD-SSC	LRR	BD-LRR	LSR	BDR-B	BDR-Z	RKLRR	IBDLR	EBDR	FRS-BDR	
2 subjects	0	x	0.3984	0.0072	0.0751	0	0	0.0005	x	x	0.0048	0.0054	
3 subjects	0.66	x	0.0958	0.0278	0.0699	0	0.1810	0.0011	x	x	0.0104	0.0300	
5 subjects	0.7300	x	0	0.4180	0.1409	0	0.0079	0.0245	x	x	0.0214	0.0845	
8 subjects	0.5524	x	0	0.5218	0.2410	0	0.0085	0.0560	x	x	0.0292	0.1626	
10 subjects	0.6483	x	0	0.5600	0.2986	0	0.0059	0.1228	x	x	0.0485	0.1967	

TABLE XVII: Conductance performance of different block diagonal representation approaches on COIL20 data set. The results are summarized for the similarity measure  $\mathbf{W} = \mathbf{X}^\top \mathbf{X}$ . All benchmark methods are 'oracle'-tuned, i.e., their tuning parameter is chosen such that minimal performance is obtained. 'x' denotes the failed results due to the generated unconnected graphs.

### F.4.3 Face Clustering:

#### F.4.3.1 ORL Data Set:

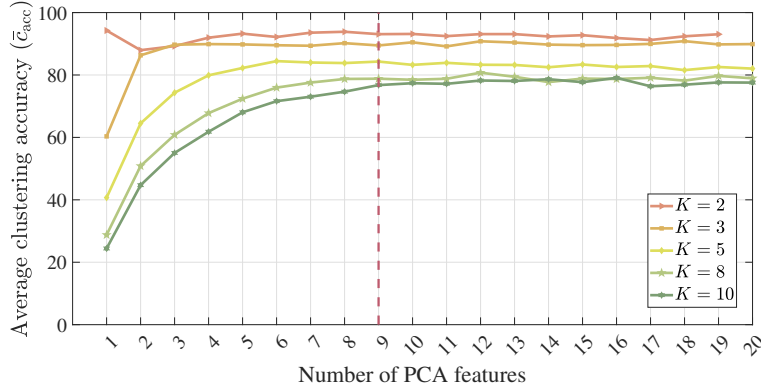


Fig. 25: Average clustering accuracy ( $\bar{c}_{acc}$ ) of FRS-BDR for increasing number of PCA features.

Subspace Clustering Performance for Different Block Diagonal Representation Methods														
ORL Data Set	$\mathbf{W}$	Minimum-Maximum Clustering Accuracy ( $c_{accmin} - c_{accmax}$ ) for Different Regularization Parameters												
		SSC	BD-SSC	LRR	BD-LRR	LSR	BDR-B	BDR-Z	RKLRR	IBDLR	FRPCAG	RSC	EBDR	FRS-BDR
2 subjects	56.8	55.0-81.9	55.1-64.0	57.6-69.1	59.1-69.1	57.7-60.5	55.0-95.6	55.3-95.4	55.0-73.7	x	90.1-91.8	58.7-61.5	95.2	93.1
3 subjects	41.5	38.8-80.8	43.4-50.7	58.6-63.4	58.0-59.7	45.1-46.6	38.9-90.5	40.0-90.5	39.0-62.9	38.8-69.0	84.1-85.8	45.4-47.4	90.5	90.1
5 subjects	28.4	26.0-77.1	31.5-41.0	51.3-57.7	57.0-66.7	36.3-38.9	26.2-80.1	30.8-80.1	26.1-60.6	25.7-70.8	77.3-82.6	34.9-36.6	83.0	84.2
8 subjects	21.8	18.6-74.4	25.3-35.8	45.0-72.6	56.7-68.5	26.8-28.5	18.9-79.1	34.6-78.5	18.6-75.4	18.5-75.1	74.6-82.2	28.7-30.0	74.1	79.4
10 subjects	18.7	16.3-74.2	22.7-36.1	41.8-72.6	62.7-72.8	24.0-25.3	16.4-78.4	31.2-78.9	16.5-72.5	16.1-72.4	70.6-81.3	25.6-27.8	69.9	77.2
Average	33.5	30.9-77.7	35.6-45.5	50.9-67.1	58.7-67.3	38.0-40.0	31.1-84.7	38.4-84.7	31.0-69.0	24.8-71.8	79.3-84.7	38.7-40.7	82.5	84.8

TABLE XVIII: Subspace clustering performance of different block diagonal representation approaches on ORL data set. The results are summarized for the similarity measure  $\mathbf{W} = \mathbf{X}^\top \mathbf{X}$ . ‘x’ denotes the failed results.

ORL Data Set	Detailed Computation time ( $t$ ) for FRS-BDR Method			
	Step 1.1	Step 1.2	Step 1.3	Step 2
2 subjects	0.001	0.002	0.005	0.002
3 subjects	0.001	0.002	0.009	0.002
5 subjects	0.002	0.005	0.018	0.010
8 subjects	0.004	0.010	0.044	0.119
10 subjects	0.007	0.014	0.079	1.810

TABLE XIX: Computation time performance of FRS-BDR method on ORL data set. The results are summarized for the similarity measure  $\mathbf{W} = \mathbf{X}^\top \mathbf{X}$ .

Computation time ( $t$ ) for Different Block Diagonal Representation Methods														
ORL Data Set	$\mathbf{W}$	Computation Time ( $t$ ) for Optimally Tuned Regularization Parameters												
		SSC	BD-SSC	LRR	BD-LRR	LSR	BDR-B	BDR-Z	RKLRR	IBDLR	FRPCAG	RSC	EBDR	FRS-BDR
2 subjects	$3 \times 10^{-4}$	0.016	0.023	0.011	0.012	$4 \times 10^{-5}$	0.009	0.009	$2 \times 10^{-4}$	x	1.791	0.027	0.003	0.005
3 subjects	$3 \times 10^{-4}$	0.018	0.025	0.012	0.014	$5 \times 10^{-5}$	0.027	0.026	$4 \times 10^{-4}$	0.133	1.959	0.042	0.003	0.006
5 subjects	$3 \times 10^{-4}$	0.034	0.047	0.013	0.017	$8 \times 10^{-5}$	0.053	0.054	0.001	0.171	1.503	0.090	0.017	
8 subjects	$4 \times 10^{-4}$	0.114	0.078	0.032	0.051	$2 \times 10^{-4}$	0.063	0.065	0.003	2.089	2.487	0.240	0.011	0.133
10 subjects	$5 \times 10^{-4}$	0.111	0.108	0.036	0.051	$3 \times 10^{-4}$	0.116	0.085	0.004	3.274	3.099	0.246	0.232	1.831
Average	$4 \times 10^{-4}$	0.058	0.056	0.021	0.029	$2 \times 10^{-4}$	0.054	0.048	0.002	1.417	2.168	0.129	0.050	0.398

TABLE XX: Computation time performance of different block diagonal representation approaches on ORL data set. The results are summarized for the similarity measure  $\mathbf{W} = \mathbf{X}^\top \mathbf{X}$  and sparsity assumed to be known for all sparse representation methods which means that computation time of FRS-BDR is detailed for Steps 1.1, 1.2 and 2.

Modularity Performance for Different Block Diagonal Representation Methods												
ORL Data Set	$\mathbf{W}$	Modularity Performance corresponding to the Maximum Clustering Accuracy of Different Block Diagonal Representation Methods										
		SSC	BD-SSC	LRR	BD-LRR	LSR	BDR-B	BDR-Z	RKLR	IBDLR	EBDR	FRS-BDR
2 subjects	-0.0305	0.2731	-1	0	0	1	0.4742	0.4664	0.1690	x	0.4827	0.4287
3 subjects	-0.0566	0.4634	-1	0	0	1	0.6276	0.6183	0.2015	0.1427	0.5913	0.5616
5 subjects	-0.0235	0.5125	-1	0	0	1	0.7381	0.7205	0.2043	0.1891	0.6659	0.6104
8 subjects	-0.1393	0.6923	-1	0	0	1	0.2905	0.2918	0.1985	0.2649	0.6905	0.5909
10 subjects	-0.7352	0.7460	-1	0	0	1	0.2743	0.2762	0.1736	0.2584	0.6766	0.5743

TABLE XXI: Modularity performance of different block diagonal representation approaches on the ORL data set. The results are summarized for the similarity measure  $\mathbf{W} = \mathbf{X}^T \mathbf{X}$ . All benchmark methods are 'oracle'-tuned, i.e., their tuning parameter is chosen such that maximal performance is achieved. 'x' denotes the failed results due to the generated unconnected graphs.

Modularity Performance for Different Block Diagonal Representation Methods												
ORL Data Set	$\mathbf{W}$	Modularity Performance corresponding to the Minimum Clustering Accuracy of Different Block Diagonal Representation Methods										
		SSC	BD-SSC	LRR	BD-LRR	LSR	BDR-B	BDR-Z	RKLR	IBDLR	EBDR	FRS-BDR
2 subjects	-0.0305	x	0.1398	0	0	1	0.0923	0.0174	x	x	0.4827	0.4287
3 subjects	-0.0566	x	-1	0	0	1	0	0.0074	x	x	0.5913	0.5616
5 subjects	-0.0235	x	-1	0	0	1	0	0.0410	x	x	0.6659	0.6104
8 subjects	-0.1393	x	-1	0	0	1	0	0.1382	x	x	0.6905	0.5909
10 subjects	-0.7352	x	-1	0	0	1	0	0.1483	x	x	0.6766	0.5743

TABLE XXII: Modularity performance of different block diagonal representation approaches on the ORL data set. The results are summarized for the similarity measure  $\mathbf{W} = \mathbf{X}^T \mathbf{X}$ . All benchmark methods are 'oracle'-tuned, i.e., their tuning parameter is chosen such that minimal performance is obtained. 'x' denotes the failed results due to the generated unconnected graphs.

Conductance Performance for Different Block Diagonal Representation Methods												
ORL Data Set	$\mathbf{W}$	Conductance Performance corresponding to the Maximum Clustering Accuracy of Different Block Diagonal Representation Methods										
		SSC	BD-SSC	LRR	BD-LRR	LSR	BDR-B	BDR-Z	RKLR	IBDLR	EBDR	FRS-BDR
2 subjects	0.2303	0.1195	1	0.0316	0.0315	0	0	0.0055	0.2539	x	0.0127	0.0099
3 subjects	0.4539	0.1390	1	0.0638	0.0985	0	0	0.0103	0.3884	0	0.0425	0.0579
5 subjects	0.5634	0.2447	1	0.1103	0.1417	0	0.1742	0.0201	0.5294	0.5862	0.0804	0.1553
8 subjects	0.9308	0.1586	1	0.1781	0.1779	0	0.5656	0.5650	0.6577	0.5854	0.1291	0.2559
10 subjects	0.7982	0.1347	1	0.2453	0.2459	0	0.6159	0.6145	0.7146	0.6306	0.1674	0.3090

TABLE XXIII: Conductance performance of different block diagonal representation approaches on the ORL data set. The results are summarized for the similarity measure  $\mathbf{W} = \mathbf{X}^T \mathbf{X}$ . All benchmark methods are 'oracle'-tuned, i.e., their tuning parameter is chosen such that maximal performance is achieved. 'x' denotes the failed results due to the generated unconnected graphs.

Conductance Performance for Different Block Diagonal Representation Methods												
ORL Data Set	$\mathbf{W}$	Conductance Performance corresponding to the Minimum Clustering Accuracy of Different Block Diagonal Representation Methods										
		SSC	BD-SSC	LRR	BD-LRR	LSR	BDR-B	BDR-Z	RKLR	IBDLR	EBDR	FRS-BDR
2 subjects	0.2303	x	0.1221	0.0316	0.0673	0	0	0	x	x	0.0127	0.0099
3 subjects	0.4539	x	0.2866	0.0642	0.1183	0	0	0	x	x	0.0425	0.0579
5 subjects	0.5634	x	0	0.1106	0.1109	0	0	0.0944	x	x	0.0804	0.1553
8 subjects	0.9308	x	0.6875	0.5875	0.2976	0	0	0.3606	x	x	0.1291	0.2559
10 subjects	0.7982	x	0	0.6190	0.3866	0	0	0.3708	x	x	0.1674	0.3090

TABLE XXIV: Conductance performance of different block diagonal representation approaches on ORL data set. The results are summarized for the similarity measure  $\mathbf{W} = \mathbf{X}^T \mathbf{X}$ . All benchmark methods are 'oracle'-tuned, i.e., their tuning parameter is chosen such that minimal performance is obtained. 'x' denotes the failed results due to the generated unconnected graphs.

F.4.3.2 JAFFE Data Set:

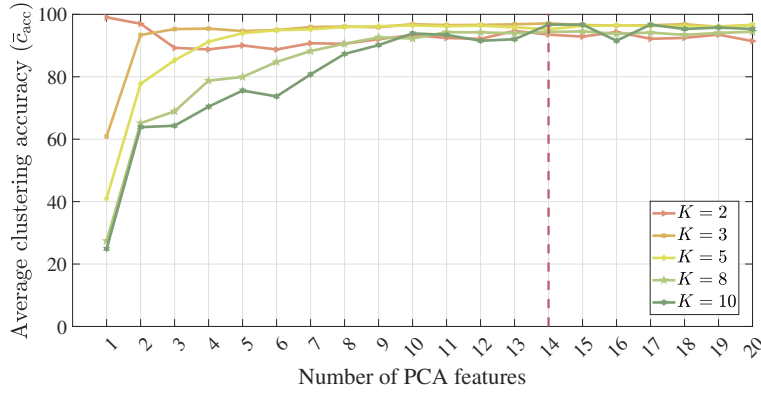


Fig. 26: Average clustering accuracy ( $\bar{c}_{acc}$ ) of FRS-BDR for increasing number of PCA features.

Subspace Clustering Performance for Different Block Diagonal Representation Methods														
Minimum-Maximum Clustering Accuracy ( $c_{accmin} - c_{accmax}$ ) for Different Regularization Parameters														
JAFFE Data Set	W	SSC	BD-SSC	LRR	BD-LRR	LSR	BDR-B	BDR-Z	RKLRR	IBDLR	FRPCAG	RSC	EBDR	FRS-BDR
2 subjects	56.1	52.1-93.3	52.8-70.4	56.4-60.7	57.1-59.0	53.4-57.1	52.3-99.7	52.4-99.7	52.4-82.0	52.0-79.6	98.8-99.8	56.3-59.1	94.9	93.4
3 subjects	39.7	36.2-95.2	37.1-59.7	49.1-78.6	49.0-65.3	39.8-45.1	36.1-98.0	36.5-98.0	36.2-76.7	35.9-75.5	96.7-98.9	43.1-44.7	92.4	96.9
5 subjects	26.4	23.3-95.3	26.4-76.5	59.9-65.7	60.0-85.0	33.1-37.8	23.2-94.2	28.3-94.2	23.3-69.0	23.1-88.0	91.4-95.3	31.7-33.0	90.7	96.4
8 subjects	19.1	15.8-93.6	18.6-91.9	56.0-85.5	80.3-89.6	24.2-38.1	15.8-94.3	34.2-94.3	15.8-87.4	15.7-94.2	89.3-94.4	24.4-25.5	82.4	94.4
10 subjects	x	13.1-93.0	16.4-93.9	54.9-92.0	85.9-92.0	11.7-55.9	12.2-91.5	25.8-91.5	13.1-92.0	12.7-94.8	84.5-97.7	x	77.9	96.7
Average	35.3	28.1-94.1	30.3-78.5	55.3-76.5	66.5-78.2	32.4-46.8	27.9-95.6	35.4-95.6	28.2-81.4	27.9-86.4	92.2-97.2	38.9-40.5	87.7	95.5

TABLE XXV: Subspace clustering performance of different block diagonal representation approaches on JAFFE data set. The results are summarized for the similarity measure  $\mathbf{W} = \mathbf{X}^T \mathbf{X}$ . ‘x’ denotes the failed results.

Detailed Computation time ( $t$ ) for FRS-BDR Method				
JAFFE Data Set	Step 1.1	Step 1.2	Step 1.3	Step 2
2 subjects	0.002	0.004	0.015	0.002
3 subjects	0.003	0.008	0.034	0.003
5 subjects	0.007	0.016	0.087	0.013
8 subjects	0.022	0.047	0.245	0.298
10 subjects	0.043	0.076	0.469	0.777

TABLE XXVI: Computation time performance of FRS-BDR method on JAFFE data set. The results are summarized for the similarity measure  $\mathbf{W} = \mathbf{X}^T \mathbf{X}$ .

Computation time ( $t$ ) for Different Block Diagonal Representation Methods														
Computation Time ( $t$ ) for Optimally Tuned Regularization Parameters														
JAFFE Data Set	W	SSC	BD-SSC	LRR	BD-LRR	LSR	BDR-B	BDR-Z	RKLRR	IBDLR	FRPCAG	RSC	EBDR	FRS-BDR
2 subjects	$3 \times 10^{-4}$	0.022	0.032	0.015	0.018	$8 \times 10^{-5}$	0.060	0.060	0.006	0.505	1.563	0.033	0.004	0.008
3 subjects	$4 \times 10^{-4}$	0.053	0.044	0.050	0.056	$3 \times 10^{-4}$	0.106	0.108	0.002	1.794	5.691	0.108	0.004	0.015
5 subjects	$4 \times 10^{-4}$	0.109	0.109	0.066	0.087	$4 \times 10^{-4}$	0.246	0.247	0.004	0.563	11.703	0.333	0.005	0.037
8 subjects	$5 \times 10^{-4}$	0.215	0.216	0.068	0.129	0.001	0.561	0.555	0.010	0.972	31.371	1.404	0.036	0.367
10 subjects	$6 \times 10^{-4}$	0.291	0.235	0.063	0.120	0.001	0.625	0.635	0.013	1.044	8.136	x	0.083	0.896
Average	$4 \times 10^{-4}$	0.138	0.127	0.052	0.082	$4 \times 10^{-4}$	0.320	0.321	0.007	0.976	11.693	0.470	0.026	0.264

TABLE XXVII: Computation time performance of different block diagonal representation approaches on JAFFE data set. The results are summarized for the similarity measure  $\mathbf{W} = \mathbf{X}^T \mathbf{X}$  and sparsity assumed to be known for all sparse representation methods which means that computation time of FRS-BDR is detailed for Steps 1.1, 1.2 and 2.

F.4.3.3 Yale Data Set:

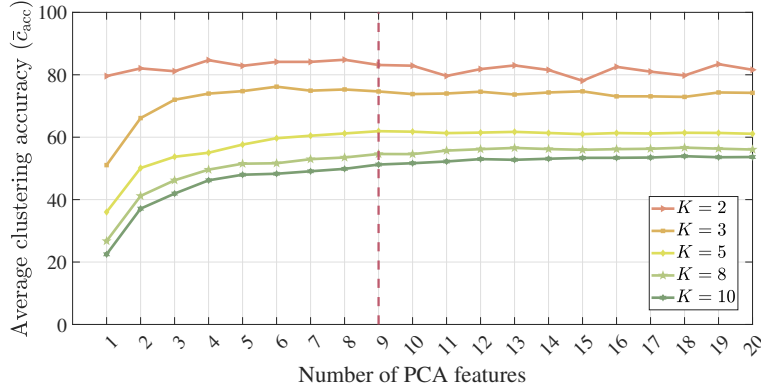


Fig. 27: Average clustering accuracy ( $\bar{c}_{acc}$ ) of FRS-BDR for increasing number of PCA features.

Subspace Clustering Performance for Different Block Diagonal Representation Methods														
Minimum-Maximum Clustering Accuracy ( $c_{accmin} - c_{accmax}$ ) for Different Regularization Parameters														
Yale Data Set	W	SSC	BD-SSC	LRR	BD-LRR	LSR	BDR-B	BDR-Z	RKLRR	IBDLR	FRPCAG	RSC	EBDR	FRS-BDR
2 subjects	55.3	54.5-75.6	54.7-58.8	55.7-60.9	57.5-60.9	54.5-57.3	53.6-84.2	54.5-83.9	54.5-60.4	x	66.1-90.4	55.5-62.2	84.1	83.1
3 subjects	41.9	38.4-67.2	43.0-46.7	51.0-51.4	50.9-53.6	42.1-43.8	38.6-68.5	39.0-68.6	38.6-52.4	38.2-55.1	61.1-69.2	43.3-49.0	71.6	74.5
5 subjects	29.8	25.5-57.9	30.5-37.4	43.6-49.8	49.2-54.4	31.1-33.2	25.7-62.3	29.9-62.2	25.4-49.9	25.2-52.9	52.9-62.7	33.8-36.9	60.2	61.7
8 subjects	21.6	18.1-52.6	22.3-29.7	37.4-47.9	47.3-50.7	23.6-25.4	18.3-51.9	28.5-51.5	18.3-48.6	17.9-49.6	44.3-57.1	27.5-30.3	53.8	54.8
10 subjects	18.7	15.6-50.0	20.2-30.2	34.5-47.5	46.2-47.9	20.8-22.0	15.8-51.6	24.5-51.6	15.9-46.3	15.4-46.3	40.3-55.0	25.3-27.3	49.2	51.2
Average	33.5	30.4-60.7	34.1-40.6	44.4-51.5	50.2-53.5	34.4-36.3	30.4-63.7	35.3-63.6	30.5-51.5	24.2-51.0	52.9-66.9	37.1-41.2	63.8	65.1

TABLE XXVIII: Subspace clustering performance of different block diagonal representation approaches on Yale data set. The results are summarized for the similarity measure  $\mathbf{W} = \mathbf{X}^\top \mathbf{X}$ . ‘x’ denotes the failed results.

Detailed Computation time ( $t$ ) for FRS-BDR Method				
Yale Data Set	Step 1.1	Step 1.2	Step 1.3	Step 2
2 subjects	0.001	0.002	0.007	0.002
3 subjects	0.001	0.003	0.013	0.003
5 subjects	0.002	0.006	0.025	0.013
8 subjects	0.005	0.012	0.056	0.046
10 subjects	0.008	0.018	0.099	0.160

TABLE XXIX: Computation time performance of FRS-BDR method on Yale data set. The results are summarized for the similarity measure  $\mathbf{W} = \mathbf{X}^\top \mathbf{X}$ .

Computation time ( $t$ ) for Different Block Diagonal Representation Methods														
Computation Time ( $t$ ) for Optimally Tuned Regularization Parameters														
Yale Data Set	W	SSC	BD-SSC	LRR	BD-LRR	LSR	BDR-B	BDR-Z	RKLRR	IBDLR	FRPCAG	RSC	EBDR	FRS-BDR
2 subjects	$3 \times 10^{-4}$	0.011	0.018	0.013	0.011	$5 \times 10^{-5}$	0.010	0.010	$2 \times 10^{-4}$	x	2.661	0.027	0.003	0.005
3 subjects	$4 \times 10^{-4}$	0.022	0.023	0.010	0.011	$6 \times 10^{-5}$	0.039	0.049	$4 \times 10^{-4}$	0.059	3.942	0.045	0.003	0.007
5 subjects	$3 \times 10^{-4}$	0.039	0.040	0.013	0.017	$1 \times 10^{-4}$	0.043	0.038	0.002	0.276	2.847	0.105	0.005	0.021
8 subjects	$4 \times 10^{-4}$	0.093	0.090	0.031	0.053	$3 \times 10^{-4}$	0.055	0.053	0.003	0.705	3.609	0.192	0.006	0.063
10 subjects	$4 \times 10^{-4}$	0.138	0.126	0.036	0.062	$4 \times 10^{-4}$	0.061	0.069	0.004	1.077	3.246	0.270	0.022	0.186
Average	$4 \times 10^{-4}$	0.061	0.059	0.021	0.031	$2 \times 10^{-4}$	0.042	0.044	0.002	0.529	3.261	0.128	0.008	0.056

TABLE XXX: Computation time performance of different block diagonal representation approaches on Yale data set. The results are summarized for the similarity measure  $\mathbf{W} = \mathbf{X}^\top \mathbf{X}$  and sparsity assumed to be known for all sparse representation methods which means that computation time of FRS-BDR is detailed for Steps 1.1, 1.2 and 2.



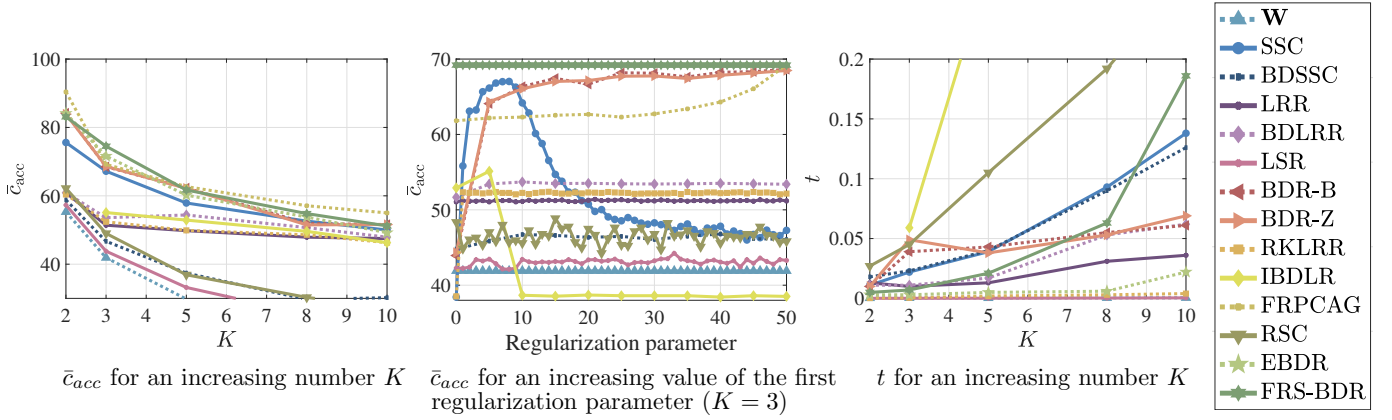


Fig. 28: Numerical results for Yale data set.

F.4.4 Additional Clustering Data Sets:

F.4.4.1 Comparisons with Popular Block Diagonal Representation Approaches:

Estimated Parameters of FRS-BDR for Different Clustering Data Sets											
Data Set	$N$	$K$	$\hat{K}$	$\bar{c}_{acc}$	$\mathbf{n} = [n_1, n_2, \dots, n_K]^T$	$\hat{\mathbf{n}} = [\hat{n}_1, \hat{n}_2, \dots, \hat{n}_K]^T$	Detailed Computation Time ( $t$ )				Estimation Error $\ \mathbf{v} - \hat{\mathbf{v}}\ $
							Step 1.1	Step 1.2	Step 1.3	Step 2	
Breast Cancer [8],	569	2	2	90.128	$[212, 357]^T$	$[173, 396]^T$	0.038	1.584	4.674	0.021	604.387
Ceramic [4],	88	2	2	98.864	$[44, 44]^T$	$[44, 44]^T$	0.002	0.010	0.031	0.007	24.271
Vertebral Column [9],	310	2,3	2	75.784	$[100, 210]^T$	$[120, 190]^T$	0.009	0.183	0.543	0.011	140.272
Iris [5],	150	3	3	96.667	$[50, 50, 50]^T$	$[51, 49, 50]^T$	0.003	0.033	0.098	0.018	48.121
Human Gait [10],	800	5	5	77.125	$[160, 160, 160, 160, 160]^T$	$[100, 128, 166, 201, 205]^T$	0.087	5.011	15.327	1.139	466.761
Ovarian Cancer [11],	216	2	2	77.315	$[95, 121]^T$	$[65, 151]^T$	0.012	0.075	0.208	0.011	131.006
Person Identification [6],	187	4	4	96.791	$[38, 40, 47, 62]^T$	$[34, 36, 52, 65]^T$	0.027	0.053	0.190	0.108	70.456
Parkinson [12],	240	2	2	58.208	$[120, 120]^T$	$[78, 162]^T$	0.006	0.095	0.266	0.013	111.626

TABLE XXXI: Estimation performance of FRS-BDR on well-known clustering data sets. The results are summarized for the similarity measure  $\mathbf{W} = \mathbf{X}^T \mathbf{X}$ .

Subspace Clustering Performance for Different Block Diagonal Representation Methods														
Data Set	$\mathbf{W}$	Minimum-Maximum Clustering Accuracy ( $c_{accmin} - c_{accmax}$ ) for Different Regularization Parameters											FRS-BDR	
		SSC	BD-SSC	LRR	BD-LRR	LSR	BDR-B	BDR-Z	RKLRR	IBDLR	FRPCAG	RSC		EBDR
Breast Cancer [8],	88.2	51.0-74.7	50.3-88.2	54.3-90.3	88.0-90.0	73.5-88.2	62.4-90.0	52.9-90.2	62.6-91.7	60.3-90.0	60.5-88.2	50.1-58.5	85.2	90.1
Ceramic [4],	98.9	51.1-98.9	51.1-100	95.5-98.9	95.5-98.9	54.5-98.9	51.1-100	51.1-98.9	51.1-95.5	51.1-98.9	50.0-100	50.0-69.3	98.9	98.9
Vertebral Column [9],	73.2	50.0-77.7	50.3-74.8	53.9-72.6	72.6-72.6	62.6-75.8	67.4-76.8	71.9-76.8	67.4-71.3	67.4-76.1	51.0-75.8	50.0-69.7	74.8	75.8
Iris [5],	78.0	34.7-82.7	34.0-83.3	38.7-80.7	80.0-98.0	78.0-82.7	34.0-96.7	65.3-96.7	34.0-80.0	34.7-84.0	34.0-89.3	35.3-50.0	98.0	96.7
Human Gait [10],	77.3	20.3-77.4	20.1-77.5	26.1-83.9	78.9-83.5	55.4-75.9	20.3-84.8	26.4-84.5	20.5-85.5	20.4-81.6	50.8-77.8	22.1-26.0	81.1	77.1
Ovarian Cancer [11],	61.7	51.4-73.6	50.9-71.3	52.3-76.4	54.2-76.4	51.9-66.2	53.7-75.9	51.9-74.1	55.6-88.4	55.6-75.5	77.8-89.3	50.0-69.4	77.8	77.3
Person Identification [6],	x	33.7-96.8	31.6-95.7	49.7-94.7	71.1-94.7	33.2-64.2	31.6-96.3	59.4-95.7	34.2-94.1	33.7-95.7	29.4-92.5	28.9-41.2	97.3	96.8
Parkinson [12],	61.3	50.4-58.8	50.0-61.3	50.4-54.2	50.4-61.3	57.9-61.3	50.4-61.3	50.0-61.3	50.4-61.7	50.4-61.3	50.0-67.5	50.4-72.1	56.7	58.2
Average	76.9	42.8-80.1	42.3-81.5	52.6-81.4	73.8-84.4	58.4-76.6	46.4-85.2	53.6-84.8	47.0-83.5	46.7-82.9	50.4-85.1	42.1-57.0	83.7	83.9

TABLE XXXII: Subspace clustering performance of different block diagonal representation approaches on well-known clustering data sets. The results are summarized for the similarity measure  $\mathbf{W} = \mathbf{X}^T \mathbf{X}$ . ‘x’ denotes the failed results due to the complex-valued eigenvectors.

Computation time ( $t$ ) for Different Block Diagonal Representation Methods														
Data Set	$\mathbf{W}$	Computation Time ( $t$ ) for Optimally Tuned Regularization Parameters											FRS-BDR	
		SSC	BD-SSC	LRR	BD-LRR	LSR	BDR-B	BDR-Z	RKLRR	IBDLR	FRPCAG	RSC		EBDR
Breast Cancer [8],	0.003	1.123	2.967	0.456	1.034	0.009	4.510	4.502	2.793	10.782	0.078	2.197	0.116	1.643
Ceramic [4],	$4 \times 10^{-4}$	0.074	0.076	0.074	0.086	$3 \times 10^{-4}$	0.139	0.137	0.174	0.918	0.511	0.052	0.007	0.019
Vertebral Column [9],	0.001	0.518	0.490	0.122	0.230	0.002	0.897	0.902	0.031	2.018	0.012	0.351	0.038	0.203
Iris [5],	$5 \times 10^{-4}$	0.161	0.166	0.070	0.066	0.001	0.030	0.025	0.024	9.330	0.056	0.226	0.012	0.054
Human Gait [10],	0.006	6.465	6.642	1.214	2.877	0.018	1.377	1.212	7.392	865.055	0.153	24.499	0.583	6.237
Ovarian Cancer [11],	0.008	3.036	3.883	8.316	8.387	0.016	5.503	0.506	9.192	17.590	3.297	0.182	0.026	0.098
Person Identification [6],	$5 \times 10^{-4}$	0.234	0.236	0.039	0.125	0.001	0.905	0.485	0.012	0.873	0.008	0.578	0.017	0.188
Parkinson [12],	0.001	0.350	0.354	0.321	0.399	0.001	0.066	0.065	0.170	2.397	1.806	0.224	0.025	0.113
Average	0.002	1.495	1.851	1.327	1.651	0.006	1.053	0.979	2.473	113.620	0.740	3.539	0.103	1.069

TABLE XXXIII: Computation time performance of different block diagonal representation approaches on well-known clustering data sets. The results are summarized for the similarity measure  $\mathbf{W} = \mathbf{X}^T \mathbf{X}$  and sparsity assumed to be known for all sparse representation methods which means that computation time of FRS-BDR is detailed for Steps 1.1, 1.2 and 2.

## F.4.4.2 Comparisons with Popular Community Detection Approaches:

Data Set	$\hat{K}$ for Different Cluster Enumeration Methods								$K$
	Louvain	Martelot	BNMF	DenPeak	Combo	MAP	Sparcode	FRS-BDR	
Breast Cancer [8],	2	1	1	3	2	1	2	2	2
Ceramic [4],	2	2	1	3	2	1	2	2	2
Vertebral Column [9],	2	2	1	3	2	1	2	2	2,3
Iris [5],	2	2	1	3	2	1	1	3	3
Human Gait [10],	3	2	1	2	3	1	2	5	5
Ovarian Cancer [11],	2	2	1	3	2	1	4	2	2
Person Identification [6],	3	3	1	47	2	2	3	4	4
Parkinson [12],	1	1	1	3	1	1	2	2	2

TABLE XXXIV: Performance of different cluster enumeration approaches on well-known clustering data sets. The results are summarized for the similarity measure  $\mathbf{W} = \mathbf{X}^\top \mathbf{X}$ .

Data Set	Modularity (mod) for Different Cluster Enumeration Methods							
	Louvain	Martelot	BNMF	DenPeak	Combo	MAP	Sparcode	FRS-BDR
Breast Cancer [8],	0.001	0.000	0.000	0.000	0.001	0.000	0.022	0.345
Ceramic [4],	0.055	0.055	0.000	0.040	0.055	0.000	0.440	0.441
Vertebral Column [9],	0.015	0.015	0.000	0.000	0.015	0.000	0.330	0.418
Iris [5],	0.016	0.016	0.000	0.016	0.016	0.000	0.000	0.472
Human Gait [10],	0.017	0.014	0.000	0.000	0.017	0.000	0.375	0.641
Ovarian Cancer [11],	0.006	0.006	0.000	0.005	0.006	0.000	0.019	0.334
Person Identification [6],	0.128	0.124	0.000	0.051	0.128	0.000	0.515	0.694
Parkinson [12],	0.000	0.000	0.000	0.000	0.000	0.000	0.179	0.342
Average	0.030	0.029	0.000	0.014	0.030	0.000	0.235	0.461

TABLE XXXV: Partitioning performance of different cluster enumeration approaches on well-known clustering data sets. The results summarized for modularity (mod) using the similarity measure  $\mathbf{W} = \mathbf{X}^\top \mathbf{X}$ .

Data Set	Conductance (cond) for Different Cluster Enumeration Methods							
	Louvain	Martelot	BNMF	DenPeak	Combo	MAP	Sparcode	FRS-BDR
Breast Cancer [8],	0.448	0.000	0.000	0.007	0.448	0.000	0.079	0.098
Ceramic [4],	0.445	0.445	0.000	0.449	0.445	0.000	0.058	0.059
Vertebral Column [9],	0.484	0.484	0.000	0.022	0.484	0.000	0.119	0.079
Iris [5],	0.424	0.429	0.000	0.433	0.424	0.000	0.000	0.183
Human Gait [10],	0.615	0.479	0.000	0.003	0.615	0.000	0.121	0.138
Ovarian Cancer [11],	0.451	0.476	0.000	0.487	0.451	0.000	0.047	0.140
Person Identification [6],	0.296	0.294	0.000	0.660	0.296	-0.035	0.095	0.047
Parkinson [12],	0.000	0.000	0.000	0.017	0.000	0.000	0.312	0.157
Average	0.395	0.326	0.000	0.260	0.395	-0.004	0.104	0.113

TABLE XXXVI: Partitioning performance of different cluster enumeration approaches on well-known clustering data sets. The results summarized for conductance (cond) using the similarity measure  $\mathbf{W} = \mathbf{X}^\top \mathbf{X}$ .

Data Set	Computation Time ( $t$ ) for Different Cluster Enumeration Methods							
	Louvain	Martelot	BNMF	DenPeak	Combo	MAP	Sparcode	FRS-BDR
Breast Cancer [8],	0.270	0.547	22.839	0.080	3.965	2.016	3.644	5.334
Ceramic [4],	0.008	0.004	0.273	0.009	0.083	0.219	0.103	0.059
Vertebral Column [9],	0.059	0.066	4.154	0.036	1.040	0.719	0.820	0.818
Iris [5],	0.012	0.010	0.752	0.017	0.241	0.375	0.323	0.178
Human Gait [10],	0.629	1.654	48.883	0.118	3.706	2.766	5.723	21.321
Ovarian Cancer [11],	0.026	0.023	1.769	0.024	0.546	0.484	0.509	0.337
Person Identification [6],	0.027	0.016	1.363	0.047	0.366	0.344	0.420	0.366
Parkinson [12],	0.029	0.032	2.307	0.027	0.003	0.578	0.540	0.425
Average	0.132	0.294	10.293	0.045	1.243	0.938	1.510	3.605

TABLE XXXVII: Computation performance of different cluster enumeration approaches on well-known clustering data sets. The results are summarized for the similarity measure  $\mathbf{W} = \mathbf{X}^\top \mathbf{X}$  and FRS-BDR is detailed for all steps.

#### F.4.5 Similarity-based Block Diagonal Ordering (sBDO) Performance Analysis:

##### F.4.5.1 Subspace Clustering Performance Comparisons with Reverse Cuthill-McKee (RCM) Algorithm:

Number of subjects	Average Clustering Accuracy ( $\bar{c}_{acc}$ ) for Different Data Sets using RCM Algorithm					
	MNIST	USPS	COIL20	ORL	JAFFE	YALE
2	89.5	92.7	87.9	81.5	89	73.8
3	79.7	87.5	82.3	74.9	93	73.6
5	67.3	77	81.7	82.7	96	60.9
8	59	65.5	77.6	79.8	94.8	54.8
10	54.7	62	75.9	76.2	92.9	51.1
Average	70.0	76.9	81.0	79.0	93.1	62.8

TABLE XXXVIII: Subspace clustering performance for different data sets using RCM algorithm in Step 1.2 of the FRS-BDR method. The results are summarized for the similarity measure  $\mathbf{W} = \mathbf{X}^\top \mathbf{X}$ .

Number of subjects	Average Clustering Accuracy ( $\bar{c}_{acc}$ ) for Different Data Sets using sBDO Algorithm					
	MNIST	USPS	COIL20	ORL	JAFFE	YALE
2	89.7	92.6	93.1	93.1	93.4	83.1
3	79.6	87.5	88.1	90.1	96.9	74.5
5	67.5	77.3	82.5	84.2	96.4	61.7
8	59.3	65.2	77.3	79.4	96.4	54.8
10	57.6	59.8	75.9	77.2	96.7	51.2
Average	70.7	76.5	83.4	84.8	96.0	65.1

TABLE XXXIX: Subspace clustering performance for different data sets using sBDO algorithm in Step 1.2 of the FRS-BDR method. The results are summarized for the similarity measure  $\mathbf{W} = \mathbf{X}^\top \mathbf{X}$ .

Data Set	$N$	$K$	$\hat{K}$	$\bar{c}_{acc}$
Breast Cancer [8],	569	2	x	x
Ceramic [4],	88	2	x	x
Vertebral Column [9],	310	2,3	x	x
Iris [5],	150	3	2	66.0
Human Gait [10],	800	5	2	20.0
Ovarian Cancer [11],	216	2	x	x
Person Identification [6],	187	4	2	26.6
Parkinson [12],	240	2	x	x

TABLE XL: Estimation performance of FRS-BDR on well-known clustering data sets. The results are summarized for the similarity measure  $\mathbf{W} = \mathbf{X}^\top \mathbf{X}$ . FRS-BDR algorithm is performed using RCM in Step 1.2. ‘x’ denotes the failed results.

Data Set	$N$	$K$	$\hat{K}$	$\bar{c}_{acc}$
Breast Cancer [8],	569	2	2	90.1
Ceramic [4],	88	2	2	98.9
Vertebral Column [9],	310	2,3	2	75.8
Iris [5],	150	3	3	96.7
Human Gait [10],	800	5	5	77.1
Ovarian Cancer [11],	216	2	2	77.3
Person Identification [6],	187	4	4	96.8
Parkinson [12],	240	2	2	58.2

TABLE XLI: Estimation performance of FRS-BDR on well-known clustering data sets. The results are summarized for the similarity measure  $\mathbf{W} = \mathbf{X}^\top \mathbf{X}$ . FRS-BDR algorithm is performed using sBDO in Step 1.2.

F.4.5.2 Block Diagonal Structure Enhancement Comparisons with Reverse Cuthill-McKee (RCM) Algorithm:

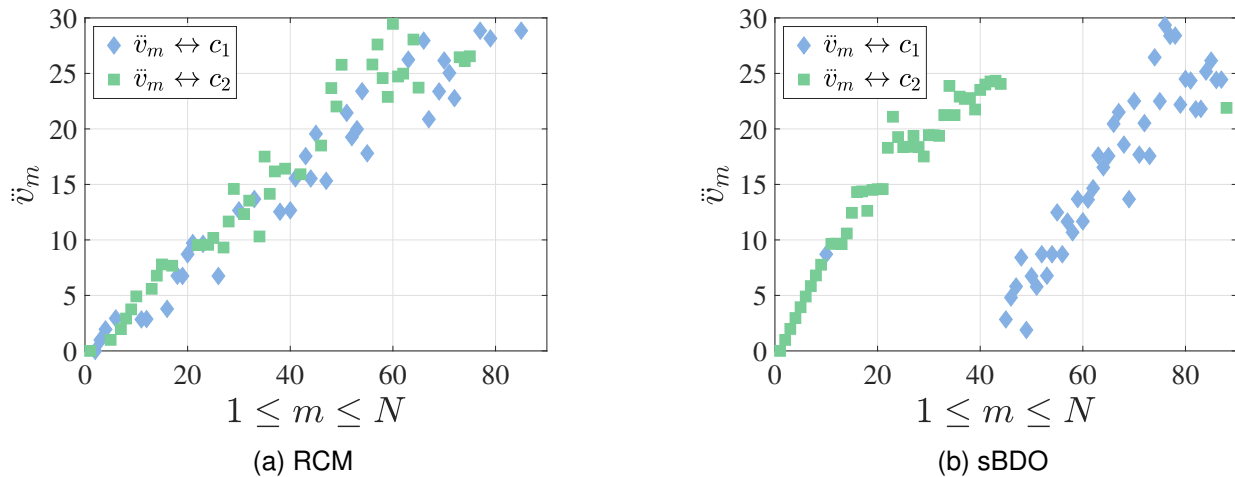


Fig. 29: Exemplary block diagonal enhancement results for Ceramic [4] data set using different block diagonal ordering algorithms in Step 1.2. Components of the obtained vector  $\check{v}$  are highlighted in two different colors based on their associations to  $K = 2$  clusters.

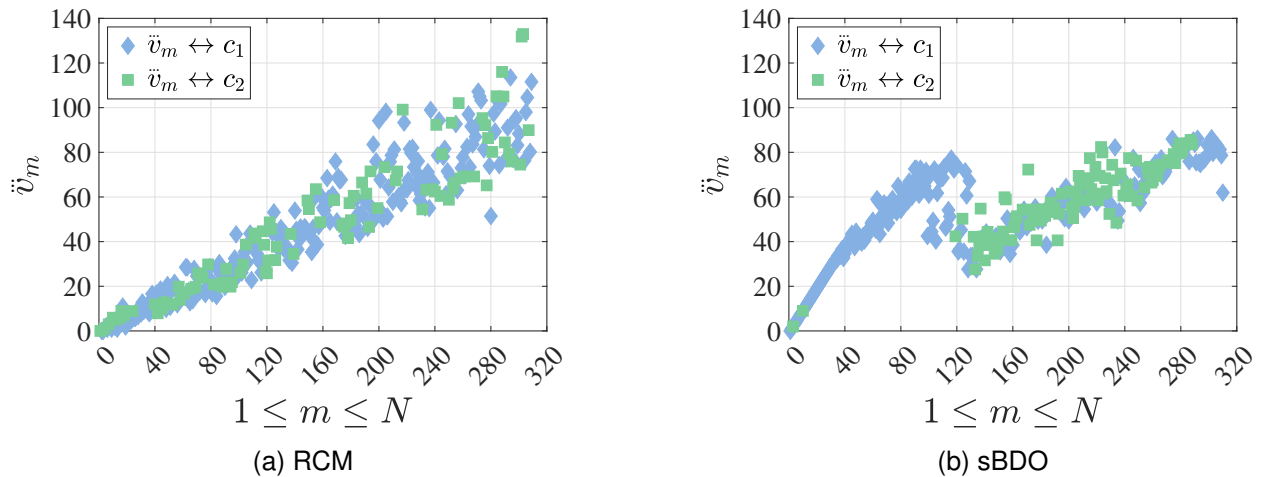


Fig. 30: Exemplary block diagonal enhancement results for Vertebral Column [9] data set using different block diagonal ordering algorithms in Step 1.2. Components of the obtained vector  $\check{v}$  are highlighted in two different colors based on their associations to  $K = 2$  clusters.

To better understand robustness of the sBDO algorithm, let consider a challenging scenario such that a heavy tailed noise that connects two groups/clusters with a large weight is selected as a starting point in the proposed sBDO method. Since the similarity coefficients are valued in range  $[-1, 1]$ , a single similarity coefficient would not lead to an unbounded effect in proposed ordering algorithm. In such cases, the algorithm starts with adding the most similar neighbor from one of the clusters. Then, the algorithm updates the set and finds the most similar neighbors based on their connectedness to the available set. This means that after the sBDO algorithm selects the first few neighbors from the same cluster, similarity of these vertices will quickly dominate the similarity of the noisy vertex. This scenario about selecting a Type II outlier in the first few iterations is visible in Fig. 30b. The real-world data example confirms the above information that selecting samples from within a cluster quickly dominates the effect of Type II outliers after a few iterations while RCM algorithm loses the cluster structure completely.

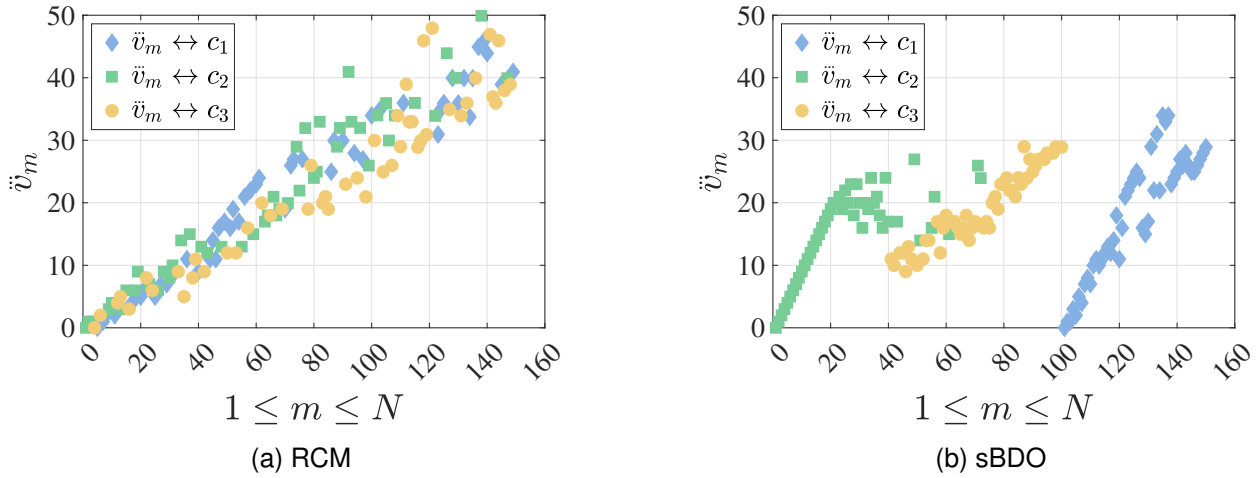


Fig. 31: Exemplary block diagonal enhancement results for Iris [5] data set using different block diagonal ordering algorithms in Step 1.2. Components of the obtained vector  $\ddot{\mathbf{v}}$  are highlighted in three different colors based on their associations to  $K = 3$  clusters.

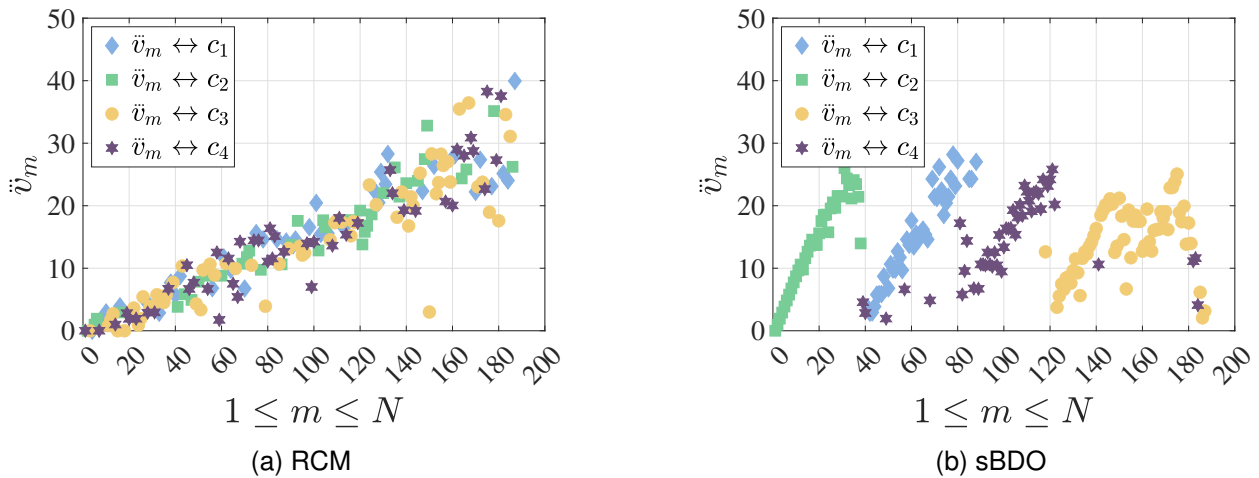


Fig. 32: Exemplary block diagonal enhancement results for Person Identification [6] data set using different block diagonal ordering algorithms in Step 1.2. Components of the obtained vector  $\ddot{\mathbf{v}}$  are highlighted in four different colors based on their associations to  $K = 4$  clusters.

#### F.4.6 Robustness Analysis:

Subspace Clustering Performance for Different Block Diagonal Representation Methods														
Noise density	W	Minimum-Maximum Clustering Accuracy ( $c_{\text{accmin}} - c_{\text{accmax}}$ ) for Different Regularization Parameters												
		SSC	BD-SSC	LRR	BD-LRR	LSR	BDR-B	BDR-Z	RKLRR	IBDLR	FRPCAG	RSC	EBDR	FRS-BDR
0	72.0	33.9-37.5	33.8-76.1	34.2-74.8	34.3-72.5	34.9-71.8	34.4-67.6	34.4-67.7	33.9-70.0	33.9-79.0	62.3-79.7	39.7-45.1	68.6	79.6
0.1	72.9	33.9-75.2	33.8-90.7	34.7-65.7	34.3-70.6	66.1-74.7	33.7-76.8	40.5-75.8	33.8-78.7	33.8-81.9	66.0-75.0	39.8-45.5	64.2	80.7
0.2	73.8	33.8-77.9	33.8-81.2	36.0-61.0	35.5-76.2	69.5-76.9	33.7-76.3	48.9-74.2	33.8-75.2	33.8-75.5	68.6-81.8	39.9-44.4	60.9	79.3
0.3	74.1	33.8-75.5	33.8-84.2	36.1-57.6	36.0-72.3	69.8-73.7	33.7-84.1	67.3-78.9	33.8-64.1	33.8-74.8	72.1-80.5	40.2-44.7	58.8	77.2
0.4	74.0	33.8-72.5	33.7-80.7	35.7-39.3	41.6-77.8	71.9-76.4	33.7-75.9	66.0-78.8	33.8-63.0	33.8-76.5	46.4-77.5	39.8-45.6	57.2	74.8
0.5	72.8	33.9-72.5	33.9-74.1	35.7-42.8	61.3-71.3	73.4-77.9	33.7-66.1	63.7-75.0	33.8-57.1	33.8-71.6	34.1-74.9	38.7-45.7	54.7	72.4

TABLE XLII: Subspace clustering performance of different block diagonal representation approaches on corrupted MNIST data set. MNIST data set is computed for  $K = 3$  clusters and the noise density, which affects approximately the defined value of pixels based on salt and pepper noise, is increased. The results are summarized for the similarity measure  $\mathbf{W} = \mathbf{X}^\top \mathbf{X}$ .

Subspace Clustering Performance for Different Block Diagonal Representation Methods														
Noise type	W	Minimum-Maximum Clustering Accuracy ( $c_{\text{accmin}} - c_{\text{accmax}}$ ) for Different Regularization Parameters												
		SSC	BD-SSC	LRR	BD-LRR	LSR	BDR-B	BDR-Z	RKLRR	IBDLR	FRPCAG	RSC	EBDR	FRS-BDR
Poisson	72.3	33.9-37.0	33.7-74.3	34.4-66.9	34.3-78.9	36.3-75.4	34.4-71.4	34.4-68.8	33.8-72.6	33.8-79.6	70.5-80.2	39.5-46.1	65.6	81.2

TABLE XLIII: Subspace clustering performance of different block diagonal representation approaches on corrupted MNIST data set. MNIST data set is computed for  $K = 3$  clusters and it is corrupted by interpreting input pixel values as means of Poisson distributions that are scaled up by  $10^{12}$ . The results are summarized for the similarity measure  $\mathbf{W} = \mathbf{X}^\top \mathbf{X}$ .

Subspace Clustering Performance for Different Block Diagonal Representation Methods														
Noise density	W	Minimum-Maximum Clustering Accuracy ( $c_{\text{accmin}} - c_{\text{accmax}}$ ) for Different Regularization Parameters												
		SSC	BD-SSC	LRR	BD-LRR	LSR	BDR-B	BDR-Z	RKLRR	IBDLR	FRPCAG	RSC	EBDR	FRS-BDR
0	70.4	34.4-55.0	36.8-77.4	35.5-68.7	35.5-69.4	38.3-71.9	36.5-85.1	34.7-85.6	34.4-80.7	34.4-86.6	65.0-78.6	37.7-48.8	77.2	87.5
0.1	78.2	34.4-59.8	35.0-77.7	36.6-54.7	36.7-80.3	35.8-74.5	34.2-74.5	35.7-76.9	34.3-63.0	34.3-77.1	40.7-77.3	36.9-47.8	68.3	77.9
0.2	73.3	34.5-64.8	34.2-75.6	36.8-41.2	38.1-77.3	37.1-72.4	34.2-70.5	35.7-71.3	34.3-53.5	34.3-64.5	39.1-75.6	38.1-46.9	62.3	73.2
0.3	67.5	34.5-63.2	34.1-67.4	37.5-41.4	38.4-71.6	40.7-69.9	34.2-66.9	38.8-68.2	34.3-47.6	34.3-58.2	39.1-78.1	36.9-47.5	56.7	67
0.4	59.9	34.4-55.1	34.2-64.6	37.2-39.6	37.9-66.2	40.5-61.5	34.1-59.4	38.1-56.8	34.4-44.3	34.3-49.8	40.6-74.6	38.0-47.7	50.3	57
0.5	50.0	34.4-49.2	34.1-54.2	36.2-39.3	37.5-57.9	39.5-53.9	34.2-52.1	39.2-53.8	34.3-41.1	34.3-43.3	39.1-72.8	36.9-47.1	44.4	48.6

TABLE XLIV: Subspace clustering performance of different block diagonal representation approaches on corrupted USPS data set. USPS data set is computed for  $K = 3$  clusters and the noise density, which affects approximately the defined value of pixels based on salt and pepper noise, is increased. The results are summarized for the similarity measure  $\mathbf{W} = \mathbf{X}^\top \mathbf{X}$ .

Subspace Clustering Performance for Different Block Diagonal Representation Methods														
Noise type	W	Minimum-Maximum Clustering Accuracy ( $c_{\text{accmin}} - c_{\text{accmax}}$ ) for Different Regularization Parameters												
		SSC	BD-SSC	LRR	BD-LRR	LSR	BDR-B	BDR-Z	RKLRR	IBDLR	FRPCAG	RSC	EBDR	FRS-BDR
Poisson	80.6	34.3-56.8	35.2-64.8	35.2-72.5	35.5-82.4	34.5-71.6	34.3-55.6	34.9-67.5	34.4-84.3	34.3-67.6	42.3-78.3	37.5-50.3	71.2	83.9

TABLE XLV: Subspace clustering performance of different block diagonal representation approaches on corrupted USPS data set. USPS data set is computed for  $K = 3$  clusters and it is corrupted by interpreting input pixel values as means of Poisson distributions that are scaled up by  $10^{12}$ . The results are summarized for the similarity measure  $\mathbf{W} = \mathbf{X}^\top \mathbf{X}$ .

## REFERENCES

- [1] J. Ding and A. Zhou, "Eigenvalues of rank-one updated matrices with some applications", *Appl. Math. Lett.*, vol 20, pp. 1223-1226, 2007.
- [2] J. R. Silvester, "Determinants of block matrices", *Math. Gazz.*, vol 84, pp. 460-467, 2000.
- [3] T. Hastie and P. Y. Simard, "Metrics and models for handwritten character recognition," *Stat. Sci.*, pp. 54-65, 1998.
- [4] Z. He, M. Zhang and H. Zhang, "Data-driven research on chemical features of Jingdezhen and Longquan celadon by energy dispersive X-ray fluorescence," in *Ceramics Int.*, vol. 42, pp. 5123-5129, 2016.
- [5] R. A. Fisher, "The use of multiple measurements in taxonomic problems," *Ann. Eugenics*, vol. 7, pp. 179-188, 1936.
- [6] F. K. Teklehaymanot, A. -K. Seifert, M. Muma, M. G. Amin and A. M. Zoubir, "Bayesian target enumeration and labeling using radar data of human gait," in *Proc. 26th European Signal Process. Conf. (EUSIPCO)*, pp. 1342-1346, 2018.
- [7] D. Cai, X. He, W. V. Zhang and J. Han, "Regularized locality preserving indexing via spectral regression," in *Proc. 16th ACM Conf. Inf. Knowl. Manage.*, pp. 741-750, 2007.
- [8] W. H. Wolberg and O. L. Mangasarian, "Multisurface method of pattern separation applied to breast cytology diagnosis," in *Proc. Natl. Acad. Sci.*, vol. 87, pp. 9193-9196, 1989.
- [9] A. R. Rocha Neto, R. Sousa, G. A. Barreto and J. S. Cardoso, "Diagnostic of pathology on the vertebral column with embedded reject option," in *Proc. Iberian Conf. Pattern Recognit. Image Anal.*, pp. 588-595, 2011.
- [10] A. -K. Seifert, M. Amin and A. M. Zoubir, "Toward unobtrusive in-home gait analysis based on radar micro-Doppler signatures," *IEEE Trans. Biomed. Eng.*, vol. 66, pp. 1-11, 2019.
- [11] T. P. Conrads, V. A. Fusaro, S. Ross, D. Johann, V. Rajapakse, B. A. Hitt, S. M. Steinberg, E. C. Kohn, D. A. Fishman, G. Whitely, J. C. Barrett, L. A. Liotta, E. F. Petricoin and T. D. Veenstra, "High-resolution serum proteomic features for ovarian cancer detection," *Endocrine-related Cancer*, vol. 11, pp. 163-178, 2004.
- [12] L. Naranjo, C. J. Perez, Y. Campos-Roca and J. Martin, "Addressing voice recording replications for Parkinson's disease detection," *Expert Syst. Appl.*, vol. 46, pp. 286-292, 2016.